

# Photobiology and metabolic interactions in the symbiotic jellyfish *Cassiopea*

Présentée le 27 janvier 2023

Faculté de l'environnement naturel, architectural et construit  
Laboratoire de géochimie biologique  
Programme doctoral en génie civil et environnement

pour l'obtention du grade de Docteur ès Sciences

par

**Niclas Heidelberg LYNDBY**

Acceptée sur proposition du jury

Dr S. Takahama, président du jury  
Prof. A. Meibom, Prof. K. Michael, directeurs de thèse  
Dr C. Ferrier-Pagès, rapporteuse  
Prof. M. Medina, rapporteuse  
Dr H. Peter, rapporteur

## Preface

This thesis manuscript is the result of 4½ years of PhD research on the photobiology and metabolic interactions in the symbiotic jellyfish *Cassiopea*. The work presented here was realized at the Laboratory for Biological Geochemistry at EPFL and the Microenvironmental Ecology & Symbiosis Lab at the University of Copenhagen.

## Acknowledgements

I would like to thank the members of the thesis jury, Dr. Satoshi Takahama, the president, Dr. Hannes Markus Peter, internal examiner, Dr. Christine Ferrier-Pagès, external examiner, and Prof. Mónica Medina, external examiner, for accepting to review this manuscript.

I would like to thank my supervisors Prof. Anders Meibom and Prof. Michael Kühn, who have taught me everything I know and supported me with invaluable insight and knowledge throughout my PhD journey.

Finally, I would like to thank my family back home in Denmark for have supported me throughout my education, all the way to the end of my PhD. And especially a huge thank to my beloved girlfriend, who has supported me immensely during the final period of my PhD, and for making my life wonderful.

Thank you all.

## Abstract

The symbiont-bearing jellyfish *Cassiopea* live a benthic lifestyle, positioning themselves upside-down on sediments in shallow waters to allow their endosymbiotic algae to photosynthesize in the sunlight. Over the last decades *Cassiopea* has become increasingly popular as a model system for photosymbiosis because, like reef-building corals, these animals rely on autotrophic assimilation of carbon from its algal symbionts. However, relatively little is still known about the photobiology of *Cassiopea*. Previous studies have focused on investigations of O<sub>2</sub> production or CO<sub>2</sub> consumption at the scale of entire individuals. Metabolic interactions between animal host and symbiont algae have been studied with bulk isotopic bulk analyses of host tissue vs. the symbiont population. Yet, this symbiosis is the result of single-cell interactions that are modulated by surrounding tissue microenvironments. Accounting for this cellular and spatial heterogeneity of interactions is thus crucial for advancing our understanding of the photobiology of *Cassiopea*.

Unlike reef-building corals, *Cassiopea* maintain their symbionts in specialized host cells, the motile amoebocytes, residing in the mesoglea of the animal. In the first chapter of this thesis, I thus explored the role of these cells in the nutrient uptake and exchange between host and symbionts. Stable isotope labelling experiments were combined with correlated scanning electron microscopy and NanoSIMS imaging, to achieve a better understanding of the fate of assimilated carbon and the photosynthate translocation *in hospite*. Amoebocytes hosting clusters of symbionts were found primarily adjacent to the subumbrella epidermis, and incubation experiments with <sup>13</sup>C-bicarbonate demonstrated that photosynthates produced by the symbiotic algae are transferred via the amoebocytes to host epidermis. Thus, the amoebocytes facilitate nutrient transfer between host and symbionts, and enable host assimilation of autotrophic carbon. Furthermore, incubations with <sup>15</sup>NH<sub>4</sub><sup>+</sup> and <sup>15</sup>NO<sub>3</sub><sup>-</sup> demonstrated that *Cassiopea* prefer NH<sub>4</sub><sup>+</sup> as their nitrogen source; assimilation of NO<sub>3</sub><sup>-</sup> was not detected in any of the holobiont compartments investigated here by NanoSIMS imaging. Both the symbiotic algae and the host animal contribute to the assimilation of NH<sub>4</sub><sup>+</sup>. In conclusion, the amoebocytes appear to be a key adaptation for the *Cassiopea* symbiosis, as they facilitate nutrient transfer *in hospite* and keeps symbionts near the most light-exposed parts of the bell to optimize photosynthesis.

In the second chapter, I investigated the photobiology and physico-chemical microenvironment of *Cassiopea* using microsensors. Photon scalar irradiance across the medusa was found to be highly heterogenous and light availability was found to be highest at the apical parts (i.e., the oral arms and manubrium) of the animal. Surface reflectance revealed that white granules (spheres of ca. 200 μm in

diameter) found in the bell tissue along rhopalia canals strongly scatter light, and scalar irradiance measurements showed that light availability was locally enhanced in tissue containing white granules in high density. Depth profiles of O<sub>2</sub> concentrations in the bell mesoglea of large individuals (> 6 cm) revealed increasing concentration of O<sub>2</sub> down towards the middle of the mesoglea (i.e., halfway between sub- and exumbrella epidermis), in light reaching levels 2-fold higher than the ambient water. During dark periods, the O<sub>2</sub> concentration slowly decreased deep in the bell but remained higher than ambient water levels, demonstrating that the mesoglea acts as a storage for O<sub>2</sub> in *Cassiopea*. Light-dark shifts further supported this as O<sub>2</sub> levels deep in the mesoglea would continue to increase in large individuals for several minutes after the light was turned off, and *vice versa* when the light was turned on. Similar observations were made for pH, but the response period was even longer (up to 10 minutes) and even small individuals showed a slow response to pH changes with light-dark shifts. Based on these observations, it is concluded that the mesoglea acts as a storage medium for *Cassiopea*, buffering O<sub>2</sub> and pH, and thereby providing a highly stable environment for *Cassiopea* symbionts.

In the third chapter, I used optical coherence tomography (OCT) to non-invasively image the micromorphology of *Cassiopea* medusae, generating 3D reconstructions of entire animals as well as individual anatomical features. Using these scans, I explored the tissue organization and spatial distribution of the algal symbionts clustered in amoebocytes, as well as the light scattering of white granules in the bell tissue. Inherent optical properties from tissue with high densities of white granules showed that these locally enhance the light availability for adjacent symbionts. These observations were combined with isotopic labelling experiments to compare the relative carbon assimilation by symbionts in bell tissue with and without white granules. Symbiont cells in tissue with white granules were significantly more enriched in <sup>13</sup>C relative to symbionts in tissue without white granules, supporting the hypothesis that the white granules locally enhance photosynthesis in the *Cassiopea* system and play an important role in host modulation of the light-microenvironment experienced by symbionts.

In the fourth chapter, I further developed a new approach to study photosynthetic performance of *Cassiopea* permitting to investigate the heterogeneity of O<sub>2</sub> evolution across the umbrella. O<sub>2</sub> imaging across the subumbrella bell, measured with planar O<sub>2</sub> optodes, indicated that photosynthetic activity was highest near the bell center, along the bell rim, and along several major radial canals during light periods. However, during darkness, the O<sub>2</sub> concentration did not show the same dynamics, with O<sub>2</sub> depleting to pre-light conditions from the bell rim towards the center in a uniform direction. This supports the conclusion of chapter 2 that the mesoglea buffers O<sub>2</sub> in the bell and that this buffering capacity is

proportional to the thickness of the mesoglea, which is largest near the bell center. Additionally, the O<sub>2</sub> concentration in the oral arms was found to be highly dynamic, as O<sub>2</sub> rapidly built up in and around the arms during light periods, and conversely, is quickly depleted during darkness. However, the O<sub>2</sub> produced in the arms did not appear to contribute to O<sub>2</sub> storage in the bell mesoglea found directly below the arms, suggesting O<sub>2</sub> might be primarily lost through gas exchange with surrounding water. The results provided here show that O<sub>2</sub> production is more heterogenous than previously thought, emphasizing that techniques – such as planar optodes – that cover entire areas of an organism are highly useful to correctly assess their productivity.

In conclusion, this thesis provides new insights into the dynamics of *Cassiopea* primary production and (sub)cellular-level nutrient assimilation. This functional understanding of the *Cassiopea* holobiont advances this important model system and identifies knowledge gaps for exciting future research venues.

## Résumé

La méduse symbiotique *Cassiopea* est benthique, vivant à l'envers et posée sur des sédiments d'eaux peu profondes, afin de fournir à ses algues endosymbiotiques une exposition à la lumière propice à leur photosynthèse. Ces dernières décennies, *Cassiopea* est devenue un organisme modèle de plus en plus populaire pour l'étude de la photosymbiose, puisque, tel que les coraux constructeurs de récifs, ces animaux dépendent de l'assimilation autotrophe du carbone par leur algues symbiotiques. Cependant, les connaissances actuelles sur la photobiologie de *Cassiopea* sont très limitées. Des études précédentes ont mesuré la production d'O<sub>2</sub> et la consommation de CO<sub>2</sub> à l'échelle de l'individu entier. Les interactions métaboliques entre l'hôte animal et ses algues symbiotiques ont été étudiées grâce à des analyses isotopiques globales du tissu hôte entier *versus* la population de symbiotes. Pourtant, la symbiose est le résultat d'interactions se produisant à l'échelle cellulaire influencées par le micro-environnement local. Prendre en compte l'hétérogénéité cellulaire et spatiale de ces interactions est donc crucial pour approfondir notre compréhension de la photobiologie chez *Cassiopea*.

A la différence des coraux constructeurs de récifs, *Cassiopea* maintient ses symbiotes dans des cellules spécialisées et mobiles, les amœbocytes, résidant dans la mésogée de l'animal. Dans le premier chapitre de cette thèse, j'ai donc exploré le rôle de ces cellules dans l'assimilation et l'échange de nutriments entre l'hôte et ses symbiotes. Pour cela, des expériences de marquage aux isotopes stables ont été combinées avec de l'imagerie corrélative en microscopie électronique à balayage et en NanoSIMS, afin de mieux comprendre le devenir du carbone assimilé et la translocation des photosynthétats *in hospite*. Les amœbocytes hébergeant des grappes de symbiotes ont été trouvés principalement près de l'épiderme oral, et les expériences d'incubation avec du <sup>13</sup>C-bicarbonate ont démontré que les photosynthétats produits par les algues symbiotiques sont transférés via les amœbocytes vers l'épiderme de l'hôte. Par conséquent, les amœbocytes facilitent le transfert des nutriments entre l'hôte et les symbiotes, et permettent l'assimilation du carbone autotrophique par l'hôte. De plus, les incubations avec <sup>15</sup>NH<sub>4</sub><sup>+</sup> et <sup>15</sup>NO<sub>3</sub><sup>-</sup> révèlent que *Cassiopea* préfère NH<sub>4</sub><sup>+</sup>, car aucune assimilation de NO<sub>3</sub><sup>-</sup> n'a été détectée dans les différents compartiments de l'holobionte lors de cette étude par NanoSIMS. Les algues ainsi que l'hôte animal contribuent à l'assimilation de NH<sub>4</sub><sup>+</sup>. En conclusion, les amœbocytes semblent être la clé de l'adaptation de la symbiose chez *Cassiopea*, en facilitant le transfert de nutriment *in hospite* et en positionnant les symbiotes près des parties de l'ombrelle les plus exposées à la lumière afin d'optimiser leur photosynthèse.

Dans le second chapitre, je me suis intéressé au micro-environnement photobiologique et physico-chimique de *Cassiopea* en utilisant des microcapteurs. Le rayonnement scalaire des photons à travers la méduse s'est avéré hautement hétérogène, et la disponibilité en lumière plus haute dans les parties apicales (par exemple les bras oraux et le manubrium) de l'animal. La réflectance de surface révèle que des granules blanches (sphères de ~200  $\mu\text{m}$  de diamètre) trouvées dans les tissus de l'ombrelle le long des canaux de rhopalie disperse fortement la lumière, et les mesures de rayonnement scalaire ont montré que la disponibilité en lumière était localement accrue dans les tissus contenant une grande densité de granules blanches. Les profils mesurant la concentration en  $\text{O}_2$  en fonction de la profondeur dans la mésoglée de l'ombrelle de larges individus (> 6cm), ont révélé une augmentation dans la concentration en  $\text{O}_2$  en descendant vers le centre de la mésoglée (par exemple à mi-chemin entre les épidermes oraux et aboraux), atteignant des niveaux deux fois plus élevés que dans l'eau environnante à la lumière. À l'obscurité, la concentration en  $\text{O}_2$  dans les profondeurs de l'ombrelle diminue progressivement, mais reste plus haute que dans l'eau environnante, ce qui suggère que la mésoglée agit comme un stockage d' $\text{O}_2$  chez *Cassiopea*. Les passages entre lumière et obscurité renforcent cette idée, comme le niveau d' $\text{O}_2$  dans la mésoglée profonde de l'ombrelle continuait à augmenter pendant plusieurs minutes dans les grands individus après l'extinction de la lumière, et *vice versa* après que la lumière fut allumée. Des observations similaires ont été faites pour le pH, mais le temps de réponse était encore plus long (jusqu'à 10 minutes), et même de petits individus ont montrés une réponse lente aux changements de pH lors des changements entre lumière et obscurité. En se basant sur ces observations, il est proposé que la mésoglée agit comme un moyen stockage chez *Cassiopea*, ayant un effet tampon pour l' $\text{O}_2$  et le pH, et par conséquent fournissant un environnement très stable pour les symbiotes de *Cassiopea*.

Dans le troisième chapitre, j'ai utilisé la tomographie en cohérence optique (TOC) pour imager de façon non-invasive la micro-morphologie des méduses de *Cassiopea*, générant ainsi des reconstructions 3D de l'animal entier et révélant des caractéristiques anatomiques de l'individu. En utilisant ces scans, j'ai exploré l'organisation des tissus et la distribution spatiale des symbiotes groupés dans les amoebocytes, ainsi que celle des granules blancs qui dispersent la lumière dans le tissu de l'ombrelle. Les propriétés optiques inhérentes aux tissus à haute densité de granules blanches ont montrées que celles-ci augmentent localement la disponibilité de lumière pour les symbiotes adjacents. Ces observations ont été combinés avec des expériences de marquages avec des isotopes stables pour comparer l'assimilation de carbone par les symbiotes dans les tissus de l'ombrelle avec ou sans granules blanches. Les cellules des symbiotes présents dans les tissus riches en granules blanches étaient



significativement plus enrichies en  $^{13}\text{C}$  que symbiotes résidant dans des tissus sans granules blanches, renforçant la conclusion que les granules blancs améliorent localement la photosynthèse dans le système *Cassiopea*, et joue un rôle important dans la modulation par l'hôte du niveau de lumière dans les micro-environnements où vivent les symbiotes.

Dans le quatrième chapitre, j'ai développé une nouvelle approche pour étudier les performances photosynthétiques de *Cassiopea* afin de mesurer l'hétérogénéité de production d' $\text{O}_2$  dans l'ombrelle. Les images de la concentration d' $\text{O}_2$  prises le long de l'ombrelle orale grâce à des « planar  $\text{O}_2$  optodes », suggèrent que l'activité photosynthétique est plus élevée près du centre et de la bordure de l'ombrelle, et le long de plusieurs canaux majeurs pendant les périodes de lumière. Cependant, lors du passage à l'obscurité, la concentration en  $\text{O}_2$  n'a pas montré les mêmes dynamiques, avec une diminution de la concentration en  $\text{O}_2$  jusqu'au niveau de pré-illumination se faisant de façon uniforme du bord vers le centre de l'ombrelle. Cela renforce la conclusion du chapitre 2 présentant la mésoglée comme un tampon de l' $\text{O}_2$  dans l'ombrelle et dont l'effet est proportionnel à l'épaisseur de la mésoglée, plus large au centre de l'ombrelle. De plus, la concentration en  $\text{O}_2$  dans les bras oraux s'est avérée très dynamique, car l' $\text{O}_2$  s'accumule rapidement dans et autour des bras pendant les périodes de lumière et de même, diminue rapidement à l'obscurité. Cependant, l' $\text{O}_2$  produit dans les bras oraux ne semble pas contribuer au stockage de l' $\text{O}_2$  dans la mésoglée de l'ombrelle, se situant directement en dessous des bras, suggérant que l' $\text{O}_2$  pourrait être principalement perdu lors d'échanges gazeux avec l'eau environnante. Ces résultats montrent que la production d' $\text{O}_2$  est étonnamment très hétérogène, soulignant l'intérêt de techniques telles que les « planar optodes », mesurant des parties entières d'un organisme, pour mesurer correctement leur productivité.

En conclusion, cette thèse fournit de nouvelles informations sur les dynamiques de production primaire et d'assimilation de nutriment au niveau (sous-)cellulaire chez *Cassiopea*. Cette compréhension fonctionnelle de l'holobiont *Cassiopea* fait avancer cette méduse en tant qu'organisme modèle important, et mets en lumière des lacunes dans les connaissances actuelles, ouvrant ainsi de nouvelles et passionnantes directions de recherche.

**Keywords:** *Cassiopea*, photobiology, photosynthesis, metabolic interactions, metabolism, light microenvironment, physico-chemical microenvironment, NanoSIMS, microsensors

## Table of Contents

Preface .....	1
Acknowledgements.....	2
Abstract.....	3
Résumé .....	6
Introduction .....	13
Morphology.....	14
Life cycle.....	17
Symbiosis and ecological expansion .....	19
<i>Cassiopea</i> holobiont metabolism .....	20
Photosynthesis and carbon assimilation .....	20
Nitrogen and phosphorus assimilation .....	21
<i>Cassiopea</i> heterotrophy.....	22
<i>Cassiopea</i> as a model system for symbiosis .....	23
Thesis objectives and knowledge gaps .....	24
General theory on major techniques used .....	26
Establishing and maintaining <i>Cassiopea</i> in culture.....	26
Nanoscale Secondary Ion Mass Spectrometry (NanoSIMS) .....	27
Basic principles of NanoSIMS.....	28
Sample preparations and requirements .....	29
General protocol for NanoSIMS preparations used in this thesis .....	30
Chapter 1: Carbon and nitrogen assimilation in <i>Cassiopea</i> : A NanoSIMS study .....	33
I. Context.....	33
Authors contribution.....	33
II. Publication .....	33
Abstract.....	33
Keywords.....	34
Introduction .....	34
Materials and Methods.....	36
<i>Cassiopea</i> husbandry .....	36
Experimental setup .....	36
Isotopic pulse labelling experiments .....	37

SEM imaging.....	39
NanoSIMS image acquisition .....	39
Statistical analyses .....	40
Results.....	40
Cassiopea histology.....	40
Stable isotope enrichment in <i>Cassiopea</i> sp. ....	41
Discussion.....	44
Translocation of photosynthetically assimilated <sup>13</sup> C.....	45
Nitrogen assimilation and resource allocation .....	46
The ecological advantages of motile symbiont-bearing amoebocytes and <i>Cassiopea</i> as a model system .....	47
Acknowledgments.....	48
Funding .....	48
Data accessibility.....	49
Competing interests.....	49
Chapter 2: Light microenvironment and O <sub>2</sub> and pH dynamics measured in the <i>Cassiopea</i> bell.....	50
I. Context.....	50
Author Contributions .....	50
II. Publication .....	50
Abstract.....	51
Introduction .....	51
Methods.....	53
<i>Cassiopea</i> maintenance .....	53
Light measurements .....	53
Microscale measurements of O <sub>2</sub> and pH .....	54
Results.....	56
Light microenvironment .....	56
Chemical microenvironment.....	57
Discussion.....	58
<i>Cassiopea</i> harbors optical microniches .....	58
<i>Cassiopea</i> harbors its photosymbionts in a buffered chemical microenvironment.....	59
Summary .....	62
Conflict of Interest .....	63
	10

Funding .....	63
Acknowledgments.....	63
Figures.....	64
Chapter 3: Non-invasive imaging of <i>Cassiopea</i> and investigation of inherent optical properties .....	74
I. Context.....	74
Author contribution .....	74
II. Publication .....	74
Abstract.....	74
Introduction .....	75
Methods.....	78
<i>Cassiopea</i> husbandry and preparation .....	78
Optical Coherence Tomography .....	78
Variable chlorophyll fluorescence imaging.....	80
Isotopic pulse labelling experiment .....	80
Symbiont density estimation .....	82
Statistical analyses .....	82
Results and Discussion .....	83
Imaging <i>Cassiopea</i> morphology.....	83
Improving depth penetration .....	87
High-resolution scans.....	90
Optical properties of <i>Cassiopea</i> bell tissue.....	91
Photosynthetic performance in different <i>Cassiopea</i> tissue compartments.....	93
Conclusion.....	96
Acknowledgements.....	96
Competing interests.....	96
Supplementary information.....	97
Chapter 4: Investigation of the O <sub>2</sub> dynamics in <i>Cassiopea</i> using O <sub>2</sub> -sensitive planar optodes .....	98
I. Context.....	98
Author contribution .....	98
II. Publication .....	98
Introduction .....	99
Methods.....	100

Cassiopea specimens .....	100
Planar optode O <sub>2</sub> imaging .....	101
Variable chlorophyll <i>a</i> fluorescence imaging .....	103
Hyperspectral imaging .....	103
Results .....	104
Variable chlorophyll <i>a</i> fluorescence .....	104
Planar optode imaging .....	106
Hyperspectral imaging .....	110
Discussion .....	111
O <sub>2</sub> dynamics in <i>Cassiopea</i> bell tissue .....	111
Light-dependent O <sub>2</sub> buildup and dark respiration .....	112
<i>Cassiopea</i> oral arm contribution to O <sub>2</sub> production .....	113
Conclusion .....	113
Acknowledgements .....	114
Supplementary information .....	114
Molecular identification .....	114
Supplementary figures .....	115
General discussion .....	118
Inorganic nutrient assimilation in <i>Cassiopea</i> and the role of amoebocytes .....	118
Nitrogen species and assimilation in <i>Cassiopea</i> .....	119
Mesoglea buffers the chemical environment of symbionts .....	120
Light scattering in <i>Cassiopea</i> .....	121
Investigating micromorphology and organization of symbionts in <i>Cassiopea</i> medusae .....	122
Photosynthesis and nutrient assimilation across the bell .....	123
Concluding remarks and future perspective .....	125
References .....	127

## Introduction

The upside-down jellyfish *Cassiopea* is a Scyphozoan jellyfish in the order of Rhizostomeae and is the sole genus in the family Cassiopeidae (Figure 1). Cassiopeidae constitutes nine recognized species (Jarms & Morandini 2019), that are found worldwide in shallow water along shores of tropical and subtropical regions (Holland et al. 2004, Arai et al. 2017, Morandini et al. 2017), typically in shallow coastal ecosystems, such as lagoons, seagrass meadows and mangroves (Bigelow 1900, Niggli & Wild 2010). *Cassiopea andromeda* (Forsskål, 1762) was originally discovered in the Red Sea by Peter Forsskål (Forsskål & Niebuhr 1775), and was later described in detail by Robert Payne Bigelow (1900) as *Cassiopea xamachana* (Jamaica; see also Mayer 1910). Bigelow realized that the medusae and polyps of *Cassiopea* contained numerous “green cells”, which were later identified as the endosymbiotic algae *Symbiodinium microadriaticum* (Freudenthal 1959, 1962). It is now well established that *Cassiopea* live in close symbiosis with photosynthetic dinoflagellates of the family Symbiodiniaceae (see recent revision from clades to genera by Lajeunesse et al. 2018), and this symbiotic relationship has encouraged scientists to adopt the *Cassiopea*-holobiont system as a model for the study of photosymbiosis (e.g. Drew 1972, Hofmann & Kremer 1981, Verde & McCloskey 1998, Lampert 2016, but see especially Medina et al. 2021).

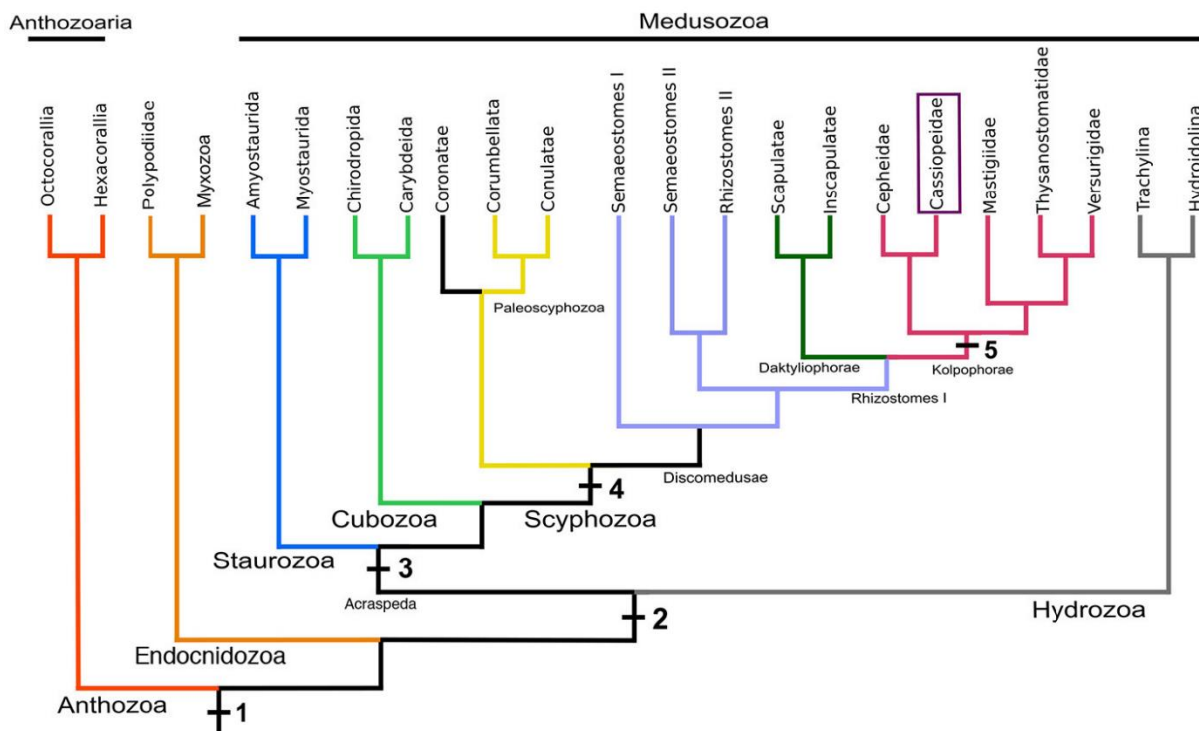


Figure 1 | Medusozoa phylogeny based on recent work (Bayha et al. 2010, Kayal et al. 2012, 2018), illustrating the phylogenetic position of the Cassiopeidae family among other Scyphozoans (1, cnidae; 2,

medusa stage; 3, rhopalia; 4, strobilation, and ephyra; 5, monodisc strobilation). Figure adopted from Ohdera et al. (2018).

## Morphology

Despite the benthic, upside-down lifestyle, the Bauplan of *Cassiopea* medusae resembles that of other scyphozoan jellyfish (Lewis Ames 2018). The body contains a typical cnidarian body composition of three layers: epidermis, mesoglea, and gastrodermis (Mayer 1910). The mesoglea is a gel-like matrix that contains collagen fibers, which form a hydrostatic skeleton supporting the body of the animal and making up the bulk volume of scyphozoan medusae. A gastric network divides the mesoglea into a sub- and exumbrella layer, with the exumbrella typically much thicker than the subumbrella layer (Bigelow 1900).

*Cassiopea* is unique among scyphozoans with the medusa stage exhibiting a flat umbrella, which facilitates a benthic lifestyle similar to corals and sea anemones. The medusa has a large, smooth and flat bell that can reach up to 25 cm in diameter, and a concave exumbrella (Figure 2), which allows the medusa to adhere to the substrate by creating a slight suction (Bigelow 1900). White coloration is typically found on the exumbrella of adult medusae, and patterns can vary greatly between individuals, but typically white radial stripes run along the major rhopalia canals out towards the bell rim and reach the rhopalia (i.e., eyespots for sensing light). The rhopalia and rhopalia canals are connected by larger bell segments of anastomosing (i.e., connective) tissue between them (Figure 3).

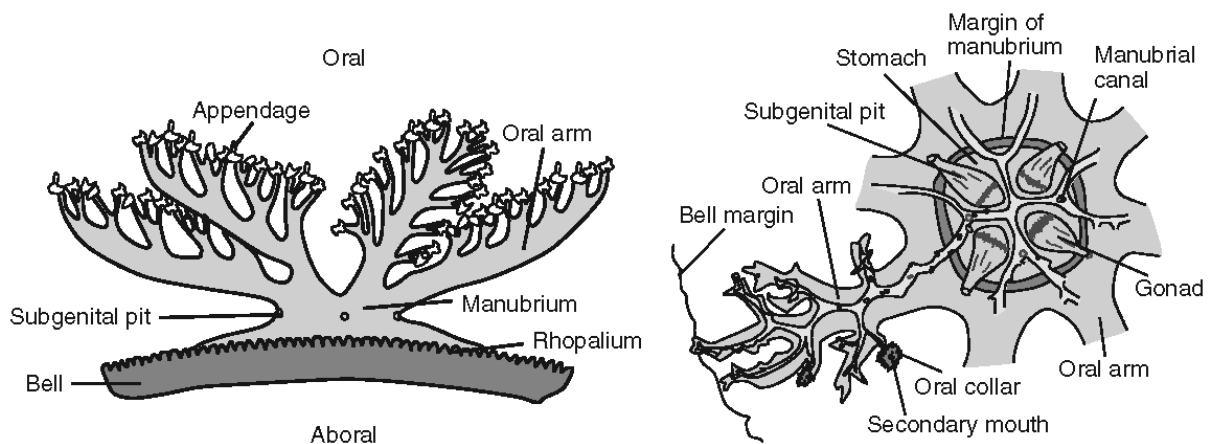


Figure 2 | Schematic overview of the main structures of the *Cassiopea* body plan. Figure adopted from Hamlet et al. (2011).

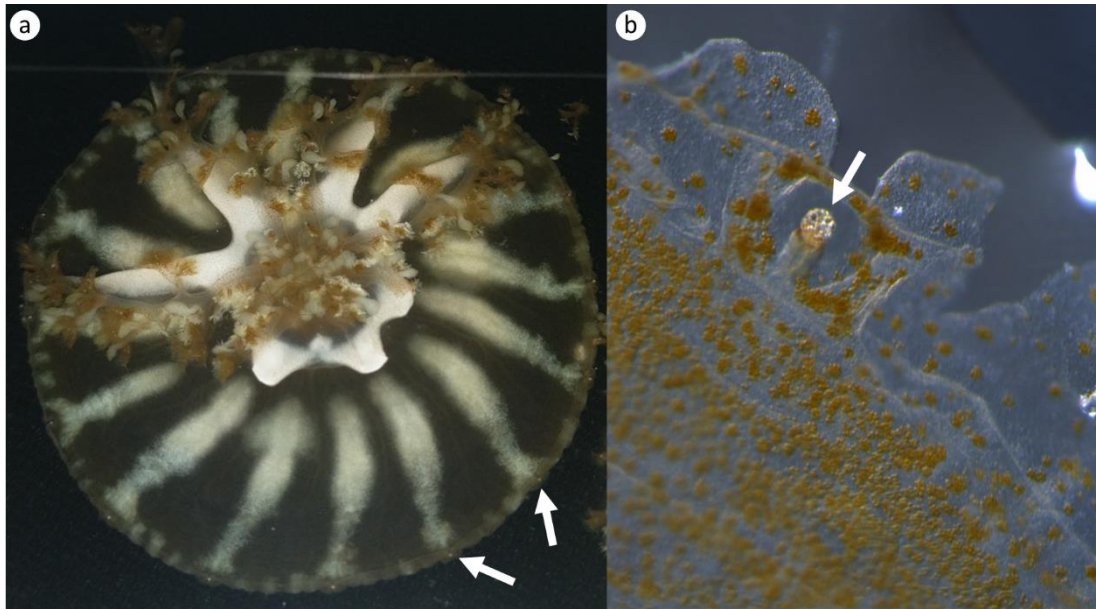


Figure 3 | White striated pattern (white granules) are clearly visible in the subumbrella and in oral arms of an adult *Cassiopea* (a). Rhopalium located in the bell rim (b). White arrows point to rhopalia location along the rim.

*Cassiopea* typically grow four pairs of round, highly branched arms at the center of the bell, the manubrium (Figure 2)(Bigelow 1900), and white coloration, similar to the rhopalia canals, is found running from the base to the apex of these oral arms. Each arm can have 9-15 branches, with the arms sometimes extending beyond the area of the bell, depending on the species (Mayer 1910). Like all rhizostome jellyfish, *Cassiopea* do not harbor traditional tentacles for feeding but instead rely on secondary mouths and vesicular appendages growing on the oral arms (Figure 2 & Figure 4). Each mouth is surrounded by fringed digitata, and both mouths and appendages are covered in cnidocytes to capture and neutralize prey before ingestion. Mouth openings run through the oral arms and into the main gastric cavity (the stomach; Figure 2) at the center of the bell. From there, the main gastric cavity branches out throughout the entire umbrella, with the radial canals in anastomosing tissue and the rhopalia canals constituting the main channels (Bigelow 1900, Avian et al. 2022).



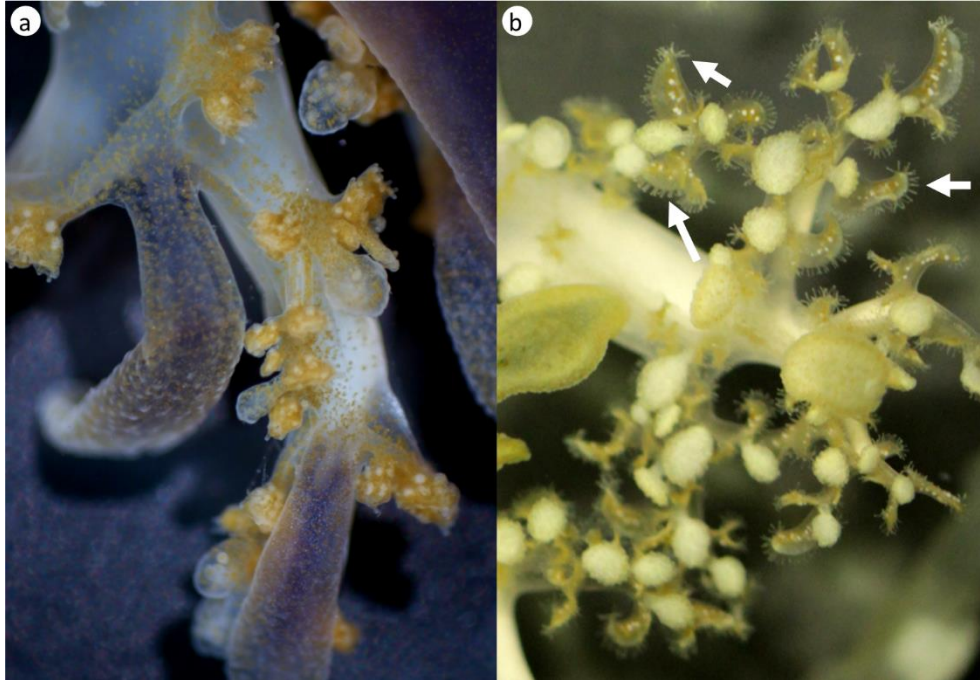


Figure 4 | Morphological diversity of oral arms. a) Large blue-colored (“Cassioblue”) vesicles, along with smaller, non-pigmented vesicles and secondary mouths. b) White pigmented vesicles along secondary mouths. Fringed digitata can be seen surrounding secondary mouths (white arrows).

In addition to the white coloration in the bell and oral arms, *Cassiopea* show a range of pigments from purple-blue to red and pink (Lampert et al. 2012). The pigments are typically associated with larger vesicles growing on the oral arms in a variety of sizes, shapes, and in different growth patterns along the oral arms depending on the individual (Bigelow 1900, Lampert et al. 2012). The two most common colors are the green and blue host pigments (Blanquet & Phelan 1987). While green pigments have yet to be identified, the blue coloration was recently described as a pigment family inherent to rhizostome jellyfish (“Cassioblue”, pigment family of Rhizostomins; Lawley et al. 2021). The exact cause of various colorations and their potential functions are not known, but the coloration is not related to the strain of dinoflagellate symbionts within the medusa (Lampert et al. 2012). The coloration has been hypothesized to play a role in photoprotection (e.g. against high irradiation or UV protection; Blanquet & Phelan 1987). Additionally, it has been suggested that different colors in *Cassiopea* could generate different light microenvironments (Lampert et al. 2012, Hamaguchi et al. 2021, Lawley et al. 2021) similar to what is known from corals (e.g. Salih et al. 2000, Dove et al. 2001, Lyndby et al. 2016, Bollati et al. 2022). The Bauplan and pigmentation of *Cassiopea* thus likely enables the host to modulate the light microenvironment experienced by algal symbionts to optimize photosynthetic performance of these (Dove et al. 2008, Wangpraseurt et al. 2012, Bollati et al. 2022).

## Life cycle

*Cassiopea* are gonochoristic (i.e., species with separate sexes), and adult females can typically be identified by the presence of specialized brooding tentacles found at the center of the bell (Hofmann & Hadfield 2002). It remains uncertain when medusae reach sexual maturity, but individuals have been observed to reproduce already when the bell has reached a diameter of 7 cm (Hofmann & Hadfield 2002). Planula larvae from sexual reproduction use bacterial cues to find a suitable place for settlement (Hofmann et al. 1978), typically in shaded and secluded areas (Fleck et al. 1999, Fleck & Fitt 1999). Once the planula has settled, it metamorphoses into a 3-4 mm long scyphistoma (i.e., a polyp) within a couple of days (Figure 5 and Figure 6)(Bigelow 1900, Curtis & Cowden 1974). Once the polyp is formed, buds begin to be produced from the aboral side of the calyx (i.e., the underside of the polyp head). Buds eventually detach, forming motile planuloids (homologous to the planula larva) that will settle and metamorphose into polyps on their own ("Asexual Budding"; Figure 5).

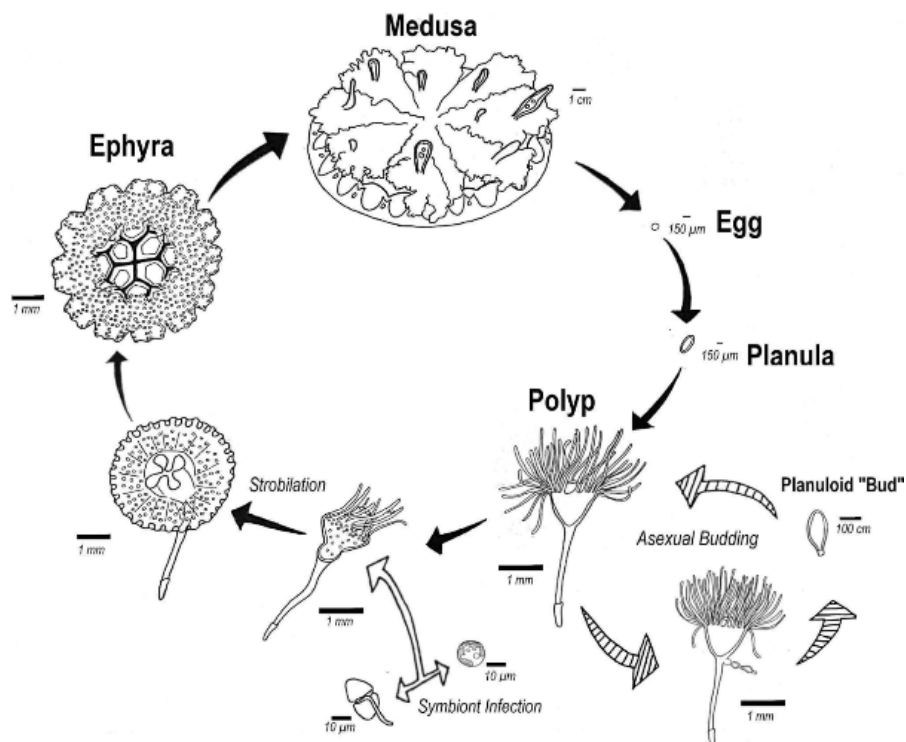


Figure 5 | Life cycle of *Cassiopea*, showing each stage of the development from the sexually produced egg up to adult medusa (black arrows), the asexual reproduction cycle (striped arrows), and the introduction of symbionts for successful strobilation (white arrows) to complete the life cycle. Figure adopted from Medina et al. (2021).

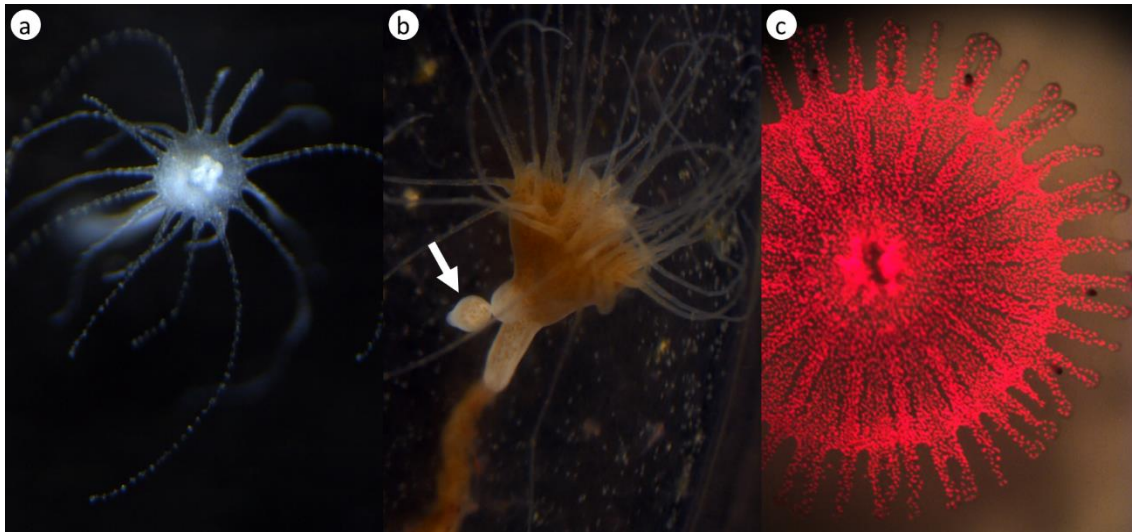


Figure 6 | Various polyp stages and newly released ephyra. a) Recently fully metamorphosed polyp without (visible) symbionts. b) Established polyp full of symbionts. A planuloid bud can be seen forming at the aboral end of the calyx (white arrow). c) Newly released ephyra. Symbionts are clearly present throughout the animal seen as auto fluorescence from chlorophyll.

*Cassiopea* are special in that the polyp requires dinoflagellate symbionts to initiate strobilation (“Symbiont Infection”; Figure 5)(Hofmann & Kremer 1981, Hofmann et al. 1996, Mellas et al. 2014). Surprisingly however, planulae do not receive these symbionts vertically from their parents, but instead need to take them up from their environment once metamorphosed (Colley & Trench 1983, Sachs & Wilcox 2006). Symbionts are acquired through phagocytosis by gastrodermal cells that subsequently develop into amoebocytes (Colley & Trench 1983, Fitt & Trench 1983). The symbionts are primarily clustered at the base of the tentacles and calyx of the polyp. While the initial uptake of symbionts appears to be unselective, mature communities are commonly dominated by a single algal strain (Thornhill et al. 2006, Mellas et al. 2014). Unlike the sexually produced planula larvae, asexually produced planuloids can bear symbionts vertically transferred from the original polyp (Figure 6)(e.g. Rahat & Adar 1980, Sachs & Wilcox 2006).

The first strobilation appears to depend on temperature (> 25 °C) and the density of symbionts in the polyp (Hofmann et al. 1978). While symbionts are required for the initiation of strobilation, studies using photosynthesis inhibitors revealed that strobilation is initiated in the absence of photosynthesis (Hofmann & Kremer 1981). *Cassiopea* are monodisc strobilating scyphozoans, meaning that only a single ephyra is produced at a time. During strobilation, polyp tentacles are reduced, the apex of the calyx begins to transition to a bell shape, while rhopalia start forming along the bell rim, and the polyp mouth start forming at the base of the first oral arms (“Strobilation”; Figure 5).

Once the ephyra is fully formed, it detaches, leaving the polyp stalk from which a new head with tentacles and mouth regrows before a new ephyra is produced (Hofmann et al. 1978). Polyps kept under optimal light and feeding regimes appear capable of producing up to two ephyra per week (Fitt & Costley 1998). Released ephyra continue to grow and metamorphose over 2-4 weeks, depending on feeding status (e.g. Muffett et al. 2022), into a fully developed juvenile medusae, that can eventually reach sexual maturation and complete the life cycle.

### Symbiosis and ecological expansion

*Cassiopea* harbor algal endosymbionts of the family Symbiodiniaceae, predominantly of the genera *Symbiodinium*, *Breviolum*, *Cladocopium*, and *Durusdinium* (formerly clades A, B, C, and D, respectively), similar to other symbiotic cnidarians (e.g. LaJeunesse 2001, Baker 2003, Thornhill et al. 2006, Mellas et al. 2014, Biquand et al. 2017). These symbionts are found in the highest densities in host-specialized amoebocyte cells directly under the subumbrella epidermis and in the oral arms, which are more light-exposed relative to the rest of the bell (Fitt & Trench 1983, Estes et al. 2003). Furthermore, symbionts are found scattered in much lower densities in the mesoglea and near the exumbrella epidermis (Hofmann et al. 1978, Colley & Trench 1983, Estes et al. 2003). Similar to reef-building corals, symbionts are responsible for the brown coloration of the animal and facilitate autotrophic assimilation of inorganic carbon and nitrogen (Welsh et al. 2009, Freeman et al. 2016).

In corals, exposure to environmental stressors like high temperatures, hypo-salinity, and acidification can result in the breakdown of the host-algal symbiosis. In this processes, which is referred to as coral bleaching, algae are lost from the animal through expulsion or digestion and the white calcium carbonate skeleton becomes visible underneath the almost transparent coral tissue (Glynn 1996, Brown 1997). In comparison, *Cassiopea* appear extraordinarily resilient to environmental stressors, and numerous studies have found them in environments deemed 'extreme' for corals (e.g. Goldfarb 1914, Morandini et al. 2017, Klein et al. 2017a, Aljbour et al. 2017, Klein et al. 2019, Newkirk et al. 2020). While bleaching can occur in *Cassiopea*, for example triggered by artificially induced heat stress or darkness (e.g. Newkirk et al. 2018, 2020), it is rarely observed naturally under present environmental conditions (Klein et al. 2019, Newkirk et al. 2020, Banha et al. 2020).

Studies have found that *Cassiopea* inhabiting different ecological niches also host different strains of symbiont algae (e.g. heat-tolerant vs. heat-sensitive strains; Fitt et al. 2021). The flexibility to associate with diverse and potentially more stress-resilient symbiont strains likely contributes to the broad thermal

tolerance of *Cassiopea* (Berkelmans & van Oppen 2006, Newkirk et al. 2020). The ecological success of *Cassiopea* is likely linked with its broad thermal tolerance (Aljbour et al. 2017, 2019, Klein et al. 2019).

The remarkable resilience of *Cassiopea* to environmental stressors and perturbations, combined with their prolific asexual reproduction and open selection of symbiont strains (Schiariti et al. 2014, Morandini et al. 2017), make the unintentional introduction to new regions by humans (e.g. transported in ballast tanks of ships) very likely; especially in the polyp stage. This potential is illustrated by the recent rapid expansion of *C. andromeda* that was originally confined to the Red Sea but has now expanded to the Mediterranean Sea (Çevik 2006, Schembri et al. 2010), the coast of Brazil (Morandini et al. 2017), and the Hawaii archipelago (Uchida 1970, Hofmann & Hadfield 2002, Holland et al. 2004).

Because of the relative robustness to a wide range of environmental conditions, the currently projected global warming trajectories (van der Zande et al. 2020) and the accompanying increase in anthropogenic pollution do not seem to have a major negative impact on *Cassiopea* population stability and growth (e.g. Stoner et al. 2011, Aljbour et al. 2018, Thé et al. 2020), but might in fact promote their proliferation throughout (sub-)tropical coastal ecosystems (Aljbour et al. 2017, Béziat & Kunzmann 2022).

### *Cassiopea* holobiont metabolism

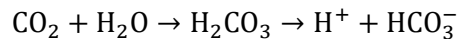
*Cassiopea* is a mixotrophic organism meaning that they can acquire nutrients via autotrophy through its photosynthesizing symbionts, and via heterotrophy through host predation (Stoecker et al. 2017, Flynn et al. 2019, Djeghri et al. 2019). Inorganic carbon and nitrogen assimilated by the photosymbionts are efficiently translocated to the surrounding host tissue (mainly  $\text{NO}_3^- + \text{NO}_2^-$ ;  $\text{NO}_x$ : Yellowlees et al. 2008, Pitt et al. 2009), and this transfer is thought to be facilitated by motile host amoebocytes (Colley & Trench 1985, Lyndby et al. 2020b). Conversely, the host is responsible for acquisition of organic molecules not sufficiently supplied through inorganic assimilation, e.g., through ingestion of zooplankton and particulate matter. However, the relative contribution of these trophic strategies is still debated (Djeghri et al. 2019).

### Photosynthesis and carbon assimilation

Similar to reef-building corals, *Cassiopea* can receive the majority of their organic carbon from endosymbionts via photosynthesis (Trench 1971, Roth 2014). Glucose and glycerol are among the major photosynthates delivered to the host. Hofmann and Kremer (1981) estimated that 5-10 % of net algal photosynthates are released to the host and suggested that this might not be enough to cover the host's daily carbon requirements. However, in a series of subsequent studies, translocation by algal symbionts

was estimated to fulfil the majority of the daily carbon demands of *Cassiopea*, or even exceeding its daily carbon requirements altogether (McCloskey et al. 1994, Verde & McCloskey 1998), independent of medusa size and season (Verde & McCloskey 1998).

While *Cassiopea* potentially receive much more organic carbon than their daily metabolic requirements, it is assumed that most of this is lost again through host-mediated processes; i.e., lost as mucus for predation and/or protection. It is also debated how the algal symbionts within *Cassiopea* are capable of maintaining high photosynthetic rates in a situation in which CO<sub>2</sub> demand for photosynthesis seems to outpace CO<sub>2</sub> produced by holobiont respiration and/or acquired from the environment. For example, it has been argued that the concentration of CO<sub>2</sub> in seawater at normal pH is low (relative to HCO<sub>3</sub><sup>-</sup>) and carbon fixation rates during photosynthesis far exceed that of holobiont respiration (Kremer et al. 1990, Verde & McCloskey 1998, Pitt et al. 2009). The majority of carbon acquired thus has to be taken up from the surrounding water, and <sup>14</sup>C-bicarbonate labelling studies have shown that *Cassiopea* actively assimilate bicarbonate (Hofmann & Kremer 1981), using carbonic anhydrase (CA; Weis et al. 1989, Al-Moghrabi et al. 1996). CA is a family of enzymes involved in the process of catalyzing the conversion of CO<sub>2</sub> to HCO<sub>3</sub><sup>-</sup> with the following reaction:



CA is also capable of the reverse reaction, i.e., converting HCO<sub>3</sub><sup>-</sup> into CO<sub>2</sub> (Keilin & Mann 1939). Estes et al. (2003) showed that CA levels corresponded with high densities of symbionts in *Cassiopea* throughout the oral arms and subumbrella bell tissue, and that bleaching resulting in lower symbiont densities also reduced CA activity. While CA activity appears to be a major factor in host-mediated CO<sub>2</sub> supply for photosynthesis, host metabolism has also been shown to increase photosynthesis. Rädcker et al. (2017) found that photosynthetic activity was increased for *Cassiopea* incubated in seawater enriched with glucose, and attributed the observed enhancement to an increase in respiration from *Cassiopea* and seawater planktonic communities in the chambers. As such, heterotrophic feeding indirectly benefits photosynthesis by increasing respiration, thereby attenuating any CO<sub>2</sub> limitations experienced by the symbionts.

### Nitrogen and phosphorus assimilation

In addition to carbon, *Cassiopea* sequester inorganic nitrogen (NH<sub>4</sub><sup>+</sup>, NO<sub>2</sub><sup>-</sup>, NO<sub>3</sub><sup>-</sup>) and phosphorus (mainly as PO<sub>4</sub><sup>3-</sup>) from the environment (Todd et al. 2006, Yellowlees et al. 2008, Pitt et al. 2009). NO<sub>3</sub><sup>-</sup> can be assimilated by the algal symbionts, and dinoflagellates have been shown to harbor the enzymes,

nitrate- and nitrite reductase, required to reduce  $\text{NO}_3^-$  into  $\text{NO}_2^-$ , and  $\text{NO}_2^-$  further into  $\text{NH}_4^+$  (Leggat et al. 2007, Yellowlees et al. 2008). While only the algal symbionts are capable of assimilating  $\text{NO}_x$  ( $\text{NO}_2^- + \text{NO}_3^-$ ), both host and symbionts are capable of assimilating  $\text{NH}_4^+$  (Miller & Yellowlees 1989, Wilkerson & Kremer 1992, Lyndby et al. 2020b), and rhizostome jellyfish, including *Cassiopea*, have been shown to preferentially take up  $\text{NH}_4^+$  over  $\text{NO}_x$  (Pitt et al. 2009, Welsh et al. 2009, Lyndby et al. 2020b). Grover et al. (2003) showed that a reef-building coral, *Stylophora pistillata*, downregulated  $\text{NO}_3^-$  assimilation pathways when  $\text{NH}_4^+$  concentrations were increased *in hospite*, and a similar inhibitory response had been proposed for *Cassiopea* (Yellowlees et al. 2008, Lyndby et al. 2020b). Furthermore, while symbionts are believed to be the main sink for  $\text{NO}_x$  assimilation in light (e.g. Welsh et al. 2009, Röthig et al. 2021), it has also been suggested, as a result of  $^{15}\text{N}$  assimilation studies, that *Cassiopea* also live in symbiosis with non-photosynthetic microbes that support  $\text{NO}_3^-$  uptake during dark periods (Welsh et al. 2009, Jantzen et al. 2010, Freeman et al. 2016).

Finally, uptake of inorganic phosphorus has been examined in symbiotic scyphozoans (Wilkerson & Kremer 1992, Pitt et al. 2005, Todd et al. 2006). Both *Cassiopea* and *Linuche unguiculata* have been found to take up phosphate from their environment (Wilkerson & Kremer 1992, Todd et al. 2006), while *Phyllorhiza punctata* did not (Pitt et al. 2005). However, inorganic acquisition of phosphorus might reflect that of nitrogen, in the sense that medusae living in oligotrophic environments have limited access and therefore actively assimilate dissolved phosphorus (Todd et al. 2006, Pitt et al. 2009). *Cassiopea* might thus be able to regulate the intake of inorganic phosphorus depending on the nutritional state of their environment.

### *Cassiopea* heterotrophy

While *Cassiopea* rely primarily on algal symbionts for the assimilation of inorganic carbon, the medusae are also known to be gluttonous eaters that rely on heterotrophy for their organic nitrogen requirements (Welsh et al. 2009). Unlike other scyphozoans, rhizostome medusae primarily feed through their secondary mouths. *Cassiopea* medusae seem to feed in two ways: 1) by exuding a mucus web full of cassinosomes (i.e., stinging cells) into the water column, immobilizing and killing prey (Ames et al. 2020), and 2) through bell pulsation, driving zooplankton up across their branched arms where appendages with cnidocytes immobilize and kill prey before consumption. The subumbrella epidermis is lined with bands of epitheliomuscular cells responsible for the contraction of the bell (Blanquet & Riordan 1981), causing jets of water to flow vertically up from the medusa (Bigelow 1900, Jantzen et al. 2010). This activity is known to enhance mass exchange across the bell surface and oral arms, and enhances predation by

actively moving zooplankton across the oral arms (Hamlet et al. 2011, Santhanakrishnan et al. 2012). Bell pulsation also moves nutrient-rich water from the sediment below the medusa, potentially providing the holobiont with an additional source of nutrients (Pitt et al. 2009, Jantzen et al. 2010). Such bioturbation might not just be beneficial to *Cassiopea*, but to their immediate environment in general (e.g. phytoplankton and other autotrophic organisms) by enhancing nutrient fluxes between the sediment and water column (Zarnoch et al. 2020). The mixotrophic lifestyle seems imperative for the *Cassiopea* holobiont to function. In fact, studies on *Cassiopea* growth and nutritional state where animals are either heterotrophically or autotrophically starved have resulted in growth stagnation or shrinkage of medusa bell size (McGill & Pomory 2008, Röthig et al. 2021, Muffett et al. 2022).

### *Cassiopea* as a model system for symbiosis

In recent years, *Cassiopea* have received increasing attention as a model system for the study of host-microbe interactions (Lampert 2016, Ohdera et al. 2018, Medina et al. 2021). *Cassiopea* are an attractive cnidarian-algal symbiosis model because they are closely related to corals (belonging to the same phylum), exhibit similar anatomical traits and tissue organization, and harbor the same genera of Symbiodiniaceae. But, unlike reef-building corals that require highly controlled aquarium conditions and specially trained personnel for completing lifecycles, *Cassiopea* are easy to work within a laboratory setting. Settled polyps rapidly reproduce asexually through budding, and motile planuloids quickly form in thoroughly fed polyps, as early as 24 hours after the parent polyp is fully developed, making upscaling of cultures fast (Van Lieshout & Martin 1992). The short time frame of the closed lifecycle of these cultures further makes *Cassiopea* an ideal candidate for transgenic studies and several gene editing workflows are currently being developed. Additionally, *Cassiopea* polyps readily take up the majority of Symbiodiniaceae strains available. Taken together, these unique characteristics make the emerging *Cassiopea*-Symbiodiniaceae model system a powerful tool to study host-microbe interactions under controlled conditions (e.g. Thornhill et al. 2006, Lampert 2016).



## Thesis objectives and knowledge gaps

The main objective of this thesis is to advance our knowledge on the metabolic interactions between the *Cassiopea* host and its endosymbiotic dinoflagellates in the context of *Cassiopea* photobiology. Previous work has focused on the bulk uptake of carbon and nitrogen species in the holobiont system, but the spatial distribution of resources at the (sub-)cellular level is missing. In this work, I aim to visualize the assimilation and exchange of inorganic nutrients between host and symbiont cells with subcellular resolution using Nanoscale Secondary Ion Mass spectrometry to provide further knowledge on the metabolic interplay in the *Cassiopea*-holobiont system. Furthermore, optical properties and the physico-chemical- and light-microenvironments are major factors in a photosymbiotic system. While such investigations have been conducted on corals over the last decades using various microsensor- and imaging techniques, surprisingly little research has been done on *Cassiopea*. Therefore, the second aim of this thesis work is to investigate the *Cassiopea*-holobiont modulation of their physico-chemical- and light-microenvironments. This is achieved through a combination of electrochemical microsensors for microscale-point measurements of the O<sub>2</sub> and pH dynamics of *Cassiopea*, and fiber-optic sensors for investigation of the light field driving these dynamics *in hospite*.

The outline of the thesis is as follows:

Chapter 1 covers the basic metabolic interactions between *Cassiopea* and its algal symbionts through a combination of stable isotope labeling experiments and NanoSIMS imaging, with a special focus on carbon assimilation and exchange facilitated by amoebocytes. This is combined with the investigation of assimilation of different sources of nitrogen (such as NH<sub>4</sub><sup>+</sup> and NO<sub>3</sub><sup>-</sup>) to identify potential preference by the holobiont.

Chapter 2 uses optical and electro-chemical microsensors to characterize the light-microenvironment of *Cassiopea* and the holobiont-modulated light field that symbionts experience. Further, O<sub>2</sub> and pH dynamics are studied in detail for the bell system of *Cassiopea*.

Chapter 3 builds on knowledge from chapter 1 and 2 by using non-invasive optical coherence tomography to explore the micromorphology of the *Cassiopea* medusa, extract optical parameters for light scattering structures (i.e., white granules), and investigates the effect of the white granules on symbionts carbon assimilation.

Chapter 4 expands on the photosynthesis and O<sub>2</sub> dynamics across the bell of *Cassiopea*, using O<sub>2</sub> sensitive planar optodes to get a complete picture of the O<sub>2</sub> dynamics as a function of symbiont densities estimated through spectral signatures of chlorophyll *a* content and absorption.

## General theory on major techniques used

This work constitutes a broad selection of techniques used to investigate the photobiology and metabolic interactions of the *Cassiopea*-holobiont system. While methods are described in each chapter, the nature of each chapter being presented as a final journal paper means method reporting focusses on reproducibility rather than underlying theory. As such, the concepts and theories underlying the major methods used in this thesis are introduced in the following.

### Establishing and maintaining *Cassiopea* in culture

Establishing a culture of *Cassiopea* in Switzerland was integral to this thesis work. 45 medusae of 5-12 cm were acquired through DeJong Marinelife in Netherlands, and kept in a 200 L tank at an aquarium facility at the University of Lausanne (Prof. Allison Daley, Animal Origins and Morphology Lab). Original animals were supposedly acquired from around Cuba and therefore assumed to be either *C. xamachana* or *C. frondosa*. However, molecular analyses have since revealed the animals to be the species *C. andromeda* (see chapter 4). While *C. andromeda* is originally from the Red Sea, individuals have reportedly been found in the Gulf of Mexico (Morandini et al. 2017).

The culture set up has undergone many iterations since the original group of animals were acquired ~3 years ago. At present, the system is running with ~180 L of artificial sea water (ASW) kept at 35 ppt, 26 °C, and a pH of 8.0-8.2. All filtration happens inside the main tank, and water is being filtrated by a protein skimmer, a UV filter, and via a filtration sock (200 µm). Additionally, biological filtration consists of a nylon bag full of corrugated, black plastic tubes for bacterial growth, and a mangrove shoot in a container with sand. The tank has 20-40 L of water replaced twice a month, and an automated top-up system supplying de-ionized water to keep water level and salinity near constant. Light is provided on a 12H-12H schedule via three 40W LED spots (cool white light) providing ~150 µmol photons m<sup>-2</sup> s<sup>-1</sup> at the water surface. Animals are kept in white, perforated plastic containers on an elevated platform to keep them separated from pumps and other equipment. To ensure water flow in the containers a small water pump with a silicon hose pumps water into each of the containers. Animals are fed *ad libitum* two times per week with freshly-hatched *Artemia* nauplii.

Adults are continuously spawning, and polyps are found settled inside corrugated black plastic tubes. Tubes with polyps were originally maintained in a separate 20 L brooding-tank with ~50 µmol photons m<sup>-2</sup> s<sup>-1</sup> on a 12H-12H schedule, with 50-100 % water being exchanged with the main holding tank weekly. Polyps were fed 4-5 times per week with *Artemia* nauplii, which ensured constant strobilation

and release of ephyra. Ephyra were maintained in the brooding-tank until reaching 1-2 cm in diameter, at which point they were moved to the main tank. This process allowed producing hundreds of individuals for the culture, and the brooding-tank has since been replaced with a brooding container directly connected to the main holding tank. The smaller brooding container ensures continuous production of ephyra, albeit at a lower rate, with reduced maintenance requirements.

## Nanoscale Secondary Ion Mass Spectrometry (NanoSIMS)

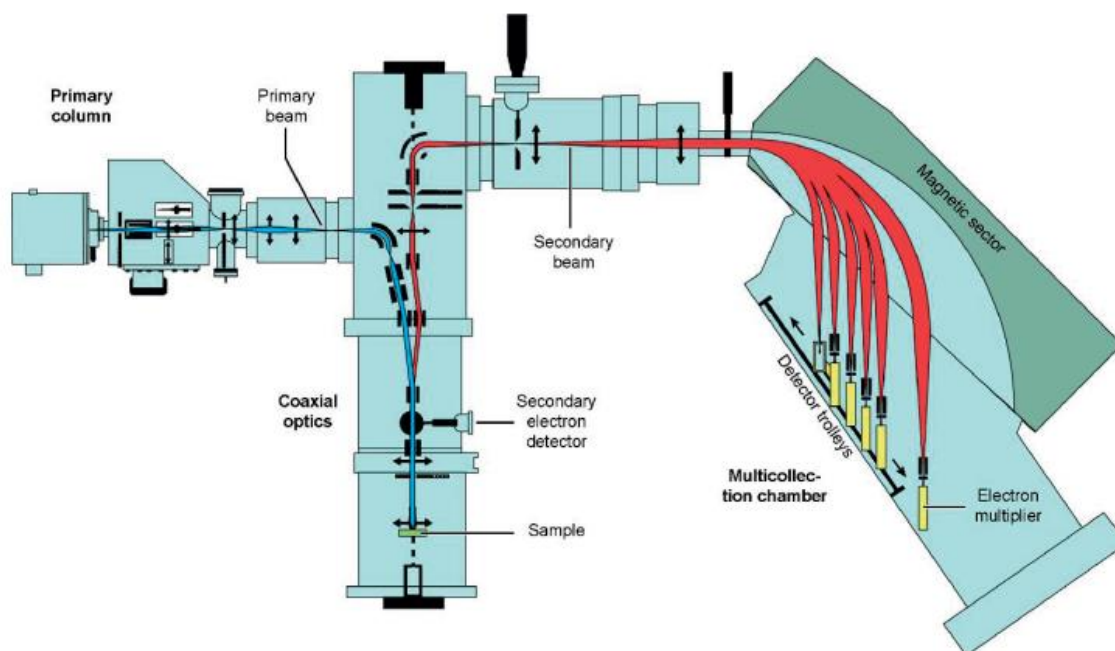


Figure 7: Schematic overview of the NanoSIMS instrument (adapted from Boxer et al. 2009). A primary ion beam ( $\text{Cs}^+$  or  $\text{O}^-$ ) accelerated (16 KeV) along the primary column and onto the sample, sputters secondary ions from the sample. Secondary ions, charged oppositely to the primary beam, are then accelerated into the mass spectrometer, where a magnet separates them according to their mass-to-charge ratio.

One of the primary tools used in this work is the Cameca NanoSIMS 50L ion microprobe mass spectrometer (simply referred to as “NanoSIMS”), which permits elemental distributions and isotopic composition of a biological sample to be imaged with subcellular lateral resolution (Hoppe et al. 2013).

NanoSIMS has been used for a broad range of studies in material science (e.g. Valle et al. 2011), cosmochemistry (e.g. Floss et al. 2006, Hoppe 2006), geochemistry (e.g. Stern et al. 2005, Wacey et al. 2011), and biology (e.g. Pernice et al. 2012, Kopp et al. 2015). In the last decade especially, NanoSIMS

have been utilized for analyses of marine biological samples, investigating incorporation of  $^{13}\text{C}$  and  $^{15}\text{N}$  into a range of aquatic organisms like cyanobacteria (Popa et al. 2007, Thompson et al. 2012), foraminifera (Nomaki et al. 2016, Lekieffre et al. 2020), marine sponges (Hudspith et al. 2021), squids (Zumholz et al. 2007, Cohen et al. 2020), sea slugs (Passarelli et al. 2013, Cruz et al. 2020), corals (Pernice et al. 2012, Kopp et al. 2015, Wangpraseurt et al. 2016), and symbiotic jellyfish (Lyndby et al. 2020b c). Of special interest here is the NanoSIMS applied to the cnidarian-dinoflagellate symbiosis (i.e., corals, sea anemones, and jellyfish), which are receiving increasing attention due to anthropogenic climate change (Hughes et al. 2003, van der Zande et al. 2020).

### Basic principles of NanoSIMS

NanoSIMS ion microprobe combines high isotopic image resolution and high mass resolution to produce quantified (with a proper standard) elemental and isotopic maps of a solid, flat sample surface. Extremely low concentrations (down to ppm) can be detected for elements that are easily ionized, and NanoSIMS is in principle capable of analyzing all elements from the periodic table that efficiently ionize from a given sample. NanoSIMS analysis involves bombarding the sample with a primary ion beam focused to a specific spot size, sputtering off atoms from the sample surface (0-10 nm), and counting secondary isotopes originating from the sample after complete separation from ions with similar masses in the mass spectrum. Strictly speaking, the NanoSIMS is therefore a destructive method although the actual damage done to a sample can in most cases be considered negligible.

In a little more detail, a focused primary ion beam of either  $\text{Cs}^+$  (ca. 100 nm spot size) or  $\text{O}^-$  (ca. 300 nm spot size) is directed at a solid sample. The impact from the primary ion beam creates a collision cascade and the displacement of near surface particles from the sample, some of which are ejected. Depending on the element and the sample matrix, a fraction (usually small) of the ejected particles are ionized. These secondary ions are accelerated through a magnetic sector mass spectrometer, which separates ions by their relative mass-to-charge ratio. The separated ions are subsequently detected individually by electron multipliers. The NanoSIMS 50L ion microprobe used in this work has 7 electron detectors, allowing for the simultaneous counting of 7 different isotopes from a given area on the sample surface. As the primary ion beam is rastered across the sample pixel by pixel, count rate maps are produced of each of these 7 isotopes. By ratioing drift-corrected count-rate images of two isotopes of interest, an isotopic map can be created, e.g., the  $^{13}\text{C}/^{12}\text{C}$  and  $^{15}\text{N}/^{14}\text{N}$  ratios.

## Sample preparations and requirements

The versatility of the NanoSIMS technique comes with some practical limitations that must be taken into consideration when producing isotopic analyses on biological samples. Proper sample preparation is crucial for successful NanoSIMS work. The NanoSIMS operates with the sample in an ultra-high vacuum. Therefore, only solid samples that are dehydrated (e.g. through ethanol dehydration) and do not degas substantially can be analyzed.

Classical preparation for NanoSIMS involves chemical fixation, tissue dehydration, and embedding in resin (see section below for detailed description of the process). Classical preparation offers a relatively easy approach, and the protocol and types of resin used can be adapted depending on the type of sample and the desired analytical outcome.

However, tissue samples undergoing this process are typically prone to alteration in tissue morphology during dehydration steps, as labile molecules are flushed from the system (Grignon et al. 1997, Grovenor et al. 2006, Loussert-Fonta et al. 2020). Furthermore, resin infiltration effectively introduces (or replaces) large amounts of C in the sample, potentially diluting the samples original  $^{13}\text{C}$ -enrichment (Loussert-Fonta et al. 2020). As such, classical preparation for NanoSIMS analyses is only adequate for samples from isotopic labelling experiments during which assimilated  $^{13}\text{C}$  and  $^{15}\text{N}$  is given sufficient time to be anabolically incorporated into tissue and organelles. Tissue organization and density play a role in the degree a sample is affected by dehydration and resin infiltration (Grovenor et al. 2006). For example, the cnidarian mesogleal matrix is largely replaced while dinoflagellate cells appear less altered due their strong cell wall that preserves their initial shape (e.g. Loussert-Fonta et al. 2020).

## Sectioning and coating

NanoSIMS isotopic analyses can only be conducted on very flat surfaces; i.e., with micrometer scale topography, or better. A common method for biological samples is to cut histological sections with precision diamond knives on a microtome in order to get a perfectly flat sample.

Samples are typically cut in ultrathin (70 nm) to semithin (200-300 nm) histological sections, and placed on glass slips, silicon wafers, or TEM-grids before metal-coating and subsequent EM and NanoSIMS imaging (see below). EM images can be correlated with NanoSIMS isotopic images to allow precise determination of isotopic compositions in individual subcellular compartments and constituents (e.g. Kopp et al. 2016, Lyndby et al. 2020b, Cruz et al. 2020).

## General protocol for NanoSIMS preparations used in this thesis

With these general considerations for SEM and NanoSIMS sample preparation, the protocol for preparation and analysis was kept as close to constant as possible throughout this thesis work.

### Chemical fixation

Samples were fixed in a solution containing 4 % Paraformaldehyde, 0.5-2.5 % Glutaraldehyde, 9 % sucrose, and mixed in 0.1M Sørensen buffer (7.8-8.1 pH).

Post isotopic labelling with stable isotopes, samples were left in chemical fixative at room temperature for up to 2 hours, and subsequently moved to cold storage at 4 °C until further processing. Samples were usually kept less than 1 week in cold storage before processing to minimize loss of labile compounds and tissue damage.

### Pre-processing staining

Samples were rinsed extensively in Sørensen buffer, 2-3 times, to remove fixative, and then micro dissected to pieces typically no larger than 2 mm<sup>2</sup>.

Samples were then treated with Osmium at 1 % for 1 hour under constant rotation and darkness. Osmium treatment is a post-fixation step necessary for the lipid preservation in the biological sample. After Osmium staining, samples were rinsed 2-3 times (15 min per rinse) in Milli-Q water.

### Sample dehydration and resin embedding

Samples were processed in an automated tissue processor (EM TP, Leica) by first dehydration and subsequent Spurr's resin infiltration as follow:

1. 5 min in Milli-Q
1. 45 min in 30 % ethanol – 70 % Milli-Q
2. 45 min in 70% ethanol – 30% Milli-Q
3. 2h 100% ethanol
4. 2h 100% ethanol
5. 2h 30% resin – 70% ethanol
6. 2h 70% resin – 30% ethanol
7. 4h 100% resin
8. 12h 100% resin + polymerizer

Samples were subsequently collected from the processor, transferred to molds with fresh 100 % resin (including polymerizer) and left in an oven at 61 °C for at least 48 hours to cure.

Resin blocks with samples were ready to cut using an ultramicrotome (Reichert Ultracut S Microtome, Leica). Sections were cut from the block by first trimming the sample block with a diamond trimming knife (Trim 45, DiATOME) to achieve a flat surface. Semithin sections of 200 nm were then cut using a diamond sectioning knife (Ultracut 45°, DiATOME).

## Sections for direct NanoSIMS analysis

Samples not intended for prior EM imaging were picked up and placed on glow discharged glass slips. Glass slips were prepared using a glow discharger (ACE600, Leica), discharging the glass slips for 10 seconds. Discharging the glass slips results in a hydrophile surface, allowing the sample-sections to be placed perfectly flat on the glass slips with no folds or wrinkles forming during subsequent air drying.

Samples for direct analyses with NanoSIMS had an additional section cut and placed on a microscope slide. Here, the section was stained with Toluidine blue and imaged with a light microscope (Axio Imager.M2m equipped with an AxioCam 506 color camera, Zeiss) for navigation of samples during NanoSIMS analyses. Samples stained with Toluidine blue were not included in NanoSIMS analyses due to the potential contamination of boron, which can be present in the Toluidine blue solution and create a mass-interference of  $^{11}\text{B}^{16}\text{O}^-$  on the  $^{12}\text{C}^{15}\text{N}^-$  ion that cannot be resolved.

## Sections for correlative EM imaging

For correlative imaging of EM and NanoSIMS, cut sections were placed on glow discharged silicon wafers. EM samples were then stained with uranyl acetate (2 %) for 10 minutes, cleaned with Milli-Q, and then stained with Reynolds lead citrate for 10 min. After staining, samples are rinsed 2-3 times (15 min per rinse) in Milli-Q water. Applying these stains improve the contrast of the sample with the EM imaging.

Samples on glass slips and silicon wafers were then gold coated with a 12.5 nm layer of gold under high vacuum (EM SCD050, Leica), and then mounted in the NanoSIMS for analyses.

### NanoSIMS analytical parameters

NanoSIMS isotopic analyses were always configured the same way:  $\text{Cs}^+$  ions were accelerated to 16 KeV and forming a beam of 2-3 pA focused to a spot-size of 100 nm on the sample surface. Image acquisition was typically done of  $40 \times 40 \mu\text{m}^2$  areas of the sample surface, with  $256 \times 256$  pixels, a dwell time of  $5000 \mu\text{s pixel}^{-1}$ , and 5 acquisition layers in total, to achieve high-quality images with sufficient counts of minor isotopes. Secondary ions,  $^{12}\text{C}_2^-$ ,  $^{13}\text{C}^{12}\text{C}^-$ ,  $^{12}\text{C}^{14}\text{N}^-$ , and  $^{12}\text{C}^{15}\text{N}^-$  were counted in parallel (multi-collection) in electron multiplier detectors at a mass resolving power ( $M/\Delta M$ ; where M is the nominal



mass and  $\Delta M$  the difference between two species to be separated) of about 9000 or more, sufficient to resolve isobaric interferences around the ions of interest, i.e.,  $^{12}\text{C}^{12}\text{CH}^-$  on  $^{13}\text{C}^{12}\text{C}^-$  and  $^{13}\text{C}^{14}\text{N}^-$  on  $^{12}\text{C}^{15}\text{N}^-$  (Hoppe et al. 2013). To minimize drift error all 5 layers were corrected for machine drift and added together before isotopic ratios were formed using the L'IMAGE software. Drift-corrected maps of  $^{13}\text{C}$  and  $^{15}\text{N}$  enrichment were obtained from the count ratios  $^{13}\text{C}^{12}\text{C}^-/^{12}\text{C}_2^-$  and  $^{12}\text{C}^{15}\text{N}^-/^{12}\text{C}^{14}\text{N}^-$ , respectively. The enrichments were expressed with the delta notations (in permille):

$$\delta^{13}\text{C} (\text{‰}) = \left( \frac{R_{\text{sample}}}{R_{\text{standard}}} - 1 \right) \times 1000$$

$$\delta^{15}\text{N} (\text{‰}) = \left( \frac{R_{\text{sample}}}{R_{\text{standard}}} - 1 \right) \times 1000$$

where  $R_{\text{sample}}$  is the ratio of the enriched sample, and  $R_{\text{standard}}$  is the ratio of a control (i.e., unlabeled) sample, prepared and analyzed in an identical manner.

# Chapter 1: Carbon and nitrogen assimilation in *Cassiopea*: A NanoSIMS study

## I. Context

Chapter 1 presents a final manuscript (as presented here) published in Proceedings Royal Society B. Chapter 1 seeks to understand the basics of metabolically exchanged nutrients between the medusa host and its endosymbiotic dinoflagellate algae.

## Authors contribution

NHL, ET, MK, and AM designed the experiment. NanoSIMS data acquisition was carried out by NHL, NR, SE, and AM. SEM imaging was carried out by NHL and LHSJ. Molecular analyses were carried out by SB. Data and statistical analyses were carried out by NHL and NR. All authors contributed to writing and editing the manuscript.

## II. Publication

# Amoebocytes facilitate efficient carbon and nitrogen assimilation in the *Cassiopea*-Symbiodiniaceae symbiosis

Niclas Heidelberg Lyndby<sup>1</sup>, Nils Rådecker<sup>1</sup>, Sandrine Bessette<sup>1</sup>, Louise Helene Søgaaard Jensen<sup>1</sup>, Stéphane Escrig<sup>1</sup>, Erik Trampe<sup>2</sup>, Michael Kühn<sup>2</sup>, Anders Meibom<sup>1,3</sup>

<sup>1</sup>Laboratory for Biological Geochemistry, School of Architecture, Civil and Environmental Engineering, Ecole Polytechnique Fédérale de Lausanne (EPFL), CH-1015 Lausanne, Switzerland.

<sup>2</sup>Marine Biological Section, Department of Biology, University of Copenhagen, DK-3000 Helsingør, Denmark.

<sup>3</sup>Center for Advanced Surface Analysis, Institute of Earth Sciences, University of Lausanne, CH-1015 Lausanne, Switzerland.

## Abstract

The upside-down jellyfish *Cassiopea* engages in symbiosis with photosynthetic microalgae that facilitate uptake and recycling of inorganic nutrients. In contrast to most other symbiotic cnidarians, algal endosymbionts in *Cassiopea* are not restricted to the gastroderm but are found in amoebocyte cells within the mesoglea. While symbiont-bearing amoebocytes are highly abundant, their role in nutrient uptake and cycling in *Cassiopea* remains unknown. By combining isotopic labelling experiments with correlated SEM and NanoSIMS imaging, we quantified the anabolic assimilation of inorganic carbon and nitrogen at the subcellular level in juvenile *Cassiopea* medusae bell tissue. Amoebocytes were clustered near the sub-umbrella epidermis and facilitated efficient assimilation of inorganic nutrients. Photosynthetically-fixed

carbon was efficiently translocated between endosymbionts, amoebocytes and host epidermis at rates similar to or exceeding those observed in corals. The *Cassiopea* holobionts efficiently assimilated ammonium, while no nitrate assimilation was detected, possibly reflecting adaptation to highly dynamic environmental conditions of their natural habitat. The motile amoebocytes allow *Cassiopea* medusae to distribute their endosymbiont population to optimize access to light and nutrients, and transport nutrition between tissue areas. Amoebocytes thus play a vital role for assimilation and translocation of nutrients in *Cassiopea*, providing an interesting new model for studies of metabolic interactions in photosymbiotic marine organisms.

## Keywords

***Cassiopea, photosynthesis, stable isotope labelling, nutrients, electron microscopy, NanoSIMS.***

## Introduction

Animal-microbe symbioses represent a fundamental pillar of life in most habitats (McFall-Ngai et al. 2013). In the marine environment, the symbiotic relationship between cnidaria and endosymbiotic dinoflagellate algae of the family Symbiodiniaceae have been key to the evolutionary success of these animals (Baker 2003, Lampert 2016, Lajeunesse et al. 2018), epitomized by reef building corals. Metabolic interactions between the coral host and endosymbiont dinoflagellate algae, as well as a diverse microbiome (collectively referred to as the coral holobiont, (Rohwer et al. 2002, Rosenberg et al. 2007, Bourne et al. 2009), facilitate efficient assimilation and recycling of organic and inorganic nutrients to support the formation and maintenance of entire coral reef ecosystems (Muscatine et al. 1981, Falkowski et al. 1984, Hatcher 1990, Kopp et al. 2015). The translocation of photosynthetically-fixed carbon from the algae to the coral host provides the major energy source for the metabolism of the host, which in turn supplies inorganic carbon to the algal photosynthesis from its respiration (Falkowski et al. 1984, Kopp et al. 2015, Lyndby et al. 2020a). Besides efficient carbon cycling, the coupling of heterotrophic and phototrophic metabolism also enables coral holobionts to efficiently assimilate and recycle otherwise limiting inorganic nutrients, such as nitrate and ammonium (Grover et al. 2008). At the same time, these tight metabolic interactions also render the corals highly vulnerable to the break-down of the symbiosis (i.e., coral bleaching), which is now reoccurring on a massive scale in many reef localities (Hughes et al. 2003, 2017, Hoegh-Guldberg et al. 2019). Whether driven by global warming of seawater or local

environmental stress, bleached corals no longer receive the same metabolic input from their diminished dinoflagellate symbiont population and can starve to death on a timescale of days and weeks, causing entire reef ecosystems to collapse (Brown 1997, Weis 2008). Because of the fundamental importance of the cnidarian-dinoflagellate symbiosis to marine life – and urged on by the coral reef crisis (Hoegh-Guldberg et al. 2019) – there is a strong effort to identify suitable model organisms that can bring forth novel experimental opportunities and help illuminate the intricate metabolic relationships between cnidarian hosts and their symbiont populations. In contrast with corals, scyphozoans seem to be thriving despite the warming of ocean waters (Purcell et al. 2007). Often referred to as the ‘true jellyfish’, this class of cnidaria also host symbiont dinoflagellate algae and one member of the scyphozoans, the upside-down jelly fish *Cassiopea*, has recently received increasing attention as a good model system for studies of host-algal metabolic interactions (Ohdera et al. 2018).

*Cassiopea* spp. exhibits unique characteristics that set it apart from corals (Ohdera et al. 2018): 1) In contrast to the sessile corals, the life cycle of *Cassiopea* is dominated by a motile medusa stage (i.e., the adult form), which allows the animal to relocate in search for environmentally optimal conditions; 2) In the medusa stage, *Cassiopea* exhibits the distinct morphological characteristics of scyphozoans (Lewis Ames 2018), with epidermis and gastrodermis spatially separated by a (compared to corals) very large mesoglea (Ruppert et al. 2004; 3) The microalgal symbionts in *Cassiopea* are, at least early in the medusa stage, predominantly found inside motile amoebocyte cells located within the mesoglea (Colley & Trench 1985, Estes et al. 2003). In contrast, corals host algal endosymbionts exclusively inside their gastrodermal cells.

Previous studies have demonstrated that active nutrient exchange does take place between *Cassiopea* and its algal endosymbiont population (Welsh et al. 2009, Freeman et al. 2016, Djeghri et al. 2020), but the analytical methods employed did not allow to disentangle – at the tissue and single cell level – the role of algal-containing amoebocytes in nutrient assimilation and the metabolic transfer to adjacent tissue structures. Here, we present a tissue- and (sub)cellular level investigation of autotrophic carbon and nitrogen assimilation and translocation in juvenile *Cassiopea* sp. medusae, in which the endosymbiotic algae are exclusively (i.e., without observed exception) restricted to amoebocytes. By coupling isotopic tracer (i.e.,  $^{13}\text{C}$ -bicarbonate,  $^{15}\text{N}$ -ammonium, and  $^{15}\text{N}$ -nitrate) incubation experiments with correlated ultrastructural imaging and ultra-high resolution stable isotopic mapping (NanoSIMS), we quantified the anabolic turnover in individual tissues and cellular compartments. This allowed us to

disentangle the role of symbiotic amoebocytes for holobiont nutrition and illuminate the ecological advantages of this unique feature of the *Cassiopea*-Symbiodiniaceae symbiosis.

## Materials and Methods

### *Cassiopea* husbandry

Adult specimens of *Cassiopea* sp. medusa originally obtained from DeJong Marinelife (Netherlands) were cultivated at the Marine Biology Section (MBS), University of Copenhagen (Helsingør, Denmark), that provides a steady supply of all life stages of the jellyfish. Juvenile *Cassiopea* sp. medusae with an umbrella diameter of 6-10 mm were reared in a 20 L aquarium. The jellyfish were fed 5 times per week with newly hatched *Artemia* nauplii. Animals used for incubations were heterotrophically starved for 24 hours before experiments started. All animals were kept at 25 °C in artificial seawater (ASW) with a salinity of 35 ppt and a pH of 8.1. Water was recycled inside the tank (20 litres) using a small filter pump. Light was maintained with a programmable LED light source (Triton R2, Pacific Sun), running a 12/12-hour day/night cycle with a downwelling photon irradiance (400-700 nm) of 500  $\mu\text{mol photons m}^{-2} \text{s}^{-1}$ , measured just above the water surface using a calibrated spectroradiometer (MSC-15, GigaHertz-Optik).

### Experimental setup

A water bath with approximately 10 L of deionized water was placed on top of 3 magnet stirrers (RCT basic, IKA GmbH). The bath was fitted with a heater to keep the water at 25 ( $\pm 0.5$ ) °C and a small pump to keep the water well mixed. All incubations were run in triplicates and each *Cassiopea* medusae was incubated in a separate 100 mL beaker filled with 95 mL ASW and positioned in the water bath. Each beaker was fitted with a mesh mounted a few centimetres above the bottom to separate the jellyfish from the magnet bar during incubations. Magnet stirrers were set to spin at 180 RPM to ensure mixing of water during incubations. The incubation chambers were illuminated by three identical tungsten halogen lamps (KL 2500 LCD, Schott AG). Each adjustable light source was equipped with a fibre guide and a collimating lens, and the incident photon irradiance for each chamber was adjusted to 350  $\mu\text{mol photons m}^{-2} \text{s}^{-1}$  (400-700 nm; Supplementary figure 1). This light level was chosen as a photosynthetically optimal irradiance (just below saturation point) based on previous measurements of relative electron transport rates (rETR) versus photon irradiance with a variable chlorophyll fluorescence imaging system (I-PAM, Walz GmbH, Germany) measuring rapid light curves (RLC; Supplementary figure 2; (Ralph & Gademann 2005). Photon irradiance measurements were done with a calibrated spectroradiometer (MSC-15, GigaHertz-Optik).

## Isotopic pulse labelling experiments

### Preparation of isotopically enriched seawater

Artificial sea water (ASW) in the main holding tank at MBS had been monitored for concentrations prior to experiments, and showed a  $\text{NO}_3^-$  level of  $0.01 \text{ mg L}^{-1}$ , suggesting overall low levels of dissolved nitrogen in the system. Approximately 15 L of this water was collected and stored in a cold room ( $4^\circ\text{C}$ ) until use, a few days later. The evening prior to start of the experiment, 1 L of the collected water was filtered (Millipore,  $0.2 \mu\text{m}$ ) and kept overnight at  $4^\circ\text{C}$ . The next morning, the filtered ASW was first stripped for dissolved inorganic carbon (DIC) by reducing the pH to  $< 3$  by the addition of 1 M HCl and subsequent flushing with ambient air for 2 hours. The pH was monitored with a calibrated pH meter (PHM220, MeterLab). Right before start of the experiment, 1 L of  $\text{CO}_2$ -stripped, low pH ASW was isotopically enriched by spiking the water with 255 mg of  $\text{NaH}^{13}\text{CO}_3$  (99 atom%, Sigma Aldrich), and 1 mL of stock solutions with either 3 mM  $\text{K}^{15}\text{NO}_3$  (99 atom%, Sigma Aldrich) or 3 mM  $^{15}\text{NH}_4\text{Cl}$  (99 atom%, Sigma Aldrich) in milli-Q water. The pH was then increased by addition of about 1 mL of 1 M NaOH. The final incubation medium had a pH of 8.0-8.1 and contained 3 mM  $\text{NaH}^{13}\text{CO}_3$  and 3  $\mu\text{M}$  of either  $\text{K}^{15}\text{NO}_3$  or  $^{15}\text{NH}_4\text{Cl}$ , with a salinity of 35 ppt. The spiked ASW solution was then heated to  $25^\circ\text{C}$  in a water bath and used for incubations.

### Pulse-label incubations

*Cassiopea* specimens contained in beakers were submitted to one out of five different pulse-label incubations, with a combination of 3 mM  $\text{NaH}^{13}\text{CO}_3$  and 3  $\mu\text{M}$   $\text{K}^{15}\text{NO}_3$  for (i) 2 hours in light, (ii) 6 hours in light, or (iii) 6 hours darkness, or with 3 mM  $\text{NaH}^{13}\text{CO}_3$  and 3  $\mu\text{M}$   $^{15}\text{NH}_4\text{Cl}$  for (iv) 6 hours in light, or (v) 6 hours in darkness (Figure 1). During the 6 hours incubations the solutions were changed at 2 and 4 hours.

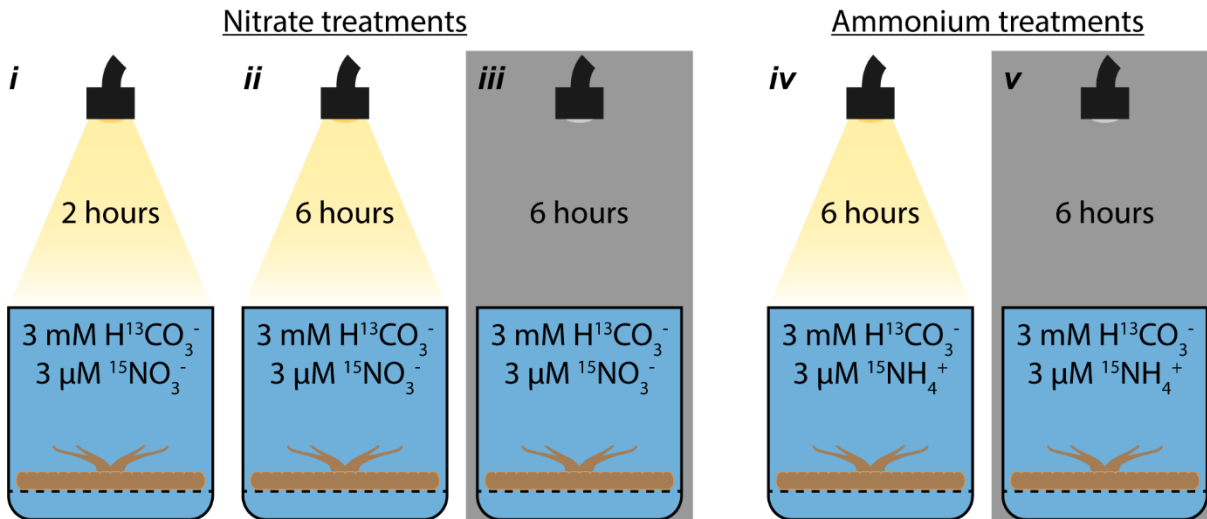


Figure 1 | Schematic overview of the 5 different incubations of *Cassiopea* sp. in stable isotope-spiked artificial seawater (ASW). All incubations were run in triplicates, and each individual jellyfish was incubated in 95 mL filtered ASW containing 3 mM NaH<sup>13</sup>CO<sub>3</sub><sup>-</sup> and either 3 μM K<sup>15</sup>NO<sub>3</sub> (incubations *i*, *ii*, and *iii*) or 3 μM <sup>15</sup>NH<sub>4</sub>Cl (incubations *iv* and *v*).

At the end of incubations, the *Cassiopea* specimens were chemically fixed in cryotubes containing 1.5 mL of 2.5 % [v/v] glutaraldehyde (Electron Microscopy Sciences), 0.5 % [v/v] paraformaldehyde (Electron Microscopy Sciences), and 0.6 M sucrose (Sigma-Aldrich) mixed in 0.1 M Sørensen phosphate buffer. The chemically fixed *Cassiopea* specimens were kept at room temperature for 2 hours and were then stored in a fridge at 4°C until transportation to Lausanne (Switzerland) in fixative for further processing.

#### Histological sectioning for EM imaging and NanoSIMS analyses

Fixed *Cassiopea* specimens were rinsed 3 times in 0.1 M Sørensen buffer with 30 minutes between changes. Samples were subsequently dissected to acquire a radial slice of the umbrella, from the central manubrium to the bell margin, as illustrated in Figure 2a-b. In order to preserve lipids in the tissue, dissected tissue was submerged in OsO<sub>4</sub> solution (2 % in milli-Q water) for 30 minutes under constant slow rotation in darkness. Samples were subsequently rinsed extensively in deionized water (3 changes at 30 to 60 minutes intervals), before further sample preparation.

Dissected tissue samples underwent dehydration via immersion in a milli-Q water/ethanol series (50, 70, 90, and 100 % ethanol), and subsequent resin infiltration with ethanol/Spurr's resin (30, 50, 75, and 100 % resin). Resin-infiltrated samples were oriented and placed in moulds filled with 100 % Spurr's resin and cured for 72 hours in an oven at 60°C. Semi-thin histological sections (500 nm) were cut from the resin blocks using an Ultracut S microtome (Leica Microsystems), equipped with a 45° histo-diamond

knife (DiATOME). 1-2 sections were placed on 10 mm round glass cover slips, coated with a ca. 12 nm layer of gold using a Leica EM SCD050 gold coater (Leica Camera AG) and mounted in a sample holder for NanoSIMS isotopic imaging. Additionally, selected thin-sections were placed on a microscope slide and stained with Epoxy Tissue Stain (Electron Microscopy Sciences) for 30 to 60 seconds on a heating plate; excessive stain was subsequently removed with deionized water, followed by heat-drying. The stained sections were imaged on an optical microscope (Axio Imager.M2m, ZEISS) to guide NanoSIMS analyses.

### SEM imaging

Semi-thin sections (500 nm) were cut as described above, and placed on silicon wafers before being stained with 4% uranyl acetate and Reynolds lead citrate solution (Electron Microscopy Sciences). Images were taken on a GeminiSEM 500 field emission scanning electron microscope (ZEISS), at 3 kV, an aperture size of 20  $\mu\text{m}$ , and a working distance of 2.5-2.7 mm, using the energy selective backscatter detector (EsB, ZEISS) with the grid set at 382-500 V. Images were acquired directly from the GeminiSEM 500 in TIFF format without further processing.

### NanoSIMS image acquisition

Isotopic imaging of semi-thin histological sections was done with a NanoSIMS 50L instrument. Images (40 $\times$ 40 or 45 $\times$ 45 $\mu\text{m}$ , 256 $\times$ 256 pixel, 5000  $\mu\text{s}$ /pixel, 5 layers) were obtained with a 16 KeV  $\text{Cs}^+$  primary ion source focused to a spot-size of about 120 nm (2 pA). Secondary ions ( $^{12}\text{C}_2^-$ ,  $^{13}\text{C}^{12}\text{C}^-$ ,  $^{12}\text{C}^{14}\text{N}^-$ , and  $^{12}\text{C}^{15}\text{N}^-$ ) were counted in individual electron-multiplier detectors at a mass resolution power of about 9000 (Cameca definition), sufficient to resolve all potential interferences in the mass spectrum.

Isotopic images were analysed using the NanoSIMS software L'Image (version 12-21-2017; developed by Dr. Larry Nittler, Carnegie Institution of Washington), and contours were carefully drawn in each image around the epidermis as well as individual amoebocytes and dinoflagellate cells. Epidermis were counted as one region of interest (ROI;  $n = 1$ ) for each image. Similarly, amoebocytes (clustered with dinoflagellates) were usually treated as one ROI per image unless cell clusters were clearly separated. Drift-corrected maps of  $^{13}\text{C}$ - and  $^{15}\text{N}$ -enrichment were obtained from the count ratios  $^{13}\text{C}^{12}\text{C}^- / ^{12}\text{C}_2^-$  and  $^{15}\text{N}^{12}\text{C}^- / ^{14}\text{N}^{12}\text{C}^-$ , respectively. Measured enrichments were expressed in the delta notation:

$$\text{Eq. 1:} \quad \delta^{13}\text{C} (\text{‰}) = \frac{r_{eC} - r_{cC}}{r_{cC}} \times 1000$$

$$\text{Eq. 2:} \quad \delta^{15}\text{N} (\text{‰}) = \frac{r_{eN} - r_{cN}}{r_{cN}} \times 1000$$



where  $r_{eC}$  and  $r_{cC}$  are the count ratios of  $^{13}\text{C}^{12}\text{C}/^{12}\text{C}_2$  in an enriched sample and a control (i.e. unlabelled) sample, respectively.  $r_{eN}$  and  $r_{cN}$  are the count ratios of  $^{15}\text{N}^{12}\text{C}/^{14}\text{N}^{12}\text{C}$  in an enriched sample and a control sample, respectively. Total numbers of technical replicates (ROIs) is provided in Supplementary table 1.

### Dinoflagellate identification

All animals used in this study contained dinoflagellate symbionts of the genus *Symbiodinium* (previously clade A; LaJeunesse et al. 2018). Algal symbionts were identified by DNA extraction, PCR amplification with genus/clade specific primers (adapted after Yamashita et al. 2011) and visualization of amplification using gel electrophoresis (see supplementary material).

### Statistical analyses

We used R (version 4.0.2) with the packages *nlme* (version 3.1-148) and *lsmeans* (version 2.30-0) to perform statistical analyses. Linear mixed model (LMM) analyses were used to test the relationship between isotopic enrichment in *Cassiopea* sp. holobiont compartments and the conditions of time, light availability, and nitrogen source taking into account the biological replicate as a random factor.  $^{13}\text{C}$  enrichment data were square root transformed to achieve normality. Tukey post hoc analyses were used for tests with more than 2 groups involved.

## Results

### Cassiopea histology

The juvenile specimens of *Cassiopea* sp. used in this study showed a high density of dinoflagellate symbionts in the sub-umbrella. All dinoflagellates were found inside amoebocytes clustered in the mesoglea, the vast majority of which were in close proximity to the (sub-umbrella) epidermal tissue layer (Figure 2b), as previously described (Colley & Trench 1985, Estes et al. 2003). Dinoflagellates were never observed outside amoebocytes or in other types of host cells or tissue layers in our juvenile specimens. Cross-sections of amoebocytes showed that dinoflagellate cells were contained in a symbiosome-like structure (orange triangles in Figure 2d-e; cf. (Colley & Trench 1983)). Furthermore, high magnification electron microscopy images of amoebocytes/symbionts showed the presence of lipid droplets inside both symbiont and amoebocyte cells (black triangles in Figure 2d-e).

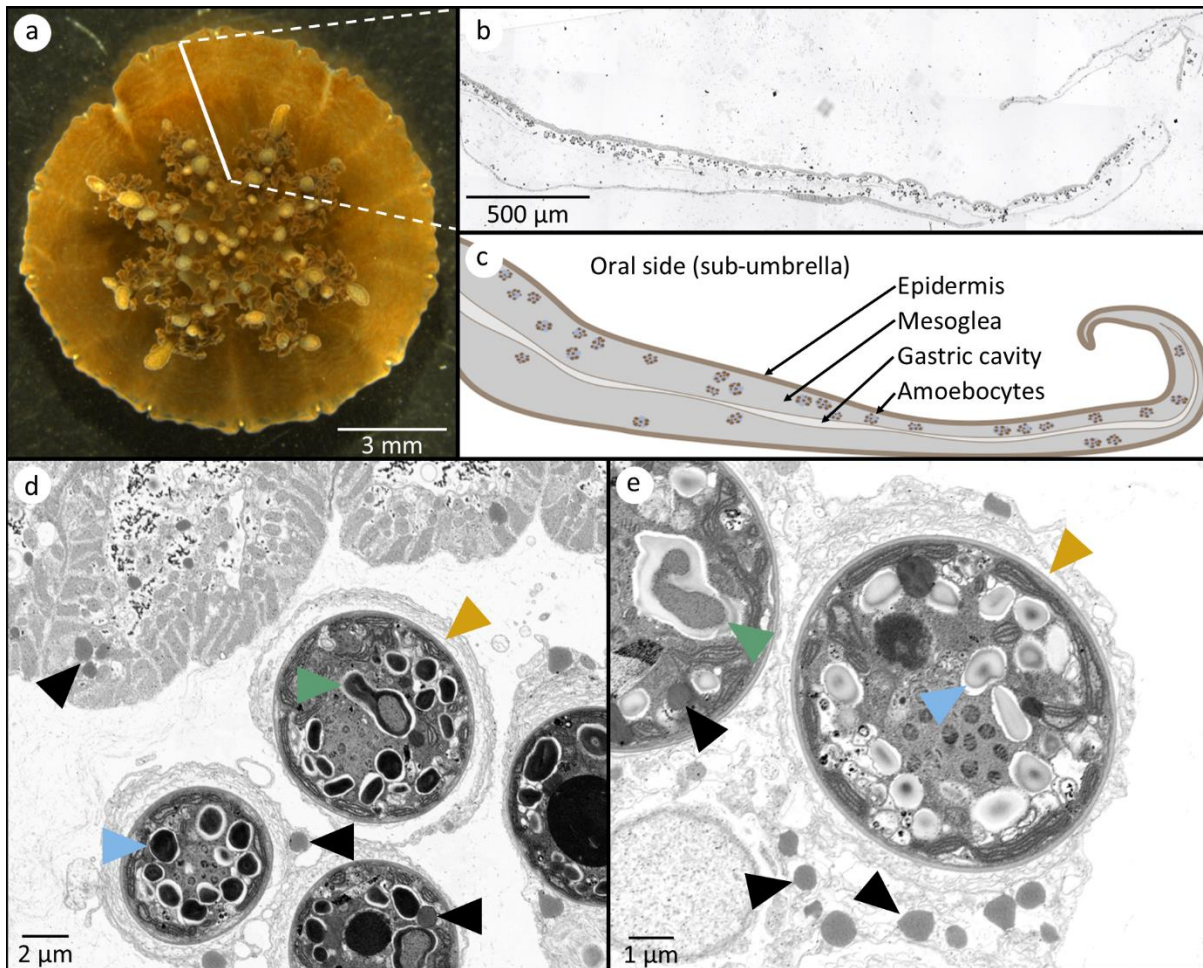


Figure 2 | Histological and electron microscopy images of *Cassiopea* tissue architecture. (a) Photograph of a juvenile *Cassiopea*. The solid white line indicates the orientation of histological sections cut for this study; i.e., cutting radially from the central manubrium region to the edge of bell. (b) Optical microscopy image of a histological section as indicated in (a). (c) Sketch of histological section illustrating key tissue structures. (d and e) Scanning electron microscopy showing the micro-architecture of host amoebocytes densely populated with symbionts next to the host epidermal tissue. Note that the grey-scale of panel (e) is inverted relative to panel (d) for increased clarity of subcellular components. Subcellular components are indicated: lipid bodies in symbionts (black triangles), pyrenoids (green triangles), and starch granules (blue triangles). Orange triangles indicate symbiosomes (i.e., host vacuolar space surrounded by a membrane similar to what is known from other symbiotic cnidarians hosting dinoflagellates) in amoebocytes.

#### Stable isotope enrichment in *Cassiopea* sp.

NanoSIMS images were acquired of compact clusters of dinoflagellate symbionts inside amoebocyte cells residing in the mesoglea, particularly in the sub-umbrella tissue area (Figure 2; a minimum of 25 dinoflagellate cells were imaged per biological sample, N = 3), including representative regions of the (sub-umbrella) epidermal tissue (Figure 3). Note that, because of the classical sample preparation methods employed here, which involves ethanol dehydration and resin embedding, most soluble compounds are lost from the tissue and only structural components, i.e., proteins, fatty acids,

RNA, DNA, etc., representing the products of anabolic metabolism, remain (Loussert-Fonta et al. 2020, Gibbin et al. 2020). Isotopic enrichments shown in the following thus represent the relative anabolic turnover of the tissue during the incubation experiments.

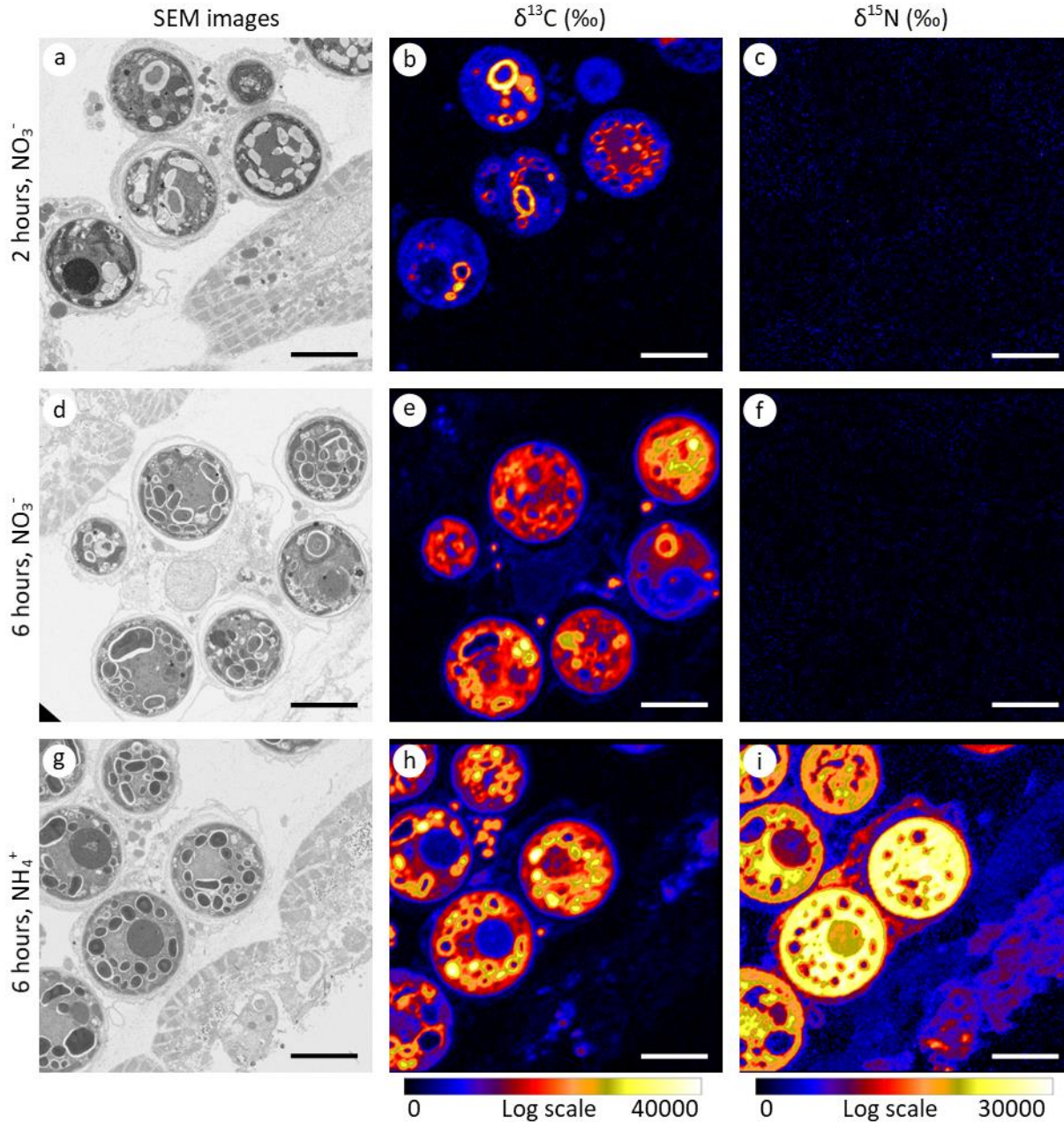


Figure 3 | Correlated SEM and NanoSIMS images for light incubations of representative tissue areas of *Cassiopea* sp. incubated with  $\text{H}^{13}\text{CO}_3^-$  and  $^{15}\text{NO}_3^-$  for 2 hours (a-c) and 6 hours (d-f), respectively, and with  $\text{H}^{13}\text{CO}_3^-$  and  $^{15}\text{NH}_4^+$  for 6 hours (g-i). Scale bars = 8  $\mu\text{m}$ .

### <sup>13</sup>C-assimilation in the holobiont

The incubation experiments described above resulted in clear <sup>13</sup>C enrichment differences between holobiont compartment, incubation time and light availability (Supplementary table 1). As expected, *Cassiopea* sp. incubated with H<sup>13</sup>CO<sub>3</sub><sup>-</sup> in darkness did not show detectable levels of <sup>13</sup>C enrichment (Supplementary table 1).

In contrast, after 2- and 6-hour light incubations, the tissue/cell types (*Symbiodinium* vs. amoebocytes vs. epidermis) showed characteristic differences in <sup>13</sup>C enrichment with the dinoflagellates showing the highest and the epidermis the lowest levels of enrichment (LMM, F(1, 219) = 280.7, p < 0.001; Figure 4a). The <sup>13</sup>C enrichment increased in all three tissue/cell types in the 6-hour compared to the 2-hour light incubation, but the relative increase was different for each compartment (LMM, F(2, 219) = 3.9, p = 0.021; Figure 4b). Specifically, *Symbiodinium* <sup>13</sup>C enrichment increased 2-fold (LMM, F(1, 4) = 3.70, p = 0.127), amoebocyte <sup>13</sup>C enrichment increased 3.6-fold (LMM, F(1, 4) = 12.9, p = 0.023), and epidermis <sup>13</sup>C enrichment increased 6.5-fold (LMM, F(1, 4) = 18.0, p = 0.013) between 2 and 6 hours, respectively (Figure 4b).

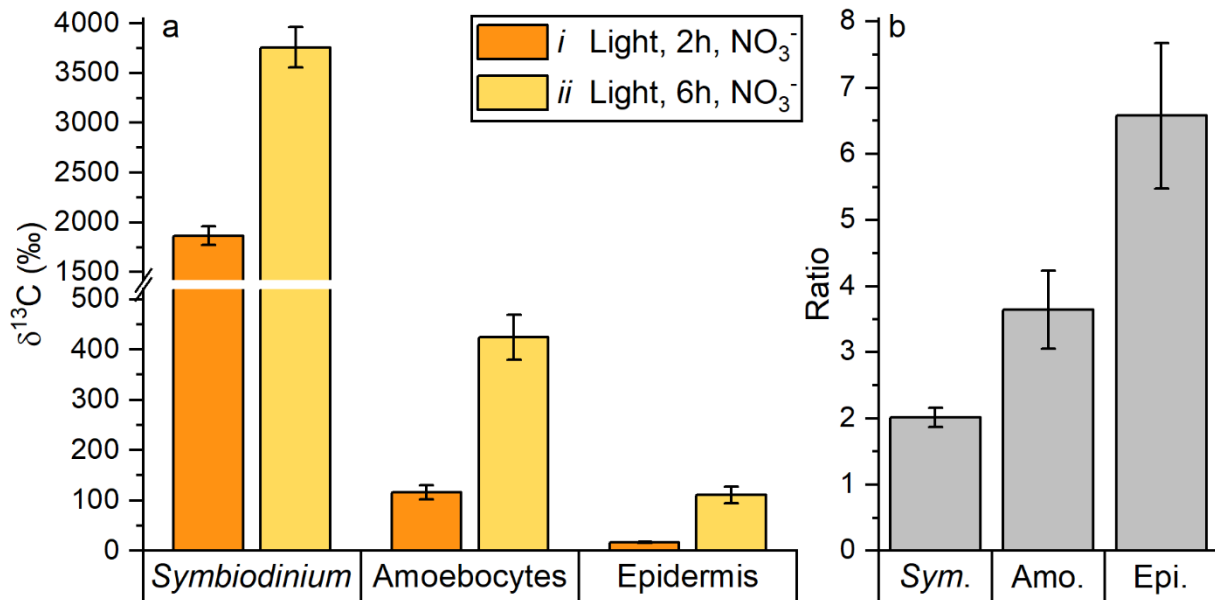


Figure 4 | (a) Observed mean <sup>13</sup>C enrichment levels in *Symbiodinium* cells and *Cassiopea* sp. host tissue for specimens incubated with <sup>13</sup>C-bicarbonate (and <sup>15</sup>N-nitrate) for 2- and 6-hours. Error bars indicate ± SE of mean. (b) Fold-change increase in <sup>13</sup>C enrichment for individual tissue areas between 2 and 6 hours. Error bars indicate ± propagated errors.

At the same time, we observed that  $^{13}\text{C}$  enrichments were not affected by the source of inorganic nitrogen available in the seawater. The 6-hour incubations with either  $^{15}\text{NO}_3^-$  or  $^{15}\text{NH}_4^+$  showed no significant differences in  $^{13}\text{C}$  enrichment across holobiont compartments (LMM,  $F(1, 4) = 0.8$ ,  $p = 0.425$ ; Supplementary table 1).

#### $^{15}\text{N}$ -assimilation in the holobiont

Regardless of incubation time and light conditions, medusae incubated with  $^{15}\text{NO}_3^-$  did not exhibit any detectable  $^{15}\text{N}$  enrichments in any of the holobiont compartments (Figure 3c, f, Figure 5, Supplementary table 1). In contrast, 6-hour incubation with  $^{15}\text{NH}_4^+$  resulted in clear  $^{15}\text{N}$  enrichments during both light and dark incubations for all holobiont compartments. Reflecting observed patterns of  $^{13}\text{C}$  enrichments, the different tissue- and cell types showed characteristic systematic  $^{15}\text{N}$  enrichments, with *Symbiodinium* exhibiting the highest and the epidermis the lowest  $^{15}\text{N}$  enrichment levels during dark as well as light incubations, respectively (LLM,  $F(2, 249) = 158.9$ ,  $p < 0.001$ ); see Figure 5 for relevant Tukey post hoc analyses. Light availability made no difference on ammonium assimilation, with  $^{15}\text{N}$ -enrichments not significantly different between light and dark incubations across holobiont compartments (LMM,  $F(1, 4) = 0.1$ ,  $p = 0.818$ ).

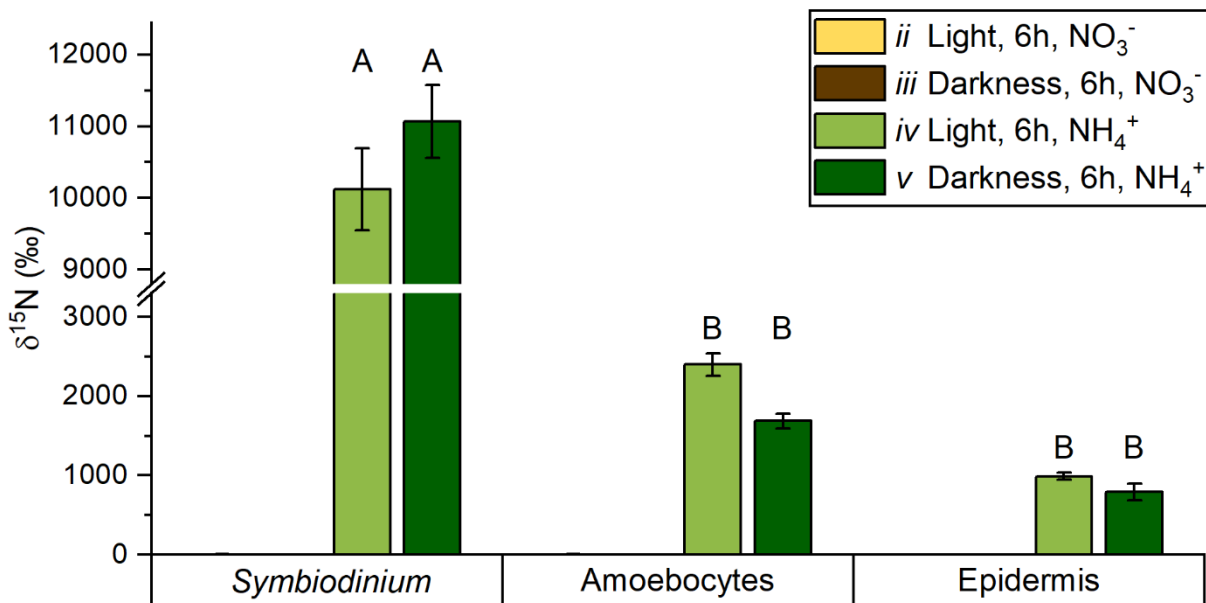


Figure 5 | Observed  $^{15}\text{N}$  enrichment levels in dinoflagellate symbionts and *Cassiopea* sp. host tissue. Error bars indicate  $\pm$  SE. Capital letters indicate significant differences ( $p < 0.05$ ; Tukey post hoc analyses).

#### Discussion

In contrast to corals and sea anemones that host their endosymbionts in the gastroderm tissue layer (Davy et al. 2012), the symbionts of juvenile *Cassiopea* sp. are predominantly found residing in

amoebocyte host cells located within the mesoglea. Metabolic interactions and translocation pathways in *Cassiopea* sp. could thus be expected to show both similarities with, and differences from those observed previously in hermatypic corals. Our findings corroborated previous reports of active nutrient exchange between *Cassiopea* and its algal symbionts. At the same time, the high resolution of quantitative NanoSIMS isotopic imaging allowed us to trace the fate of assimilated nutrients in the symbiosis, and quantify their anabolic partitioning across cells and tissues. We clearly observed that motile amoebocytes facilitated efficient assimilation of inorganic nutrients from seawater, and made isotopically enriched nutrients available for anabolic processes in other tissue layers, strongly suggesting that amoebocytes represent a key adaptation of scyphozoan jellyfish to a symbiotic lifestyle.

### Translocation of photosynthetically assimilated $^{13}\text{C}$

The anabolic turnover of photosynthetically-fixed carbon in *Cassiopea* sp. was found to display non-linear behaviour as a function of time in all investigated holobiont compartments. The enrichment level of any cell or tissue at any given time point reflects the balance between anabolic incorporation and catabolic consumption of isotopically-enriched compounds. As cells become more and more enriched over time, the catabolic consumption of isotopically-enriched compounds increases. Consequently, the increase in enrichment over time is expected to asymptotically approach the saturation point (i.e., 100%  $^{13}\text{C}$  enrichment). Such non-linearity was observed in *Symbiodinium* cells in which, over a 3-fold increase in incubation time (from 2 to 6 hours), only a 2-fold increase in  $^{13}\text{C}$  enrichment was observed (from ca. 1860 to 3760‰; Figure 4). Similarly, a non-linear trend was observed in the amoebocytes and epidermis, which showed a roughly 3.5- and 6.5-fold increase in  $^{13}\text{C}$  enrichment (from ca. 120 ‰ to 420 ‰ in amoebocytes, and from ca. 20‰ to 110‰ in epidermis), respectively, between the 2- and 6-hour light incubations (Figure 4). This implies that the rate of anabolic incorporation of isotopically-enriched compounds must have accelerated over time in the host tissue. The relative increase in the  $^{13}\text{C}$  enrichment levels over time, thus, reflects the delay at which photosynthetically-fixed  $^{13}\text{C}$  became available to the respective cell/tissue. The increasing ratios between 2- and 6-hour incubations allow to disentangle the order of translocation of photosynthetically-fixed carbon in the *Cassiopea*-Symbiodiniaceae symbiosis: Symbiodiniaceae translocate photosynthates to hosting amoebocytes, which subsequently can release labelled carbon substrates to other compartments of the holobiont, such as the epidermis.

Importantly, the efficiency of carbon translocation in the *Cassiopea*-Symbiodiniaceae symbiosis appears comparable to that of the coral-Symbiodiniaceae symbiosis. Using a similar methodological approach, Kopp *et al.* (Kopp *et al.* 2015) observed a qualitatively similar, non-linear  $^{13}\text{C}$  enrichment curve

for storage structures in dinoflagellates hosted by the hermatypic coral *Pocillopora damicornis* during a 6-hour pulse labelling with  $\text{H}^{13}\text{CO}_3^-$ . However, that study found slightly less efficient translocation dynamics, i.e.,  $^{13}\text{C}$  enrichment in adjacent host tissue was lower than the  $^{13}\text{C}$  enrichment in the *Cassiopea* amoebocytes and similar to epidermal tissue in the present study. To the degree that such qualitative comparison is possible (i.e., considering differences in experimental setup, dinoflagellate species, distribution and density) this – at least qualitatively – indicates that translocation of  $^{13}\text{C}$ -enriched photosynthates is certainly not less efficient in *Cassiopea* compared to that in a symbiotic coral. This conclusion is perhaps surprising considering that symbiotic corals rely on up to 95% of their metabolic energy demand being supplied in the form of photosynthates translocated from their dinoflagellate symbionts (Muscatine et al. 1981, Edmunds & Davies 1986, Kopp et al. 2015). However, our observations are consistent with previous studies on metabolic interactions between *Cassiopea* and their symbiont population, which indicate that *Cassiopea* can cover up to 170% of daily carbon demand via autotrophic carbon assimilation, regardless of host size (Verde & McCloskey 1998).

Our results thus suggest a very efficient and high-throughput system for autotrophic carbon assimilation in *Cassiopea*, in which a state of saturation of internal storage structures in symbionts is quickly reached and assimilated carbon is rapidly translocated (via amoebocytes) to the host for downstream biosynthesis (Figure 4). While we conclude that amoebocytes play a major role in the highly efficient nutrient translocation in the *Cassiopea* holobiont, the exact pathways and underlying mechanisms of such a system in *Cassiopea*, with the added complexity of photosynthates passing from the symbionts, via the amoebocytes, through the mesoglea to the epidermis, remain to be explored.

#### Nitrogen assimilation and resource allocation

Patterns of  $^{15}\text{NH}_4^+$  assimilation in the *Cassiopea* holobiont mirrored those previously described in corals (Pernice et al. 2012).  $^{15}\text{NH}_4^+$  was efficiently assimilated by both host and symbionts, regardless of light availability (Figure 5). As both algal endosymbionts and the cnidarian host have the cellular machinery for the metabolic incorporation of  $\text{NH}_4^+$  (Miller & Yellowlees 1989, Yellowlees et al. 2008), the observed  $^{15}\text{N}$  enrichment patterns reflect a combination between the cellular incorporation of  $^{15}\text{NH}_4^+$  and the translocation of fixed  $^{15}\text{N}$  between the symbiotic partners. Despite the spatial separation of amoebocytes from the surrounding seawater, Symbiodiniaceae showed the highest  $^{15}\text{N}$  enrichment levels in the *Cassiopea* holobiont. This implies that the close proximity of amoebocytes to the animals' external surface facilitates the, presumably, diffusion-controlled transport of  $\text{NH}_4^+$  to the algal symbionts.

In contrast to this,  $^{15}\text{NO}_3^-$  assimilation was not observed (or was below the detection limit of the NanoSIMS, which was roughly 0.2 % enrichment over the natural isotope ratio) regardless of light availability (Figure 5). In line with this, Welsh *et al.* (Welsh *et al.* 2009) found that *Cassiopea* sp. collected from South East Queensland, Australia, showed only a low net  $\text{NO}_3^- + \text{NO}_2$  ( $\text{NO}_x$ ) uptake in the light but attributed a high release of  $\text{NO}_x$  during dark incubations to the presence of surface-associated nitrifying bacteria. Likewise, Freeman *et al.* (Freeman *et al.* 2016) found that  $^{15}\text{NO}_3^-$  assimilation in *Cassiopea xamachana* was highest in body parts with lowest Symbiodiniaceae density. In light of these studies, our findings suggest that Symbiodiniaceae associated with *Cassiopea* either have limited access to  $\text{NO}_3^-$  from seawater or exhibit downregulated pathways for  $\text{NO}_3^-$  uptake due to high *in hospite* ammonium availability (Yellowlees *et al.* 2008, Allemand & Furla 2018). Such reduced  $\text{NO}_3^-$  assimilation by algal symbionts could indirectly benefit the cnidarian host as previous studies have linked high rates of  $\text{NO}_3^-$  assimilation to reduced rates of carbon translocation from algal symbionts, and increased bleaching susceptibility of corals during heat stress (Wiedenmann *et al.* 2012, Ezzat *et al.* 2015). Given the wide tolerance to temperatures and salinity that *Cassiopea* exhibits in its natural environment (Holland *et al.* 2004, Morandini *et al.* 2017) (unlike what is commonly known for corals), we hypothesize that a reduced or absent assimilation of  $\text{NO}_3^-$  by endosymbiotic Symbiodiniaceae may increase stress tolerance of the *Cassiopea* holobiont by enhancing energy availability for the host and reducing the bleaching susceptibility of the symbiosis.

### The ecological advantages of motile symbiont-bearing amoebocytes and *Cassiopea* as a model system

Amoebocytes have not been widely studied in cnidarians (Gold & Jacobs 2013, Smith 2016), but they are considered to be beneficial to non-symbiotic jellyfish by acting as part of the immune system (Hartenstein 2006, Smith 2016), and take part in general tissue maintenance (Chapman 1999, Ladouceur *et al.* 2013). Amoebocytes in *Cassiopea* have additionally been linked to the establishment of dinoflagellate symbiont populations via phagocytosis in the polyp stage (Colley & Trench 1983, Fitt & Trench 1983). The results of the present study further highlight the role of amoebocytes in the *Cassiopea* holobiont as a key adaptation to facilitate efficient symbiotic nutrient cycling in medusae.

In symbiotic corals, endosymbiotic dinoflagellates are found exclusively in the gastrodermis, which is in direct contact with the gastrovascular cavity and in close proximity to surrounding seawater, from which it is only separated by a thin mesoglea and epidermal tissue layer. In contrast, the thick mesoglea that makes up the bulk part of the medusa constitutes a significant spatial barrier separating gastrodermis



from epidermis and may hinder efficient uptake of nutrients from the seawater by algal symbionts through the gastrodermis. Motile, symbiont-bearing amoebocytes may help *Cassiopea* holobionts to overcome these barriers to nutrient uptake created by the scyphozoan morphology. On one hand, amoebocytes facilitate the relocation of algal symbionts from the gastroderm to other parts in the animal with close proximity to the surface, and better access to nutrients from the seawater. On the other hand, the motile nature of amoebocytes also allow for the release of autotrophically assimilated nutrients in the vicinity of other tissue layers thereby ensuring a more efficient exchange of nutrients in the holobiont. Symbiotic amoebocytes may thus be considered “cargo-ships”, efficiently shuttling symbionts to (photosynthetically and nutrient-wise) optimal locations inside the thick mesoglea, as well as efficiently transporting assimilated nutrients back to host tissue.

Taken together, symbiotic amoebocytes likely reflect a key adaptation of symbiotic scyphozoans to facilitate efficient assimilation and exchange of nutrients. In addition to this, a reduced or absent  $\text{NO}_3^-$  uptake of algal symbionts may further allow *Cassiopea* to thrive in highly dynamic habitats with strong fluctuations in salinity, nutrient availability and temperature conditions. At the same time, its unique characteristics set the *Cassiopea*-Symbiodiniaceae symbiosis apart from most other cnidarian-algal symbiotic assemblages. Whilst corals and many other symbiotic cnidarians are in global decline due to anthropogenic environmental change, *Cassiopea* spp. appear to thrive, producing massive blooms and undergoing rapid geographical expansion in the Anthropocene (Arai 2001, Ohdera et al. 2018). Future studies harnessing the unique advantages and characteristics of the *Cassiopea*-Symbiodiniaceae model system may reveal key processes underlying the functioning and breakdown of cnidarian-algal symbioses in general.

## Acknowledgments

We thank Sofie Lindegaard Jakobsen at the Marine Biology Section, University of Copenhagen for her excellent assistance with maintenance and care of the *Cassiopea* culture for the duration of this study, and for assistance with equipment for experimental setups. The authors thank Thomas Krueger and Margaret Caitlyn Murray, who performed initial NanoSIMS pilot experiments upon which this study builds. Finally, we thank the Electron Microscopy Facility at the University of Lausanne for use of their facilities and expert advice about histological sample preparation.

## Funding

This study was supported by grants from the Swiss National Science Foundation (AM; 200021\_179092), and an Investigator award from the Gordon and Betty Moore Foundation (MK; Grant no. GBMF9206, <https://doi.org/10.37807/GBMF9206>).

**Data accessibility**

Raw data will be made publicly available via the Dryad data repository upon acceptance of the manuscript.

**Competing interests**

The authors declare no competing interests.

## Chapter 2: Light microenvironment and O<sub>2</sub> and pH dynamics measured in the *Cassiopea* bell

### I. Context

Chapter 2 presents a completed manuscript that has been submitted to *Frontiers in Ecology and Evolution* for an article collection on Holobiont Interactions. In this chapter the physico-chemical microenvironment and optical microniches of *Cassiopea* is investigated using microsensors.

Chapter data originates from the master's thesis project by Margaret Caitlyn Murray, and data and manuscript were later adapted by me and Margaret into its current form. Chapter 2 represents a completed manuscript that has (at the time of the thesis was handed in) been submitted to *Frontiers in Ecology and Evolution* for a special topic contribution.

### Author Contributions

MCM, NHL, ET, and MK designed the experiment. Data acquisition was done by MCM, ET, and MK. Data and statistical analyses were carried out by MCM, NHL, ET, and MK. All authors contributed to writing and editing of the manuscript.

### II. Publication

# The mesoglea buffers the physico-chemical microenvironment of photosymbionts in the upside-down jellyfish *Cassiopea* sp.

**Niclas Heidelberg Lyndby<sup>1†</sup>, Margaret Caitlyn Murray<sup>2†</sup>, Erik Trampe<sup>2</sup>, Anders Meibom<sup>1,3</sup>, Michael Kühl<sup>2\*</sup>**

<sup>1</sup>Laboratory for Biological Geochemistry, School of Architecture, Civil and Environmental Engineering, Ecole Polytechnique Fédérale de Lausanne, 1015 Lausanne, Switzerland

<sup>2</sup>Marine Biological Section, Department of Biology, University of Copenhagen  
Strandpromenaden 5, DK-3000 Helsingør, Denmark

<sup>3</sup>Center for Advanced Surface Analysis, Institute of Earth Sciences, University of Lausanne, 1015 Lausanne, Switzerland.

#### \* Correspondence:

Michael Kühl  
mkuhl@bio.ku.dk

† **First authorship:** These authors share first authorship.

**Keywords: Symbiosis, jellyfish, microenvironment, photosynthesis, respiration, light.**

## Abstract

The jellyfish *Cassiopea* has a conspicuous lifestyle, positioning itself upside-down on sediments in shallow waters thereby exposing its photosynthetic endosymbionts (Symbiodiniaceae) to light. Several studies have shown how the photosymbionts benefit the jellyfish host in terms of nutrition and O<sub>2</sub> availability, but little is known about the internal physico-chemical microenvironment of *Cassiopea* during light-dark periods. Here, we used fiber-optic sensors to investigate how light is modulated at the water-tissue interface of *Cassiopea* sp. and how light is scattered inside host tissue. We additionally used electrochemical and fiber-optic microsensors to investigate the dynamics of O<sub>2</sub> and pH in response to changes in the light availability in intact living specimens of *Cassiopea* sp.

Mapping of photon scalar irradiance revealed a distinct spatial heterogeneity over different anatomical structures of the host, where oral arms and the manubrium had overall higher light availability, while shaded parts underneath the oral arms and the bell had less light available. White host pigmentation, especially in the bell tissue, showed higher light availability relative to similar bell tissue without white pigmentation. Microprofiles of scalar irradiance into white pigmented bell tissue showed intense light scattering and enhanced light penetration, while light was rapidly attenuated over the upper 0.5 mm in tissue with symbionts only.

Depth profiles of O<sub>2</sub> concentration into bell tissue of intact, healthy/living jellyfish showed increasing concentration with depth into the mesoglea, with no apparent saturation point during light periods. O<sub>2</sub> was slowly depleted in the mesoglea in darkness, and O<sub>2</sub> concentration remained higher than ambient water in large (> 6 cm diameter) individuals, even after 50 min in darkness. Light-dark shifts in large medusae showed that the mesoglea slowly turns from a net sink during photoperiods into a net source of O<sub>2</sub> during darkness. In contrast, small medusae showed a more dramatic change in O<sub>2</sub> concentration, with rapid O<sub>2</sub> buildup/consumption in response to light-dark shifts; in a manner similar to corals. These effects on O<sub>2</sub> production/consumption were also reflected in moderate pH fluctuations within the mesoglea. The mesoglea thus buffers O<sub>2</sub> and pH dynamics during dark-periods.

## Introduction

Symbiont-bearing jellyfish in the genus *Cassiopea* exhibit a conspicuous lifestyle by settling upside-down on sediment, exposing the subumbrella and oral arms to light. The oral side (i.e., the subumbrella side) of the medusa is particularly dense in intracellular microalgal symbionts, which are dinoflagellates

of the family Symbiodiniaceae (Lampert 2016). In contrast to corals where symbionts are found in endoderm cells, symbiont algae in *Cassiopea* are kept in clusters in host-specialized amoebocyte cells, directly below the epidermis in the mesoglea of the bell and oral arms (Colley & Trench 1985, Estes et al. 2003). Similar to many photosymbiotic corals and anemones, *Cassiopea* rely on a metabolic exchange of carbon and nitrogen between the host animal and its algal symbionts (Welsh et al. 2009, Freeman et al. 2016, Lyndby et al. 2020b). Translocation of autotrophically acquired carbon from the algal symbionts to the host covers a significant part of its daily carbon requirement, estimated to be at a similar or greater level than what is known from reef-building corals (Muscatine et al. 1981, Verde & McCloskey 1998).

While most photosymbiotic cnidarians require a rather stable environment to maintain a healthy symbiosis, *Cassiopea* appears extraordinarily resilient to fluctuating environmental conditions (Goldfarb 1914, Morandini et al. 2017, Klein et al. 2019, Aljbour et al. 2019, Banha et al. 2020) and are increasingly regarded as an invasive species (Mills 2001, Morandini et al. 2017). *Cassiopea* are typically found in shallow waters (e.g. lagoons, around seagrass beds, and mangroves) in tropical and subtropical regions (Drew 1972, Hofmann et al. 1996) that are prone to strong diel fluctuations in both temperature, and salinity, as well as high solar irradiance (Anthony & Hoegh-Guldberg 2003, Veal et al. 2010). Human activities in such coastal ecosystems can further add to strong fluctuations in both nutrient input, O<sub>2</sub> availability, and pH (Stoner et al. 2011, Klein et al. 2017a, Rowen et al. 2017, Arossa et al. 2021).

The photobiology and optical properties of marine symbiont-bearing cnidarians have been studied in detail in reef-building corals, showing adaptations in host growth patterns, microscale holobiont light modulation, and colony-wide symbiont organization to enable and optimize symbiont photosynthesis for the benefit of the host. There has been a special focus on coral skeletons and host pigments (e.g. Falkowski et al. 1984, Kühl et al. 1995, Wangpraseurt et al. 2014b, Lyndby et al. 2019, Kramer et al. 2021, Bollati et al. 2022). Studies have shown that *in vivo* light exposure of symbionts is modulated on a holobiont level to enhance photosynthesis, including alleviating photodamage and bleaching (Lesser & Farrell 2004, Enríquez et al. 2005, Marcelino et al. 2013, Wangpraseurt et al. 2017a), altering inter- and intracellular pH (e.g. Kühl et al. 1995, Gibbin et al. 2014), and directly affecting holobiont temperature (Jimenez et al. 2008, 2012, Lyndby et al. 2019). Recently, these experimental insights were integrated in a first multiphysics model of radiative, heat and mass transfer in corals, simulating how coral tissue structure and composition can modulate the internal light, O<sub>2</sub> and temperature microenvironment of corals (Taylor Parkins et al. 2021). Given a similar global distribution and a benthic lifestyle relying on host-symbiont metabolic interactions, it is feasible to assume that *Cassiopea* exhibit similar traits, but few studies have

investigated to what extent *Cassiopea* modulate their physicochemical microenvironment (Klein et al. 2017a, Arossa et al. 2021).

In this study, we use a combination of optical and electro-chemical microsensors to investigate the internal microenvironment of *Cassiopea* sp. medusae. We explore how light is modulated by host morphology and distinct anatomical features. Furthermore, we show how the size of animals and the thickness of their bell mesoglea affects the intracellular physicochemical microenvironment of intact, living *Cassiopea* sp. medusae.

## Methods

### *Cassiopea* maintenance

Medusae of *Cassiopea* sp. were acquired via DeJong Marinelife (Netherlands) in 2018, and since cultivated at the aquarium facility at the Marine Biology Section in Helsingør, University of Copenhagen (Denmark). According to the commercial provider, the obtained specimens originated from Cuba indicating the species *Cassiopea xamachana* or *C. frondosa*, but no species identification was performed. The medusae were kept in artificial seawater (ASW; 25°C, 35 ppt, pH of 8.1) in a 60 L glass aquarium, under a 12h-12h day-night cycle using LED lamps (Tetra, Pacific Sun) providing an incident photon irradiance (400-700 nm) of  $\sim 300 \mu\text{mol photons m}^{-2} \text{ s}^{-1}$ , as measured with a cosine corrected mini quantum sensor (MQS-B, Walz, Germany), connected to a calibrated irradiance meter (ULM-500, Walz, Germany). Animals were fed with living *Artemia* sp. nauplii twice a week, and 25% of the aquarium water was replaced with fresh filtered ASW (FASW) 1 hour after feeding. Additionally, water was continuously filtered using an internal filter pump, a filter sock (200  $\mu\text{m}$ ), and a UV filter. Additionally, an air pump was used to ensure water remained oxygenated at all times.

### Light measurements

#### Photon scalar irradiance

Mapping of photon scalar irradiance in  $\mu\text{mol photons m}^{-2} \text{ s}^{-1}$  (PAR; 400–700 nm) on the jellyfish tissue surface was performed with a submersible spherical micro quantum sensor (3.7 mm diameter; US-SQS/L, Walz, Germany) connected to a calibrated irradiance meter (ULM-500, Walz, Germany). Measurements were conducted inside an aquarium tank filled with ASW and the inside covered with a black cloth to avoid internal reflections from the container. The medusa was placed in the aquarium and illuminated vertically from above by a fiber-optic tungsten-halogen lamp (KL-2500 LCD, Schott GmbH, Germany), equipped with a collimating lens. Photon scalar irradiance was measured holding the sensor at a  $\sim 45^\circ$  angle, while measuring light on the surface of the animal within 7 areas of interest (AOI) of one

animal (Figure 8B). Measurements were normalized against the incident downwelling photon irradiance, as measured over the black cloth covering the inside of the container relative to each AOI on the animal.

### **Spectral scalar irradiance & reflectance**

Both spectral scalar irradiance and reflectance measurements required the medusa to be fixed in place on a large rubber stopper using hypodermic needles, and placed in a container filled with seawater. Incident light was provided vertically from above with a fiber-optic halogen lamp (KL-2500 LCD, Schott GmbH, Germany) fitted with a collimating lens. Spectral scalar irradiance was measured using a fiber-optic scalar irradiance microprobe (spherical tip diameter  $\sim 100 \mu\text{m}$ ; Rickelt et al. 2016). Spectral reflectance was measured using a fiber-optic field radiance probe ( $400 \mu\text{m}$  diameter; Kühl 2005). Both sensors were connected to a fiber-optic spectrometer (USB2000+; Ocean Optics, USA), and spectral information was acquired using SpectraSuite software (Ocean Optics, USA). Sensors were mounted on a manual micromanipulator (MM33, Märzhäuser Wetzlar GmbH, Germany) attached to a heavy-duty stand to facilitate precise positioning of sensors on the medusa. Sensors were positioned visually using a dissection microscope, while ensuring oral arms and other anatomical features did not shade the tissue studied. The spectral reflectance probe was positioned by first moving the sensor to the surface of the medusa, then moving the sensor 1 mm away. Similarly, the scalar irradiance probe was first positioned to touch the surface tissue of the medusa (depth =  $0 \mu\text{m}$ ) and was then moved into the medusa in vertical steps of  $200 \mu\text{m}$ . Both sensors were held by the micromanipulator in an angle of  $45^\circ$  relative to the incident light. The recorded spectral scalar irradiance was normalized against the incident, downwelling spectral irradiance measured over the black cloth covering the inside of the container relative to each measuring position on the medusae. The recorded spectral reflection spectra were normalized against a reference spectrum measured with an identical setup over a 99% white reflectance standard (Spectralon, Labsphere) in air.

### **Microscale measurements of $\text{O}_2$ and pH**

#### **General setup**

For all  $\text{O}_2$  and pH measurements, individual medusae were placed in a cylindrical plexiglass chamber with aerated, filtered ASW. Medusae were illuminated with a fiber-optic halogen lamp (KL-1500 LED, Schott GmbH, Germany) equipped with a collimating lens, and providing defined levels of incident photon irradiance (0, 42, 105, 160, 300, and  $580 \mu\text{mol photons m}^{-2} \text{s}^{-1}$ ; 400-700 nm), as measured for specific lamp settings with a calibrated photon irradiance meter equipped with a spherical micro quantum sensor (ULM-500 and US-SQS/L, Heinz Walz GmbH, Germany).  $\text{O}_2$  concentration measurements showed  $\text{O}_2$  production

saturated at  $300 \mu\text{mol photons m}^{-2} \text{ s}^{-1}$ , but production was not inhibited at maximum intensity of  $580 \mu\text{mol photons m}^{-2} \text{ s}^{-1}$ .

Concentration profiles and dynamics were measured above and inside anastomosing bell tissue of 3 small (25-48 mm) and 2 large (63-67 mm) medusae. The microsensor tip was carefully positioned at the tissue surface-water interface while watching the tissue surface under a dissection microscope. For profiling, the sensor was inserted in vertical steps of  $100 \mu\text{m}$  until reaching the approximate center of the mesoglea, relative to the subumbrella and exumbrella bell epidermis.

### Oxygen measurements

The  $\text{O}_2$  concentration measurements were done using a robust fiber-optic  $\text{O}_2$  optode (OXR230  $\text{O}_2$  sensor,  $230 \mu\text{m}$  diameter tip,  $< 2 \text{ s}$  response time; PyroScience GmbH, Germany) connected to a fiber-optic  $\text{O}_2$  meter (FireSting, PyroScience GmbH, Germany). The sensor was linearly calibrated in  $\text{O}_2$ -free and 100 % air saturated seawater at experimental temperature and salinity. The sensor was mounted slightly angled relative to the incident light (to avoid shadowing) on a motorized micromanipulator (MU1, PyroScience GmbH, Germany) attached to a heavy-duty stand, facilitating visual sensor positioning with a dissection microscope. Data acquisition was done using the manufacturer's software (Profix, PyroScience GmbH, Germany). Measurements were performed at room temperature ( $22^\circ\text{C}$ ) in a dark room under defined light conditions, and the temperature was continuously recorded in the experimental chamber with a submersible temperature sensor (TSUB21, PyroScience GmbH, Germany) connected to the  $\text{O}_2$  meter.

For light-dark measurements, the  $\text{O}_2$  sensor tip was inserted approximately midway between sub- and exumbrella epidermis (depth ranging from  $\sim 800$  to  $3000 \mu\text{m}$  from the surface depending on the specimen size). Once the depth of interest was reached, the local  $\text{O}_2$  concentration dynamics were measured at  $10 \text{ s}$  intervals during experimental manipulation of the light. Local rates of net photosynthesis and post-illumination respiration were estimated from the measured linear slope of  $\text{O}_2$  concentration versus time measurements (using linear fits in the software OriginPro 2020b) under light and dark conditions, respectively. The local gross photosynthesis was then estimated as the sum of the absolute values of net photosynthesis and respiration.

The  $\text{O}_2$  concentration depth profiles were recorded at vertical depth intervals of  $100$ - $200 \mu\text{m}$  during constant light or darkness. The measurements were recorded once the  $\text{O}_2$  concentration reached a steady-



state at each depth, starting from deepest inside the tissue and moving the sensor up until the sensor tip was retracted up into the overlying turbulent water column (100 % air saturation).

#### pH measurements

pH was measured using a pH glass microelectrode (PH-100, 100  $\mu\text{m}$  tip diameter, response time < 10 s, Unisense, Denmark) combined with an external reference electrode and connected to a high impedance mV-meter (Unisense, Denmark). A motorized micromanipulator (MU1, PyroScience GmbH, Germany) was used for positioning of the sensor, and data were recorded using SensorTrace Logger software (Unisense, Denmark). Prior to measurements the sensor was calibrated at room temperature using IUPAC standard buffer solutions at pH 4, 7, and 9 (Radiometer Analytical, France). Dynamic changes in mesoglea pH levels were measured during experimental dark-light transitions and *vice versa*. pH depth profiles were measured under constant light or darkness, and were recorded from the middle of the bell and up into the water column in steps of 200  $\mu\text{m}$ , until the sensor tip was retracted into the overlying turbulent water column (pH level of 8.1-8.4).

## Results

### Light microenvironment

#### Photon scalar irradiance

Macroscopic mapping of integral photon scalar irradiance of photosynthetically active radiation (PAR, 400-700 nm) in 4 distinct regions of an intact, living *Cassiopea* sp. revealed a heterogeneous light field across the medusa tissue facing the incident light as well as across the tissue. The manubrium center experienced the highest scalar irradiance reaching 166 % of incident photon irradiance (Figure 8). Oral arms experienced a photon scalar irradiance reaching  $140 \pm 19$  % of incident photon irradiance, while light availability just below the oral arms was significantly lower ( $75 \pm 12$  % of incident photon irradiance). The light levels of rhopalial canals reached  $124 \pm 30$  % of incident photon irradiance and light levels of anastomosing tissue reached  $96 \pm 8$  % of incident photon irradiance on the subumbrella side. On the exumbrella side, more light penetrated the anastomosing tissue ( $65 \pm 14$  % of incident photon irradiance), while the least amount of light penetrated through the rhopalial canals ( $39 \pm 9$  % of incident photon irradiance).

#### Reflectance

The oral arms and rhopalial canals of *Cassiopea* reflected more light than the manubrium and anastomosing tissue, with oral arms reflecting 9.5 %, rhopalial canals 7 %, the manubrium 4.8 %, and anastomosing tissue 3 % of incident irradiance (Figure 9).

## Spectral scalar irradiance

Depth profiles of spectral scalar irradiance in live *Cassiopea* tissue showed spectral absorption signatures of chlorophyll (Chl) *a* (430–440, 675 nm), Chl *c* (460, 580–590, 635 nm), and peridinin (480–490 nm), throughout the anastomosing tissue and near rhopalia canals (Figure 10). Spectral scalar irradiance at the tissue-water interface (0  $\mu\text{m}$ ) revealed a local enhancement near the rhopalia canals, while light was more readily absorbed on anastomosing tissue. Depth profiles show a steady attenuation of light within the first 400  $\mu\text{m}$  of the bell near rhopalia canals (Figure 10A). In contrast, scalar irradiance was slightly enhanced at 200 and 400  $\mu\text{m}$  in the anastomosing tissue, until a strong attenuation was observed at 600  $\mu\text{m}$  depth (Figure 10B).

## Chemical microenvironment

### Oxygen depth profiles

The  $\text{O}_2$  concentration depth profiles were measured in a *Cassiopea* sp. medusa (45 mm  $\emptyset$ ) under a saturating photon irradiance of 300  $\mu\text{mol photons m}^{-2} \text{s}^{-1}$  (Figure 11). The  $\text{O}_2$  concentration increased strongly in deeper parts of the bell tissue below 1 mm depth, rising from 315 ( $\pm 21$ ) to 445 ( $\pm 40$ )  $\mu\text{mol O}_2 \text{l}^{-1}$  at a depth of 3.7 mm. A maximal  $\text{O}_2$  concentration was measured at 4 mm, reaching  $\sim 500 \mu\text{mol O}_2 \text{l}^{-1}$  (not shown in figure).

Similarly,  $\text{O}_2$  depth profiles were measured in darkness in 3 different medusae (38–67 mm  $\emptyset$ ), with either 0, 15, or 50 min of darkness prior to the profile (Figure 12). Profiles reveal high  $\text{O}_2$  depletion in the top 1 mm layer of the bell with increasing length of dark incubation, while measurements deeper into the bell showed a less dramatic decrease of  $\text{O}_2$  concentration in the mesoglea of the medusae.

### Light-dependent oxygen dynamics

The  $\text{O}_2$  dynamics measured approximately in the middle of the mesoglea between the sub- and exumbrella epidermis showed a delayed response to changes in light in large individuals, while the response in smaller medusae appeared immediately after a light-dark switch or *vice versa* (Figure 13). The  $\text{O}_2$  concentration measured in 2 large and 3 small medusae showed that the  $\text{O}_2$  content continued to increase in the mesoglea of large medusae several minutes after light was turned off, indicative of diffusive supply from the surrounding tissue with a higher symbiont density and/or photosynthetic activity prior to onset of darkness (Figure 14).

Locally measured photosynthesis versus photon irradiance curves showed that photosynthesis increased linearly with irradiance until saturation was approached at  $\sim 300 \mu\text{mol photons m}^{-2} \text{s}^{-1}$  (Figure 15). At saturating irradiance, net photosynthesis rates in bell tissue ranged from 0.08  $\mu\text{mol O}_2 \text{l}^{-1} \text{s}^{-1}$  in large

individuals, to  $0.18 \mu\text{mol O}_2 \text{ l}^{-1} \text{ s}^{-1}$  in small medusae. Similarly, the estimated gross photosynthesis was roughly 2-fold higher in small medusae, at  $0.26 \mu\text{mol O}_2 \text{ l}^{-1} \text{ s}^{-1}$  vs.  $0.14 \mu\text{mol O}_2 \text{ l}^{-1} \text{ s}^{-1}$  in large medusae. Post-illumination respiration rates were  $0.04\text{-}0.07 \mu\text{mol O}_2 \text{ l}^{-1} \text{ s}^{-1}$  in large medusae regardless of illumination, while post-illumination respiration in small medusae increased to a maximum of  $0.18 \mu\text{mol O}_2 \text{ l}^{-1} \text{ s}^{-1}$  at maximum photon irradiance ( $580 \mu\text{mol photons m}^{-2} \text{ s}^{-1}$ ). The respiration at saturating photon irradiance ( $300 \mu\text{mol photons m}^{-2} \text{ s}^{-1}$ ) was  $0.08 \mu\text{mol O}_2 \text{ l}^{-1} \text{ s}^{-1}$  in tissue of small medusae.

#### Spatio-temporal dynamics of pH

pH depth profiles measured after a combined 15 minutes light, 15 minutes darkness incubation showed that pH dropped rapidly to below ambient water pH at the bell tissue-water interface ( $0 \mu\text{m}$ ) in both the large and small medusae (Figure 16). pH then increased rapidly again within the first  $1000 \mu\text{m}$  of the bell tissue (to above ambient water pH), and kept increasing to a maximum depth of  $4000 \mu\text{m}$  to a final pH of  $\sim 8.8$  for both specimens. The pH dynamics over experimental light-dark shifts showed a similar pattern to what was observed with  $\text{O}_2$  dynamics: pH changed relatively quickly in the small medusa, while a much longer delay (usually  $> 10$  min after the light change) was observed with the large medusa (Figure 17).

## Discussion

### *Cassiopea* harbors optical microniches

Light availability in the host is a key factor for an efficient photosymbiosis. It has been shown that host morphology and tissue plasticity, host pigmentation, and symbiont density can modulate the scattering and absorption of photons in tissue of reef building corals, creating optical microniches in a colony (D'Angelo et al. 2008, Wangpraseurt et al. 2014b, 2019, Bollati et al. 2022); and we note that the coral skeleton is also important for the coral light microenvironment (e.g. Enríquez et al. 2005, 2017). In *Cassiopea*, we found distinct spatial heterogeneity over the surface tissue in various regions of an adult medusa (Figure 8). Local photon scalar irradiance was highest near apical parts of the animal, while it dropped by 30-80 % underneath the same anatomical structures (Figure 8A). The largest decrease was observed between measurements on the subumbrella and exumbrella epidermis along the rhopalia canal, which dropped by 80 % on the exumbrella side. Additionally, spatial heterogeneity was observed over the subumbrella bell tissue, with rhopalia canals experiencing on average  $\sim 30$  % higher photon flux compared to the anastomosing tissue right next to it.

Depth profiles of spectral scalar irradiance measured in tissue close to rhopalia canals and in anastomosing tissue showed that light scattered differently within the upper  $600 \mu\text{m}$  of the two regions

(Figure 10). Profiles in anastomosing tissue showed small variations in spectral scalar irradiance measured in the top 400  $\mu\text{m}$  of this region (Figure 10B). Such small variations indicate the presence of a dense symbiont population spread out in the top 400  $\mu\text{m}$  of the mesoglea, between the subumbrella epidermis and the gastric network (Estes et al. 2003). Similar studies on corals have shown that light can be scattered by host tissue and symbionts in the surface layers, enhancing the chance of photon absorption (Wangpraseurt et al. 2012, 2014a, Jacques et al. 2019). In contrast, we observed a strong light attenuation over the first 400  $\mu\text{m}$  of the tissue near rhopalia canals, with an initial enhancement of local scalar irradiance that quickly attenuated to levels below what was observed at the same depth in anastomosing tissue (Figure 10B). *Cassiopea* contain distinct white striated patterns in dense layers along the rhopalia canals in the bell and under oral arms (see white patches in Figure 8B) (Bigelow 1900). While little is known about host pigments in *Cassiopea* and other rhizostome jellyfish (Hamaguchi et al. 2021, Lawley et al. 2021), our reflection data (compare e.g. rhopalia canal with anastomosing tissue in Figure 9) suggests that the white pigmented tissue can play a role in scattering and reflection of light in *Cassiopea* medusae, similar to host pigments and the skeleton in reef building corals (Wangpraseurt et al. 2014a, Jacques et al. 2019). More detailed analyses are required to understand the full potential of light-modulating host pigments in *Cassiopea*, and how the holobiont might respond and grow under various light regimes.

#### ***Cassiopea* harbors its photosymbionts in a buffered chemical microenvironment**

We investigated the light-driven dynamics of  $\text{O}_2$  and pH on the surface and inside the bell tissue of *Cassiopea* medusae. Depth profiles of  $\text{O}_2$  concentration measured at saturating irradiance showed the presence of a diffusive boundary layer (DBL) over the bell tissue (Figure 12). In light, the  $\text{O}_2$  concentration increased towards the bell tissue-water interface and continued to increase as the sensor penetrated deeper into the tissue and mesoglea (Figure 11). We measured to a maximum depth of 4 mm into the mesoglea reaching an  $\text{O}_2$  concentration of roughly 2-fold that of the surrounding seawater concentration. A similar study, measuring  $\text{O}_2$  in cut-off oral arms of *Cassiopea* sp., found that  $\text{O}_2$  concentration was highest near symbiont populations (i.e., near the epidermis), while it decreased to a more constant level deeper into the oral arm mesoglea (Arossa et al. 2021). However, our measured depth profiles in bell tissue did not show any indication that  $\text{O}_2$  buildup would stagnate or decrease at this point, suggesting even higher concentrations might be possible in the bell mesoglea relative to oral arms. Passive accumulation of  $\text{O}_2$  has been reported in non-symbiotic jellyfish like *Aurelia labiata* (Thuesen et al. 2005), which was found to build up  $\text{O}_2$  in the mesoglea when in  $\text{O}_2$ -rich water, indicating that the mesoglea can act as a natural reservoir for  $\text{O}_2$  in jellyfish. However, similar to measurements in oral arms of *Cassiopea*

sp. (Arossa et al. 2021), measured depth profiles of O<sub>2</sub> concentrations in non-symbiotic jellyfish like *Aurelia* appear to have the highest O<sub>2</sub> concentration near the tissue-water interface, with a steady decline towards the center of the bell (Thuesen et al. 2005). In contrast our measurements indicate that the presence of photosynthetic endosymbionts harbored within amoebocytes in the mesoglea (Colley & Trench 1985, Medina et al. 2021) leads to internal O<sub>2</sub> production and accumulation in deeper tissue layers during photo periods (Kühl et al. 1995, Arossa et al. 2021).

The diffusion of O<sub>2</sub> through cnidarian tissue and mesoglea has received little attention, however, Brafield and Chapman (1983) determined an O<sub>2</sub> diffusion coefficient of  $7.69 \times 10^{-6} \text{ cm}^2 \text{ s}^{-1}$  (Fick's law) in the mesoglea of the sea anemone *Calliactis* sp. Such a low diffusion coefficient in the mesoglea (as compared to seawater) will impede mass transfer, especially in cnidarians with a particularly thick mesoglea like jellyfish and sea anemones, and is probably a key factor in the observed buffering of O<sub>2</sub> dynamics in the *Cassiopea* sp. bell. We further investigated the dynamics of O<sub>2</sub> in darkness and found that the top 1 mm layer of *Cassiopea* bell tissue turned from a net O<sub>2</sub> source into a sink (Figure 12). Measurements in the DBL showed a switch from a net export from the tissue into the surrounding seawater to a diffusive import of O<sub>2</sub> from the seawater within the first 15 min (compare DBLs in Figure 12). A more pronounced depletion of O<sub>2</sub> was observed in the top 1 mm of the bell after 50 min darkness. The higher O<sub>2</sub> consumption near the subumbrella epidermis probably reflects the presence of abundant musculature required for bell pulsation and motility of jellyfish (Blanquet & Riordan 1981, Thuesen et al. 2005, Aljbour et al. 2017), as well as the presence of a dense population of endosymbionts (Estes et al. 2003, Lampert 2016). Both have previously been ascribed to heavy diel fluctuations of O<sub>2</sub> measured in *Cassiopea* oral arms (Arossa et al. 2021). However, the O<sub>2</sub> concentration remained high at depths deeper than 1 mm into the bell even after 50 min of darkness, reflecting a lower cell density and diffusive transport of O<sub>2</sub>.

In the present study, experimental light-dark shifts performed on intact small (< 5 cm) and large (> 6 cm) *Cassiopea* sp. showed that the O<sub>2</sub> concentration in small medusae with a (relatively) thin bell of 2 mm thickness changed almost immediately in response to light-dark shifts similar to observed O<sub>2</sub> dynamics in corals and dissected oral arms of *Cassiopea* (Figure 13A) (Kühl et al. 1995, Arossa et al. 2021). Unlike the fast response observed in small medusae, larger medusae with a thicker bell tissue showed a much slower response of O<sub>2</sub> levels to changes in light (Figure 13B). In fact, detailed O<sub>2</sub> dynamics measured in several large and small medusae revealed a consistent pattern where O<sub>2</sub> would continue to build up in the thick mesoglea of larger medusae for a few minutes after onset of darkness (Figure 14). These observations indicate that O<sub>2</sub> generated in other regions with higher photosynthetic activity due to higher

light levels and/or higher symbiont density can diffuse into and accumulate in the mesoglea, from where it is not efficiently exchanged with the surrounding water due to the relatively low O<sub>2</sub> diffusivity in mesoglea (Brafield & Chapman 1983).

Furthermore, an inverse relationship between medusa size and photosynthetic rate have previously been reported (Verde & McCloskey 1998). We observed a similar inverse relationship, with smaller medusae on average reaching roughly 2-fold higher photosynthetic rates (net and gross) at photon irradiances above 200 μmol photons m<sup>-2</sup> s<sup>-1</sup> (Figure 15). Post-illumination respiration also increased in small individuals, while larger medusae did not show changes to respiration after illumination. The combined effect of the diffusive properties of mesoglea, the relative thickness of the mesoglea, and the overall size of the animal might together explain why the O<sub>2</sub> dynamics is more pronounced in medusae (and other cnidarians) with a thin mesoglea like in juvenile *Cassiopea* bell or oral arms, while the O<sub>2</sub> dynamics in medusae with a thick mesoglea is much more buffered.

Consistent with the measured O<sub>2</sub> dynamics, we found that pH changes in the mesoglea were affected by changes in light, because pH increases due to photosynthetic carbon fixation in the light and decreases during darkness due to respiration (Figure 17). This relationship between photosynthesis, respiration, and pH seems prevalent in symbiotic cnidaria (e.g. Kühl et al. 1995, de Beer et al. 2000, Chan et al. 2016, Klein et al. 2017a, Arossa et al. 2021), largely driven by the shifting equilibrium between carbonate species (i.e., CO<sub>2</sub>, H<sub>2</sub>CO<sub>3</sub>, HCO<sub>3</sub><sup>-</sup>, CO<sub>3</sub><sup>2-</sup>) and the balance between photosynthesis and respiration. de Beer et al. (2000) found that pH in coral tissue followed the trend of O<sub>2</sub> during experimental light-dark shifts but with a delayed response (seconds to minutes), and attributed the delay to hypothetical processes, such as proton pumps and other similar cross-tissue transport, that would buffer pH in coral polyps (Palmer & Van Eldik 1983). External buffering has also been reported in polyps of *Cassiopea*, where Klein et al. (2017b) found that polyps retained their internal pH at ambient water pH during the night, and only symbiotic polyps would increase their internal pH during photoperiods due to a shifting carbonate equilibrium. We observed a similar, but much longer (>10 min) delay before a pH change was observed in the mesoglea of large medusa after light-dark shifts (Figure 17B). While external buffering is likely to occur in medusae of *Cassiopea* as well, the pH dynamics inside the mesoglea is probably more affected by diffusive transport phenomena. Depth profiles done in both small and large medusae thus show that within 15 min of darkness the top 1 mm of the bell tissue became more acidic relative to ambient water pH (0.3-0.5 pH lower; Figure 16), while pH in deeper tissue layers (>1000 μm into the bell) remained

alkaline and above ambient water pH. This strongly suggest that the mesoglea has a buffering effect on pH in the bell tissue of *Cassiopea*.

The buffering capacity of the mesoglea could be of benefit for both host and symbionts. A reservoir of O<sub>2</sub> can e.g. act as a steady supply of O<sub>2</sub> to both host musculature, needed for bell pulsation, and to symbionts during dark periods or exposure to hypoxia (Thuesen et al. 2005). Similarly, buffering pH could lower the possibility of the holobiont experiencing cellular acidosis (Smith & Raven 1979, Gibbin et al. 2014) that would otherwise disrupt cell-function (Madshus 1988). Thus, symbionts harbored in amoebocytes in the *Cassiopea* mesoglea may exist in a more stable ecological niche as compared to algae in corals that are more prone to rapid chemical dynamics. We speculate that the buffering of the chemical microenvironment in the mesoglea of *Cassiopea*, might also be reflected in the fact that *Cassiopea* medusae generally seem to only engage with a specific type of Symbiodiniaceae. Indeed, specific strains of Symbiodiniaceae have been speculated to be favored by different hosts in symbiotic cnidarians (Schoenberg & Trench 1980, Biquand et al. 2017), including *Cassiopea* (Colley & Trench 1983, Fitt 1985). While specificity is generally attributed to a combination of symbiont cell size and a hospitable host microenvironment (Biquand et al. 2017), Fitt (1985) found a correlation between symbiont cell size and respective photosynthesis and respiration rates, and proposed that only specific symbiont strains are able to establish symbiosis due to metabolic rates matching the hosts specific microenvironment. As such, the *Cassiopea*-Symbiodiniaceae symbiosis may be successful even in extreme environments as *Cassiopea* is capable of maintaining less stress-tolerant species due to the buffering nature of the *Cassiopea* chemical microenvironment.

## Summary

In comparison to corals, *Cassiopea* shares similar optical properties to that of reef-building coral tissue. Both macroscale host anatomy and microscale structures play a role in modulating the internal light field experienced by the symbionts via light scattering. Precisely how these structures affect symbiont photosynthesis remains to be explored further. Furthermore, our microsensor measurements indicated a buffering of chemical dynamics in the thick mesoglea matrix of *Cassiopea* sp. medusae, suggesting that the internal physico-chemical microenvironment of the holobiont remains more constant when experiencing abrupt changes in light conditions. This is in strong contrast to the rapid dynamics seen in coral tissue, which has a much thinner mesoglea and where the endosymbionts are found within endoderm cells. We hypothesize that the stabilization of the internal host microenvironment can be beneficial to the holobiont during unfavorable external environmental conditions such as hypoxia, where

stored O<sub>2</sub> in the mesoglea might act as an important reserve for keeping internal homeostasis. This may also be key to the apparent success of *Cassiopea* to invade and persist coastal tropical habitats with strong environmental fluctuations, that often preclude coral colonization. However, further studies are required to determine the effect of the buffering capacity of large individuals in combination with true environmental stressors over short and long periods.

### **Conflict of Interest**

The authors declare that the research was conducted in the absence of any commercial or financial relationships that could be construed as a potential conflict of interest.

### **Funding**

This study was supported with an Investigator award from the Gordon and Betty Moore Foundation (MK; Grant no. GBMF9206, <https://doi.org/10.37807/GBMF9206>) and the Swiss National Science Foundation (AM; Grant no. 200021\_179092).

### **Acknowledgments**

We thank Sofie Lindegaard Jakobsen for excellent technical assistance with keeping *Cassiopea* specimens used in this study.



## Figures

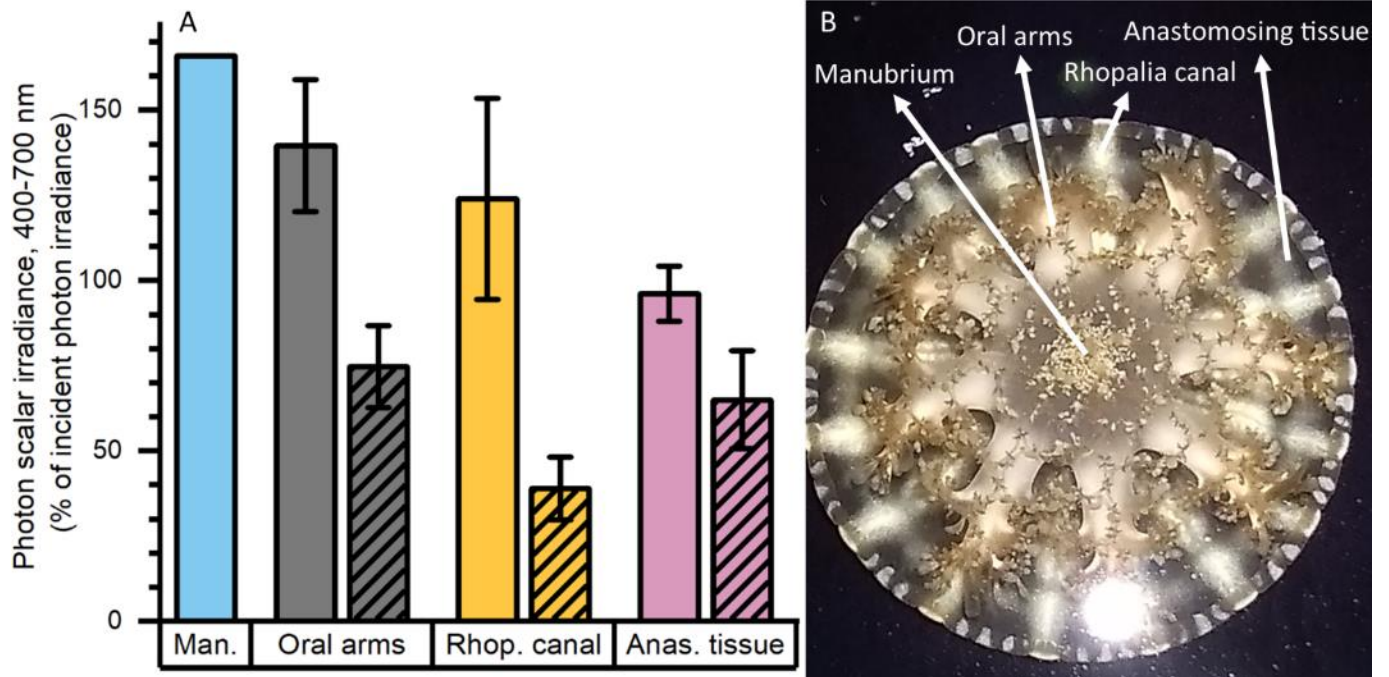


Figure 8 | Normalized photon scalar irradiance (PAR, 400-700 nm) measured at (A) the manubrium center (Man.), oral arms, rhopalia canals (Rhop. canal) and anastomosing tissue (Anas. tissue) on a single adult medusa of *Cassiopea*. Bright colors indicate values measured above, and shaded colors the values below the medusa. (B) Overview of the specimen with exemplary positions for measurements (white arrows). Light intensities were mapped at the tissue-water interface (above and below the medusa) at respective anatomical structures ( $n = 7-17$ ) using a submersible spherical quantum sensor (see methods), and normalized against the incident photon irradiance intensity measured at the same sensor positions without the medusae above a black surface. Note, only one measurement was performed above the manubrium center.

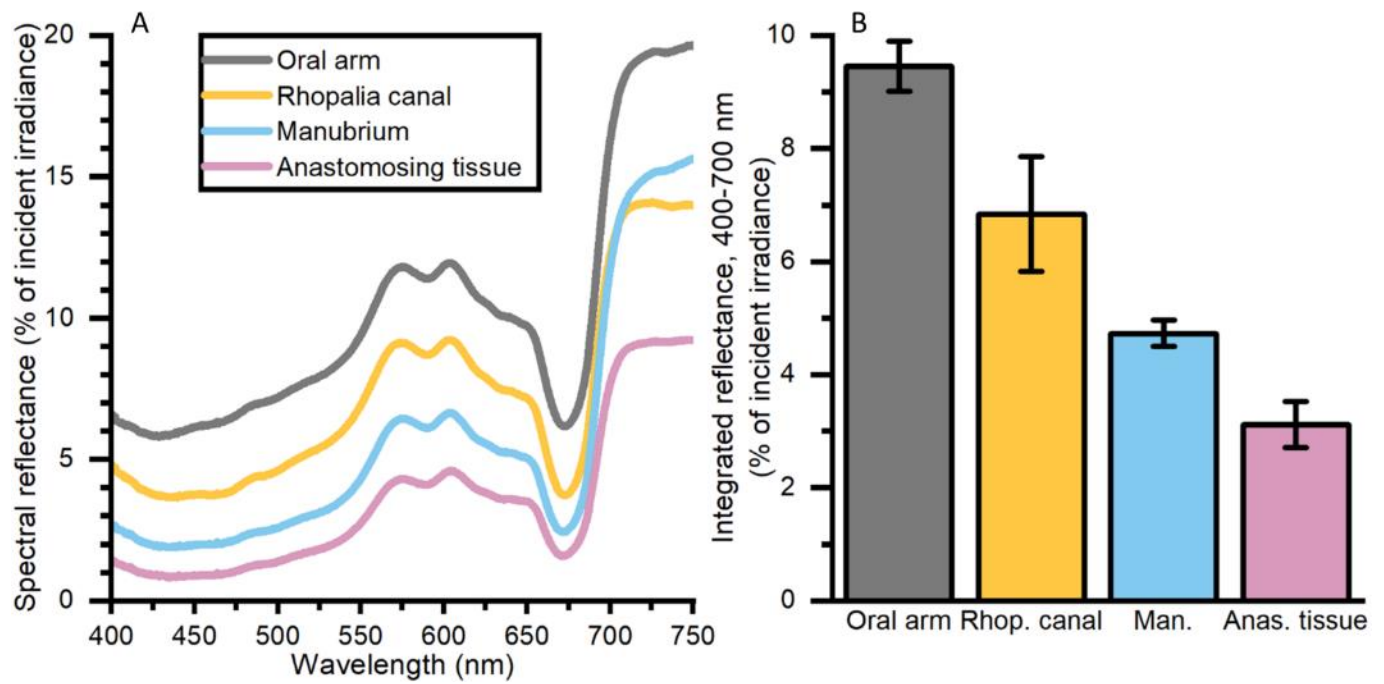


Figure 9 / Spectral reflectance (in % of incident irradiance) (A) measurements, and integrated reflectance (400-700 nm) (B) averaged for 4 AOIs depicting differing morphological tissue regions of one large *Cassiopea* medusa. Data represent mean  $\pm$ SEM ( $n = 3$  for each tissue type). For increased clarity standard errors are not shown in panel A, but are reflected in the  $\pm$ SEM shown for integrated values in panel B.

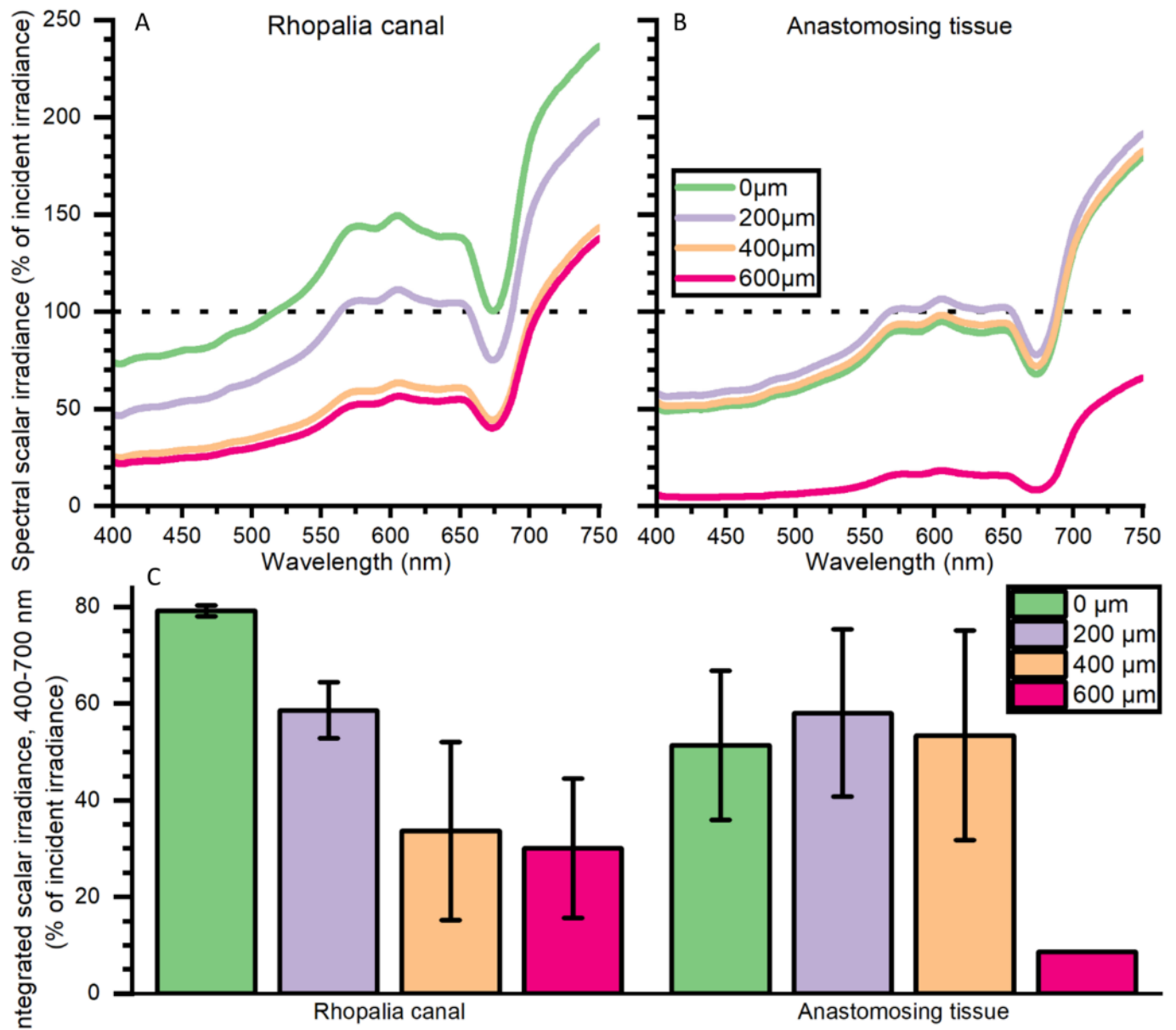


Figure 10 | Spectral scalar irradiance (in % of incident irradiance) measured near the subumbrella rhopalial canal (A) and anastomosing tissue (B), and integrated scalar irradiance (400-700 nm) (C). Data represent mean  $\pm$ SEM of 2 rhopalial canals and 3 anastomosing tissue areas (except for the 600  $\mu$ m). For increased clarity standard errors are not shown in panel A and B, but are reflected in the  $\pm$ SEM shown for integrated values in panel C.

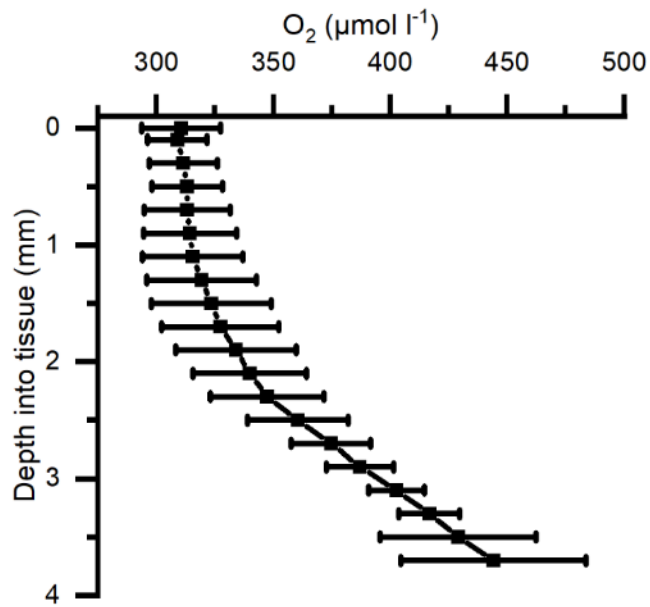


Figure 11 | Average of depth profiles of O<sub>2</sub> concentration in *Cassiopea* tissue measured under a photon irradiance (400-700 nm) of 300 μmol photons m<sup>-2</sup> s<sup>-1</sup> in the bell of a medusae. n = 3 biological replicates with 1 profile each.

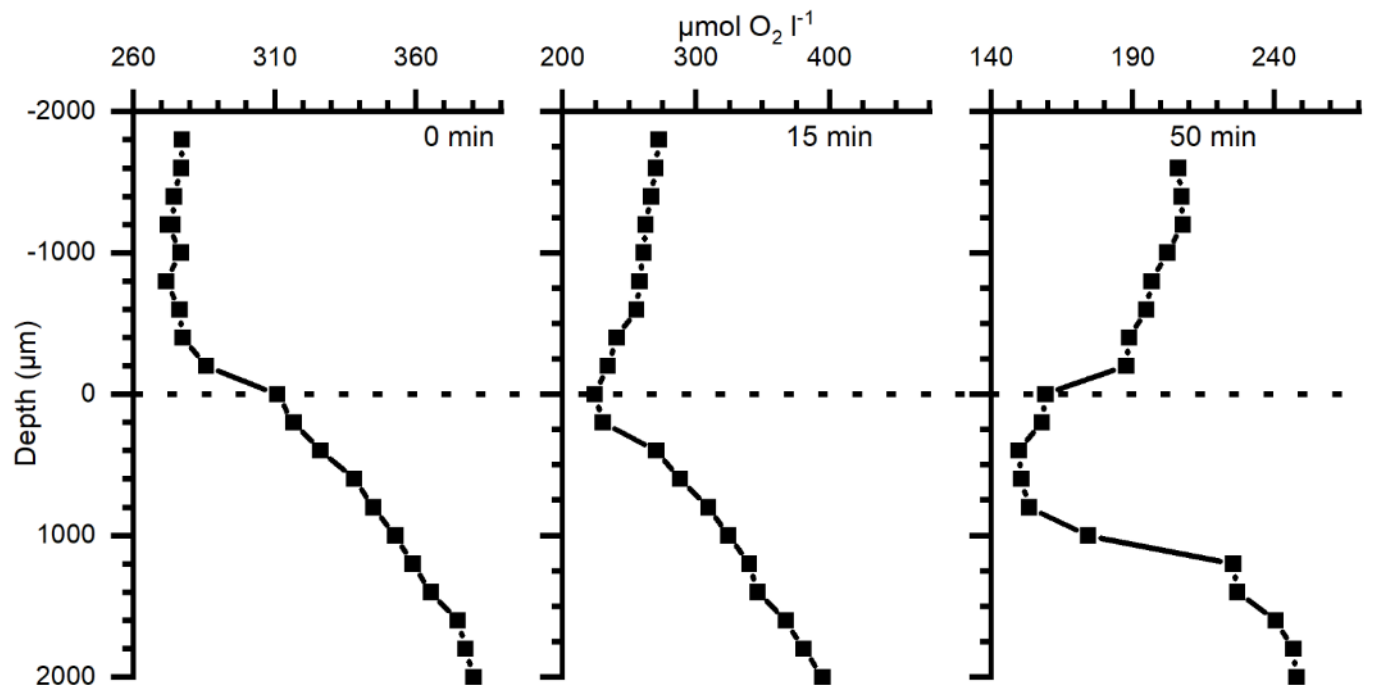


Figure 12 | Depth profiles of O<sub>2</sub> concentration in bell tissue of 3 different *Cassiopea* specimens (38-67 mm Ø) incubated in darkness for 0, 15, and 50 min, respectively (38, 67, and 63 mm Ø individual, respectively), prior to measurements. Zero depth indicates the tissue-water interface. Note differences in the x-axis scales.

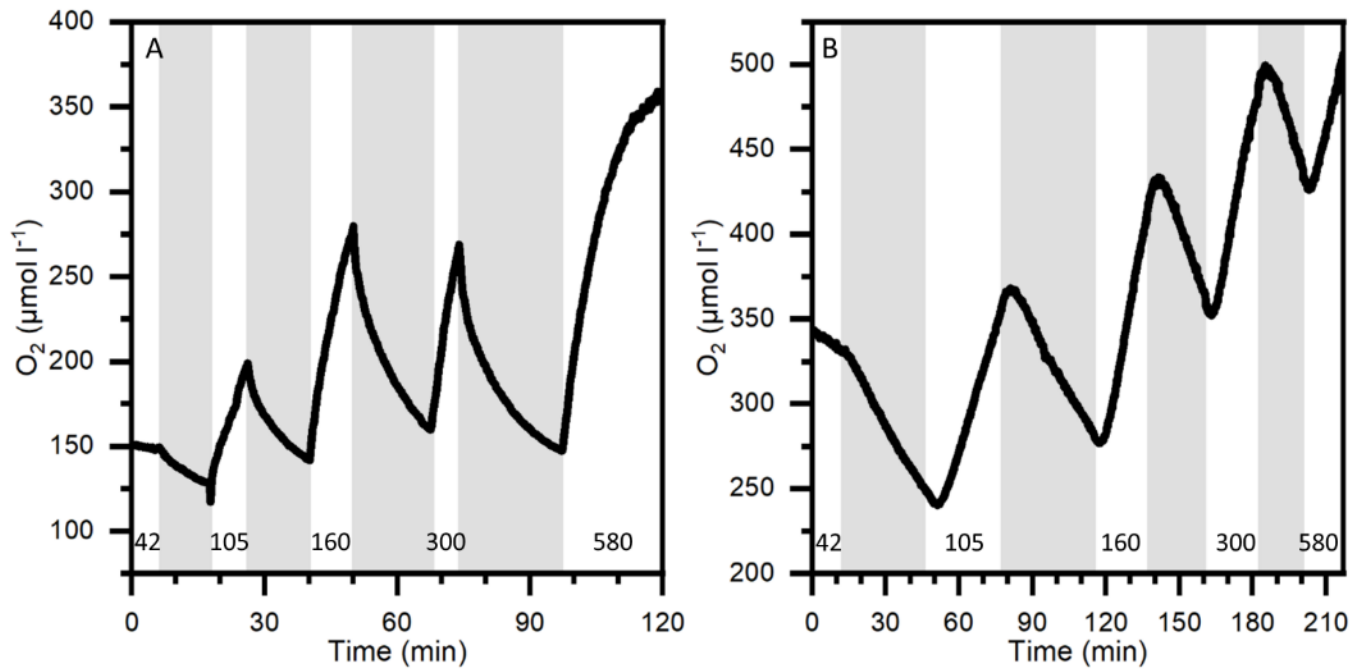


Figure 13 |  $O_2$  dynamics at 1 mm depth into the bell of a small medusa (A) and 3 mm into the bell of a large medusa (B) during light-dark shifts. Gray areas indicate dark shifts and white areas indicate photo periods of increasing incident photon irradiance (400-700 nm) noted with numbers in units of  $\mu\text{mol photons m}^{-2} \text{s}^{-1}$ . Note differences in x- and y-axes.

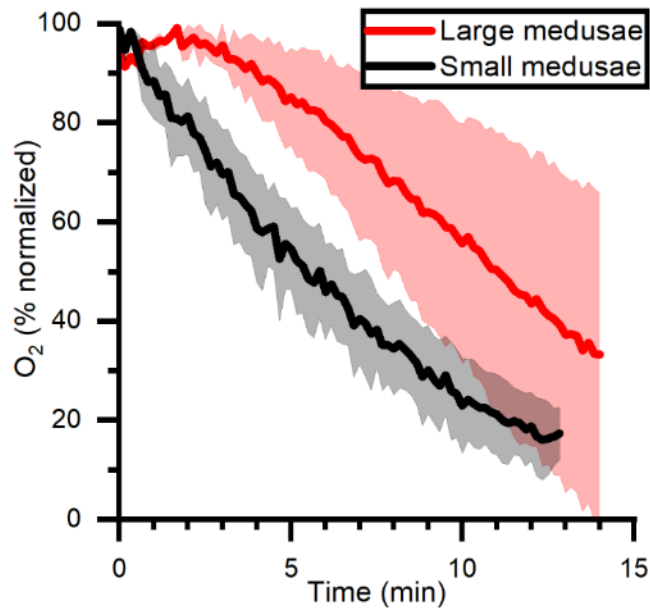


Figure 14 | O<sub>2</sub> dynamics measured in mid-bell mesoglea (roughly halfway deep in the bells) of large and small medusae from onset of darkness at 0 min, after a previous illumination with an incident photon irradiance (400-700 nm) of 580  $\mu\text{mol photons m}^{-2} \text{s}^{-1}$ . Data is normalized against maximum oxygen concentration measured in each medusa, and then averaged for large (n=2) and small (n=3) individuals  $\pm$ SEM.

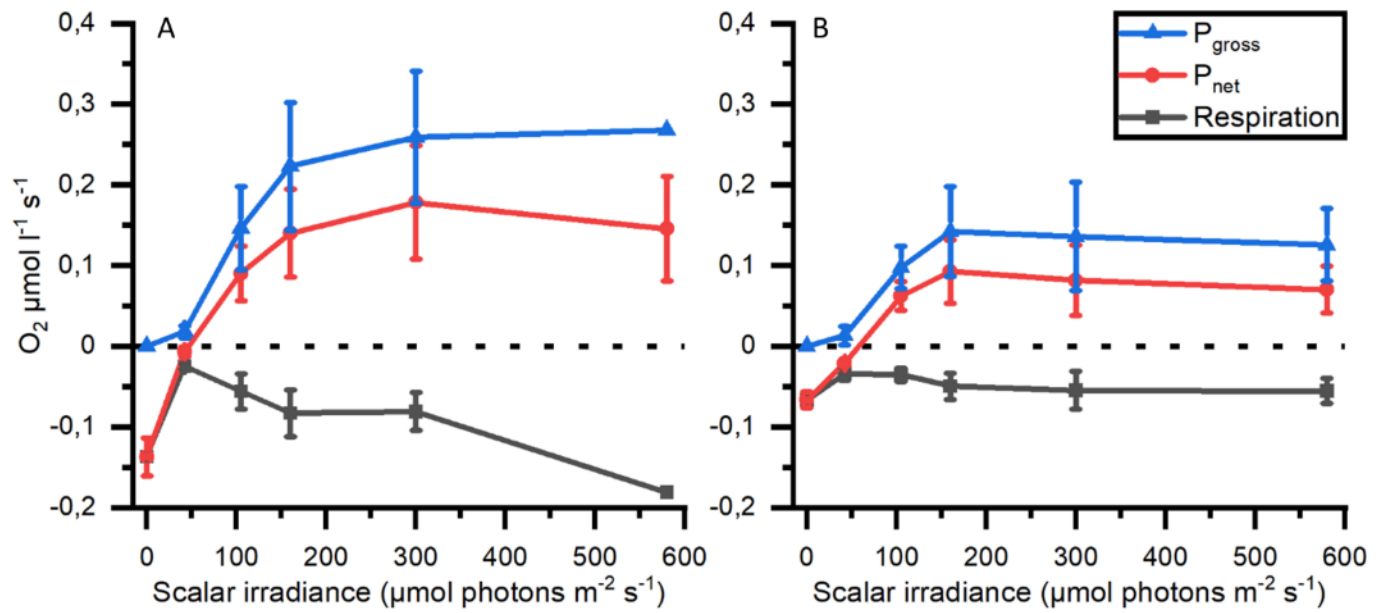


Figure 15 | Respiration, net ( $P_{\text{net}}$ ) and gross photosynthesis ( $P_{\text{gross}}$ ) measured mesoglea of small (A;  $n=3$ ) and large (B;  $n=2$ ) medusae as a function of photon scalar irradiance (400-700 nm).



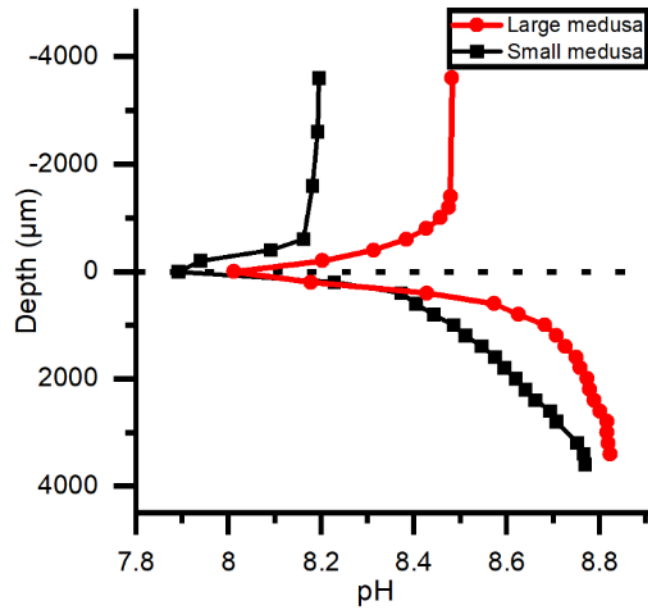


Figure 16 | pH depth profiles measured in the bells of a small and large medusae. Both individuals were kept under an incident photon irradiance (400-700 nm) of  $580 \mu\text{mol photons m}^{-2} \text{s}^{-1}$  light for >15 minutes and then in darkness for ~15 minutes before profiles were done.

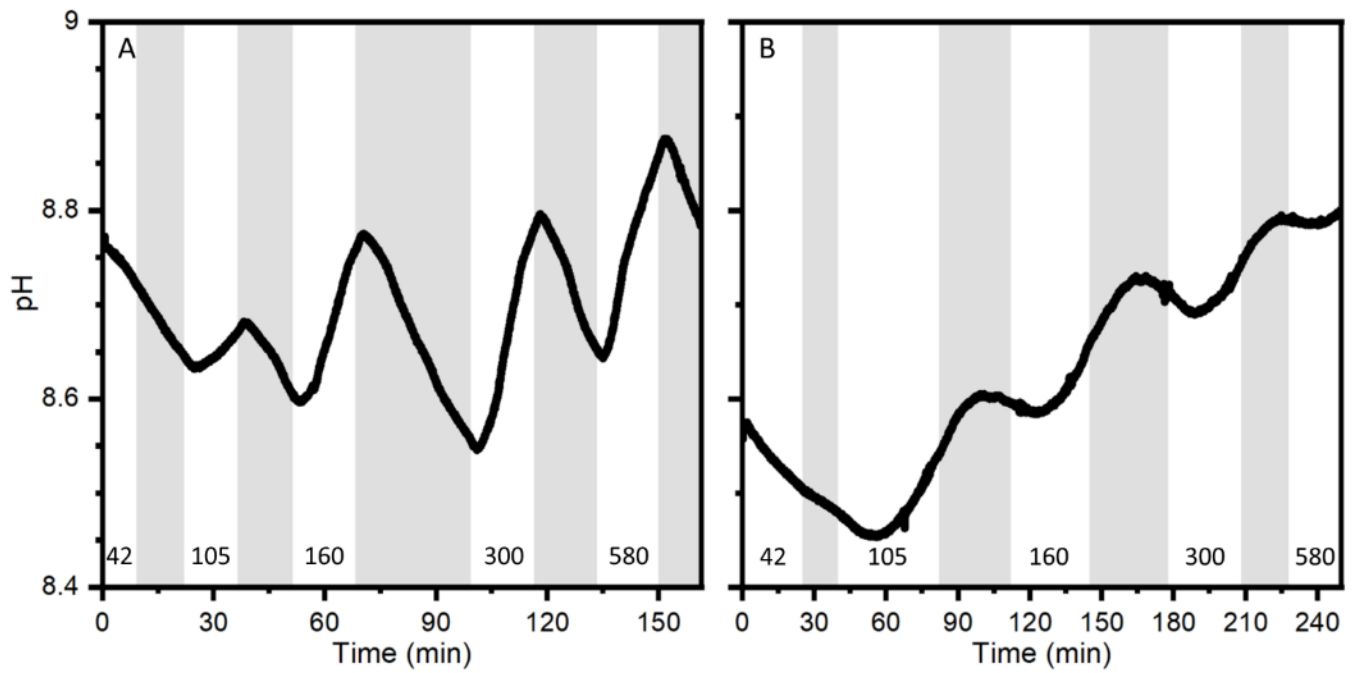


Figure 17 | pH dynamics measured with a pH microsensor positioned at a depth of 1.6 mm into the bell of a small medusa (A) and 2 mm into the bell of a large medusa (B) during experimental light-dark shifts. Gray areas indicate dark shifts and white areas indicate photo periods of increasing incident photon irradiance (400-700 nm) noted with numbers in units of  $\mu\text{mol photons m}^{-2} \text{s}^{-1}$ . Note difference in x-axes.

## Chapter 3: Non-invasive imaging of *Cassiopea* and investigation of inherent optical properties

### I. Context

Chapter 3 presents a completed manuscript that is intended for submission to Journal of Experimental Biology. In this chapter the Bauplan of *Cassiopea* medusa is investigated using non-invasive optical coherence tomography, and the optical microniches observed in *Cassiopea* is put into context of nutrient assimilation.

### Author contribution

NHL, SM, AM, and MK designed the experiment. NHL, SM, SB, and SLJ carried out experiments and data collection. NHL, SM, MK, and AM analyzed the data. All authors contributed to writing of the manuscript.

### II. Publication

# Non-invasive investigation of the morphology and optical properties of the upside-down jellyfish *Cassiopea* with optical coherence tomography

Niclas Heidelberg Lyndby<sup>1</sup>, Swathi Murthy<sup>2</sup>, Sandrine Bessette<sup>1</sup>, Sofie Lindegaard Jakobsen<sup>2</sup>,

Anders Meibom<sup>1,3</sup>, Michael Kühl<sup>2</sup>

<sup>1</sup>Laboratory for Biological Geochemistry, School of Architecture, Civil and Environmental Engineering, Ecole Polytechnique Fédérale de Lausanne, CH-1015 Lausanne, Switzerland

<sup>2</sup>Marine Biological Section, Department of Biology, University of Copenhagen, Strandpromenaden 5, DK-3000 Helsingør, Denmark

<sup>3</sup>Center for Advanced Surface Analysis, Institute of Earth Science, University of Lausanne, CH-1015 Lausanne, Switzerland.

### Abstract

The jellyfish *Cassiopea* rely on photosynthetic endosymbionts to provide inorganic carbon, but how holobiont morphology and optical properties affect the light microclimate and photosynthesis in symbiotic jellyfish remains largely unexplored. Here, we use optical coherence tomography (OCT) to study *Cassiopea* medusa morphology at high spatial resolution on live specimens. We include detailed 3D

reconstructions of external micromorphology, and show the spatial distribution of endosymbionts clustered in amoebocytes and white granules in the bell tissue. Furthermore, we use OCT data to extract inherent optical properties from light scattering white granules in *Cassiopea* and show that white granules enhance local light availability for symbionts in close proximity. Individual granules had a scattering coefficient of  $\mu_s = 200\text{-}300\text{ cm}^{-1}$ , and an anisotropy factor of  $g = 0.7$ , while large tissue regions filled with white granules had a lower  $\mu_s = 40\text{-}100\text{ cm}^{-1}$ , and  $g = 0.8\text{-}0.9$ . We combined OCT information with an isotopic labelling experiment to investigate the effect of enhanced light availability in whitish tissue regions. Algal symbionts located in whitish tissue exhibited significantly higher carbon fixation as compared to symbionts in anastomosing tissue (i.e., tissue without light scattering white granules). Our findings support previous suggestions that white granules in *Cassiopea* play an important role in the host modulation of the light-microenvironment.

**Keywords:** *Medusa, morphology, symbiosis, chlorophyll fluorescence, light scattering, optical properties*

## Introduction

Characterization of anatomical structures and morphology is important to understand the interplay between host light-modulation and photosymbiont spatial organization in complex holobionts, such as corals and other photosymbiotic cnidarians. External structures can be relatively easily identified using macro- and microscopic imaging in the visible wavelength range on intact individuals with various levels of preparation (Sivaguru et al. 2014, Shapiro et al. 2016). However, imaging deeper into tissue is challenging with conventional and laser scanning microscopes, where the observational depth is typically limited to a few hundred micrometers before absorption and scattering of light reduces image quality substantially, and fluorescent labelling of structures is often necessary to achieve sufficient contrast (Salih 2012). Invasive tissue clearing of fixed specimens can enhance light penetration for 3D reconstruction of intact whole organisms (Dekkers et al. 2019). However, serial sectioning in combination with light or electron microscopy is often necessary to obtain a combination of macrostructural observations and detailed information of internal organization (Colley & Trench 1985). This is both destructive and slow, and involves tissue sample preparation steps that can create artefacts in tissue organization (Huebinger et al. 2018, Loussert-Fonta et al. 2020).

In this context, optical coherence tomography (OCT) (Huang et al. 1991, Schmitt 1999, Fercher et al. 2003), which enables non-invasive *in vivo* imaging of live specimens using near infrared (NIR)

wavelengths, presents an attractive alternative imaging modality. OCT allows for high-resolution tomographic scanning of tissue in real time, and enables 3D reconstruction of large samples with a potential depth of penetration of several millimeters depending on the scattering properties of the sample (Schmitt 1999, Wangpraseurt et al. 2017b). Previous studies have utilized OCT for visualizing and quantifying structural characteristics such as surface area, volume and porosity in biofilms (Wagner et al. 2010, Depetris et al. 2021), terrestrial plants (Hettinger et al. 2000), and marine invertebrates (Speiser et al. 2016), including scleractinian corals (Wangpraseurt et al. 2017b, 2019).

The OCT measuring principle is analogous to ultrasound imaging and is based on the detection of directly backscattered light from refractive index mismatches in a sample, measured as the echo time delay and intensity of directly backscattered light from internal microstructures in materials or tissues (Fujimoto et al. 2000). OCT imaging uses low coherent NIR light to generate tomographic data composed of axial point measurements (A-scan) that are used to generate two-dimensional cross-sectional images (B-scan) or three-dimensional data cubes (C-scan) of backscattered photons using interferometry. Besides providing structural information from tomographic measurements of relative backscatter intensity, OCT systems can also be calibrated for absolute measurements of reflectivity. In combination with a theoretical bio-optical model based on an inverse Monte Carlo method (Levitz et al. 2010), calibrated OCT datasets can be used to extract optical properties, i.e., the scattering coefficient,  $\mu_s$  ( $\text{mm}^{-1}$ ) and anisotropy of scattering,  $g$  (where  $g = 1$  indicates completely forward scattered, and  $g = 0$  indicates isotropic scattering) from a sample. More details on the basic principle of OCT can be found elsewhere (Huang et al. 1991, Schmitt 1999, Fercher et al. 2003). Furthermore, we note that OCT can also be combined with spectroscopic measurements to obtain a wider range of optical parameters and higher spatial resolution (Spicer et al. 2019).

The optical properties in corals have received increased attention over the last decade, and both coral tissue and skeleton have been found to exhibit strong light scattering properties (Enríquez et al. 2005, 2017, Wangpraseurt et al. 2012, 2014a, Lyndby et al. 2016, Spicer et al. 2019). Host-produced fluorescent pigments (FPs) in particular enable cnidarians to enhance scattering of incident light in the tissue, and the backscatter of light from the coral calcium carbonate skeleton further enhances light capture and photosynthesis by the endosymbiotic dinoflagellate algae (Enríquez et al. 2005, Terán et al. 2010, Marcelino et al. 2013, Wangpraseurt et al. 2014a, 2017a, Swain et al. 2016, Lyndby et al. 2016). Wangpraseurt et al. (2017b) used OCT imaging for real-time quantification of tissue movement in coral polyps, providing insights into symbiont and FP movement and density. They demonstrated how optical

properties not only differ between tissue regions, but that tissue movement can lead to dynamic modifications of local optical properties of the coral tissue, potentially enhancing or reducing photon absorption (Wangpraseurt et al. 2019). However, we are not aware of such use of OCT for investigating other cnidarians.

The so-called up-side-down jellyfish *Cassiopea* is currently promoted as an important model system for cnidarian photo-symbiosis (Ohdera et al. 2018, Medina et al. 2021). *Cassiopea* hosts photosynthetic algae belonging to the same dinoflagellate family (Symbiodiniaceae) as symbionts in scleractinian corals (Lampert 2016). Adult *Cassiopea* medusa live mostly in shallow benthic environments, where they position themselves up-side down on the sediment basking in the sun to expose their photosynthesizing algae that supplement the carbon demand of the heterotrophic host with autotrophically acquired carbon (Welsh et al. 2009, Freeman et al. 2016, Lyndby et al. 2020b). The symbiont algae are found concentrated in the host tissue on the oral side of the bell and in oral arms of the medusa (Colley & Trench 1985, Estes et al. 2003). *Cassiopea* exhibit a range of colors from purple-blue to reddish (Lampert et al. 2012, Lampert 2016) but most commonly have a blue pigmentation associated with the bell disc and oral vesicles (Blanquet & Phelan 1987), which was recently identified as Rhizostomins (Lawley et al. 2021). Another common trait of adult *Cassiopea* is the whitish appearance of certain tissue regions containing granules, which is most pronounced in the oral arms and stretches radially from manubrium to the bell margin and rhopalia (Bigelow 1900). The function of the white granules in *Cassiopea* is still unknown, but it has been suggested to play a role in the mitigation of photodamage and enhancement of photosynthesis (Blanquet & Phelan 1987, Phelan et al. 2006), where the white granules and colored pigments in *Cassiopea* might serve similar functions to that of the skeleton and host pigments in corals.

Here, we used non-invasive OCT imaging to i) visualize the structure of live *Cassiopea* sp. medusae, and ii) provide details of specific anatomical features in intact, living specimens as well as cut-out samples from living specimens. We identified two highly heterogeneous tissue regions in the bell, namely the rhopalia canals with white granules and the anastomosing tissue primarily containing clusters of symbionts. Optical properties were extracted from these regions using the OCT data, and a labelling experiment using stable isotopes of  $^{13}\text{C}$ -bicarbonate and  $^{15}\text{N}$ -ammonium was conducted to test if the different optical properties altered photosynthetic performance of symbionts found in the two tissue regions.

## Methods

### *Cassiopea* husbandry and preparation

*Cassiopea* sp. medusae acquired from DeJong Marinelife (Netherlands) were cultivated at the Marine Biology Section (MBS), University of Copenhagen (Helsingør, Denmark) in a 50 L aquarium. Medusae were fed 5 times per week with recently hatched *Artemia* nauplii, and supplemented with AF Amino Mix (Aquaforest) 2-3 times per week. Medusae were kept at 25 °C in artificial seawater (ASW) with a salinity of 35 ppt and a pH of 8.2. Water was recycled inside the tank using a small internal filter, as well as UV light filtration. Illumination was maintained with a programmable LED aquarium lamp (Triton R2, Pacific Sun) running a 12/12-hour day/night cycle with a downwelling photon irradiance (400-700 nm) of  $350 \mu\text{mol photons m}^{-2} \text{s}^{-1}$ , as measured just above the water surface using a calibrated spectroradiometer (MSC-15, GigaHertz-Optik). We used *Cassiopea* medusae in a size range from 7 mm up to several cm in diameter to scan the internal and external anatomy of the *Cassiopea* medusa life stage.

### Optical Coherence Tomography

We used a spectral domain OCT imaging system (Ganymede II, Thorlabs GmbH) comprised of a base unit with a non-coherent NIR light source (930nm; GAN611) and a scanning system (OCTG9) fitted with either the OCT-LK3-BB lens kit (field of view 10×10 mm, lateral resolution 8  $\mu\text{m}$ , effective focal length 36 mm) for complete medusa scans, or an OCT-LK2-BB kit (field of view 6×6 mm, lateral resolution 4  $\mu\text{m}$ , effective focal length 18 mm) for closeup scans with a higher resolution. The axial resolution was 5.8  $\mu\text{m}$ . For imaging, animals and cut-out tissue samples were kept in a small petri dish submerged in either filtered ASW or 100 % glycerol, typically with a distance of 4 mm between the liquid and tissue surface. Prior to the OCT imaging, animals were anaesthetized with  $\text{MgCl}_2$  (50 % w/v in ASW) that was added dropwise to the petri dish until the individual stopped pulsing. Cut-out tissue, if not stable in a favorable orientation relative to the OCT system, was fixed with hypodermic needles onto a cork surface covered with dark-cloth to reduce light reflection.

### Extraction of optical parameters using OCT

Optical properties like the scattering coefficient  $\mu_s$  [ $\text{cm}^{-1}$ ] and the anisotropy of scattering  $g$  can be estimated from OCT scans of biological tissues using theoretical models of light propagation based on the inverse Monte Carlo method (Levitz et al. 2004, Thrane et al. 2005). A more detailed description of optical parameter extraction from OCT scans of tissue can be found elsewhere (Fercher et al. 2003, Wangpraseurt et al. 2019).

Briefly, OCT B-scans were acquired with a resolution of 581×1024 pixels, over a fixed depth interval of 2.8 mm, and variable distance in the X-plane. The setup was optimized to yield the highest signal at a fixed distance of 0.4 mm from the top of the scan. The OCT reflectivity (R) was calibrated before measurements using homemade reflectance standards with an immersion oil-glass, a water-glass, and an air-glass interface. R values from the standards were determined using Fresnel's equation:

Eq. 1: 
$$R = \left( \frac{n_1 - n_2}{n_1 + n_2} \right)^2$$

using the refractive index (n) for air (1), water (1.33), immersion oil (1.46), and quartz glass (1.52). The OCT signal (in decibel, dB), from the samples, was then converted to the depth-dependent R via a linear fit of  $\log_{10}(R)$  versus OCT intensity values (see Wangpraseurt et al. 2019 for details).

Calibration of the focus function of the objective lens was performed by measuring the OCT signal fall off, in steps of 0.1 mm, from either side of the focal plane ( $z = 0.4$  mm) to  $z = 0$  and 0.8, respectively. The signal loss from the focal plane follows an exponential decay function. The determined R values from the sample scans were corrected by dividing with the exponential fit. Then the corrected R values were plotted against sample depth (z, distance from focal volume) and fitted to the exponential decay function:

Eq. 2: 
$$R(z) = \rho \times e^{-\mu \cdot z}$$

where  $\rho$  (dimensionless) is the light intensity and  $\mu$  is the signal attenuation ( $\text{cm}^{-1}$ ) from the focal volume. The fit was considered satisfactory if  $R^2 > 0.5$ . The first few pixels from each scan were excluded due to high reflectivity at interface, arising from the refractive index mismatch between the water and epidermis.

Using the grid method (Levitz et al. 2010), values of  $\rho$  and  $\mu$  were matched to  $g$  and  $\mu_s$  based on the theory described in other previous studies (Samatham et al. 2008, Wangpraseurt et al. 2019). It was assumed that the *Cassiopea* tissue absorption at 930 nm was negligible and the absorption was dominated by water ( $\mu_a = 0.43 \text{ cm}^{-1}$ ). The effective numerical aperture (NA) was 0.11. The refractive index of the tissue was estimated to be 1.473 (see results and discussion).

The targeted areas for extraction of optical properties in *Cassiopea* tissue were i) bell tissue with white granules (along rhopalia canals), and ii) symbiont clusters in anastomosing tissue. Scans in ASW were done on intact tissue and tissue, where the epidermis was removed by gently peeling the epidermis from the underlying bell using tweezers.



Raw OCT files, and selected animated figures, for figures 1-6 can be found in the supplementary information.

### Variable chlorophyll fluorescence imaging

The absorptivity and PSII quantum yield in the exposed bell tissue areas on each medusae were imaged with a variable chlorophyll fluorescence imaging system using blue LED's (I-PAM, IMAG MIN/B, Walz; (Ralph et al. 2005) providing weak, non-actinic measuring light pulses, strong saturating light pulses, as well as actinic light levels of known photon irradiance. All measurements of variable chlorophyll fluorescence were performed, and AOIs drawn, by using the software ImagingWin (v2.41a, Walz).

For this, medusae were individually dark acclimated for 15 minutes in a petri dish filled with ASW. During dark acclimation, the absorptivity was measured. The maximal PSII quantum yield ( $F_v/F_m$ ) was then measured by applying a strong saturation pulse ( $>3000 \mu\text{mol photons m}^{-2} \text{s}^{-1}$  for 0.8 s). Rapid light curves (RLCs), i.e., relative PSII electron transport as a function of photon irradiance, were subsequently measured by measuring the effective PSII quantum yield,  $Y(II)$ , and the relative electron transport rate,  $rETR (= Y(II) \times PAR)$ , at a range of increasing photon irradiance levels of photosynthetically active radiation, PAR (400-700 nm;  $0-700 \mu\text{mol photons m}^{-2} \text{s}^{-1}$ ).

The surface areas of 6 areas of interest (AOI) on the exposed bell of each medusae were estimated with the built-in analysis function using the ImagingWin software. Pixels were converted to an estimated surface area:

Eq. 3: 
$$P \times 0.0025 = A \text{ mm}^2$$

where P is the number of pixels in a given AOI, 0.0025 is the estimated conversion factor from the software, and A is the final area in  $\text{mm}^2$ . The AOIs were chosen based on visible white granules along rhopalia canals and the anastomosing tissue connecting the canals.

### Isotopic pulse labelling experiment

#### Experimental setup

A tank with  $\sim 10$  L of deionized water was placed on top of 3 magnet stirrers (RCT basic, IKA GmbH). A heater and a small water pump were fitted in the bath to keep water homogenously at  $25 (\pm 0.5) ^\circ\text{C}$ . A white LED lamp (KL2500 LED; Schott AG) equipped with 3-furcated fiber guide was used for homogenous illumination over each magnet stirrer. Each fiber guide was fitted with a collimating lens, and light was adjusted to an incident photon irradiance of  $350 \mu\text{mol photons m}^{-2} \text{s}^{-1}$  (400-700 nm), as measured with a calibrated spectroradiometer (MSC-15, GigaHertz Optik). The photon irradiance was chosen based on the

average RLCs (Figure 26c), where all individuals showed light saturation above 500  $\mu\text{mol photons m}^{-2} \text{s}^{-1}$ . Isotopic labelling was done in 100 mL plastic beakers placed in the thermal bath and fitted with a magnet bar, as well as a mesh at the bottom to separate medusae from the rotating magnet (200 RPM).

#### Water preparation and pulse labelling

Prior to the labelling experiment, 1 L of isotopically enriched ASW was prepared: Filtered ASW (35 ppt, 8.2 pH; 0.2  $\mu\text{m}$ , Millipore) was stripped of dissolved inorganic carbon by lowering pH to < 3 with 1M HCl, and was then flushed with atmospheric air over night. The ASW was then enriched with 3mM  $\text{NaH}^{13}\text{CO}_3$  (99 atom%, Sigma Aldrich), brought back up to experimental pH (8.2) with 1M NaOH, and 3 $\mu\text{M}$   $^{15}\text{NH}_4\text{Cl}$  (99 atom%, Sigma Aldrich) was added. The mix was left to equilibrate with the experimental temperature of the thermal bath (25 °C) before pulse labeling began.

Three *Cassiopea* medusae of roughly 3.5-4 cm in diameter were chosen for the labelling experiment. For each medusa; 3-4 oral arms were removed using a tweezer and razor blade in order to expose one half of the medusa bell surface area. Medusae were subjected to 6 hours of pulse labeling in 80 mL of isotopically enriched ASW, with a change of isotopically enriched ASW every 2 hours. At the end of pulse labelling, one quarter of the bell from each medusae was chemically fixed in 10 mL of 2.5 % [v/v] glutaraldehyde (Electron Microscopy Sciences), 4 % [v/v] paraformaldehyde (Electron Microscopy Sciences), and 0.6 M sucrose (Sigma-Aldrich) mixed in 0.1 M Sørensen phosphate buffer. Chemically fixed *Cassiopea* samples were kept at room temperature for 2 hours and then stored at 4 °C in fixative until further processing.

#### Histological sectioning for NanoSIMS analyses

A detailed description of sample preparations can be found in (Lyndby et al. 2020b). Briefly, isotopically labelled animals had a piece of the bell cut out including both anastomosing tissue and the rhopalia canal with visible white granules. The cut-out pieces were divided into the two respective tissue regions, and a smaller piece roughly halfway between manubrium and margin was extracted and embedded in Spurr's resin. Semi-thin histological sections with a thickness of 200 nm were then cut with a Ultracut S microtome (Leica Microsystems), placed on glass slips and gold coated with a layer of 12.5 nm gold (Leica EM SCD050, Leica Camera AG) for NanoSIMS imaging.

#### NanoSIMS image acquisition

Isotopic imaging of semi-thin histological sections was performed with a NanoSIMS 50L instrument (Hoppe et al. 2013). Images (40 $\times$ 40  $\mu\text{m}$ , 256 $\times$ 256 pixels, 5000  $\mu\text{s}$ /pixel, 5 layers) were obtained with a 16 KeV  $\text{Cs}^+$  primary ion beam focused to a spot-size of about 120 nm (with a beam current of 2.2 pA).

Secondary ions ( $^{12}\text{C}_2^-$ ,  $^{13}\text{C}^{12}\text{C}^-$ ,  $^{12}\text{C}^{14}\text{N}^-$ , and  $^{12}\text{C}^{15}\text{N}^-$ ) were counted in individual electron-multiplier detectors at a mass resolution of about 9000 (Cameca definition), sufficient to resolve all potential interferences in the mass spectrum (Lechene et al. 2006, Clode et al. 2007, Pernice et al. 2015, Gibbin et al. 2018, Nuñez et al. 2018).

Isotopic images were analyzed using the software L'IMAGE developed by Dr. Larry Nittler. Contours were drawn in each image around the epidermis as well as around individual amoebocytes and dinoflagellate cells. The epidermis in each NanoSIMS image was treated as a single region of interest (ROI;  $n = 1$ ). Similarly, amoebocytes were treated as one ROI per image unless their cell clusters were clearly separated. Due to low amounts of symbionts in the exumbrella tissue, NanoSIMS analyses only include subumbrella tissue. Drift-corrected maps of  $^{13}\text{C}$ - and  $^{15}\text{N}$ -enrichment were obtained from the count ratios  $^{13}\text{C}^{12}\text{C}^-/^{12}\text{C}_2^-$  and  $^{15}\text{N}^{12}\text{C}^-/^{14}\text{N}^{12}\text{C}^-$ , respectively. Measured enrichments were expressed in delta notation:

$$\text{Eq. 4: } \delta^{13}\text{C} (\text{‰}) = \left( \frac{R_{\text{enriched}}}{R_{\text{control}}} - 1 \right) \times 1000$$

$$\text{Eq. 5: } \delta^{15}\text{N} (\text{‰}) = \left( \frac{R_{\text{enriched}}}{R_{\text{control}}} - 1 \right) \times 1000$$

where  $R_{\text{enriched}}$  and  $R_{\text{control}}$  are the count ratios of an enriched sample and a control (i.e., unlabeled) sample, respectively. Total numbers of technical replicates (ROIs) are provided in Supplementary table 1.

### Symbiont density estimation

The density of symbionts was estimated from bell tissue corresponding roughly to AOIs drawn in ImagingWin (Walz GmbH). For each cut-out section, the subumbrella epidermis was carefully peeled off using a pair of tweezers, leaving the thick mesoglea (bulk mass of the bell) with the ex-umbrella epidermis still attached; simply referred to as “mesoglea” from this point. The subumbrella epidermis and the mesoglea were analyzed separately by homogenizing the tissue in 1.5 mL of filtered (0.45  $\mu\text{m}$ ) ASW using a T10 Standard Ultra Turrax handmixer (IKA) until samples were completely homogenized. Then 1 mL of the tissue slurry was transferred to a Sedgewick-rafter cell S52 (Pyser-SGI), and dinoflagellate cells were counted in 10 random squares on a microscope (AxioStar Plus, Zeiss). A total of 3 biological individuals were used, each of which 6 tissue regions were extracted (3 rhopalia canals and 3 anastomosing tissue regions).

### Statistical analyses

We used R (version 4.0.5) with the packages nlme (version 3.1-157) to perform statistical analyses. Linear mixed model (LMM) analyses were used to test the relationship between isotopic enrichment in

*Cassiopea* holobiont compartments in 2 bell tissue regions (near rhopalia canals and in anastomosing tissue) taking into account the biological replicate as a random factor.  $^{13}\text{C}$  enrichment data for amoebocytes, and  $^{15}\text{N}$  enrichment data for symbionts and host epidermis were square root transformed to achieve normality.

## Results and Discussion

### Imaging *Cassiopea* morphology

Due to the near-neutral buoyancy of *Cassiopea* jellyfish, even small vibrations during OCT imaging can cause the sample to move, creating distortion in the scans. Scanning speed and reference light intensity was thus adjusted to achieve a relative short scan-duration without sacrificing signal intensity. The field of view (FOV 7×7×2.8 mm; X-Y-Z) was adjusted to exactly cover the animal diameter, and the number of pixels in each direction was kept to a minimum (350×350×1024 pixel; X-Y-Z) (Figure 18a). The scan pattern resulted in a voxel size of 20×20×2.74  $\mu\text{m}$  (X-Y-Z). Given that the average diameter of dinoflagellate symbionts found in *Cassiopea* are typically around 10  $\mu\text{m}$  (Fitt 1985, Biquand et al. 2017), this voxel size provided sufficient resolution to identify symbiont clusters in form of amoebocytes (that typically host >10 cells per unit, e.g., Lyndby et al. 2020b), even from complete specimen scans (Figure 18b).

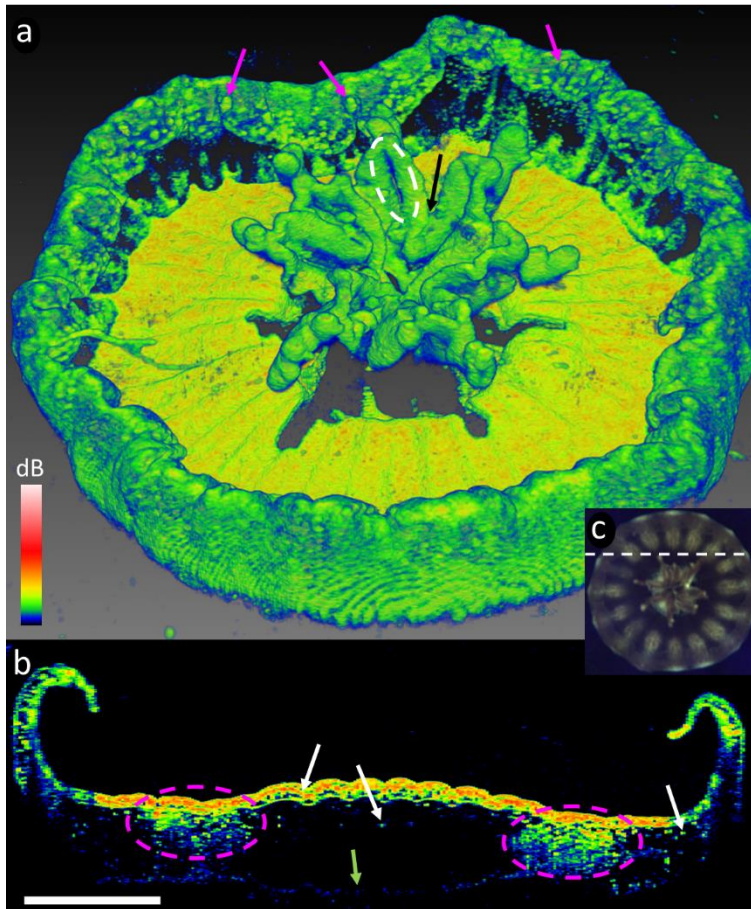


Figure 18 | (a) 3D scan (C-scan) of an entire juvenile *Cassiopea* sp. medusa, using a FOV of  $7 \times 7 \times 2.8$  mm (X-Y-Z), a resolution of  $350 \times 350 \times 1024$  pixels, giving a voxel size of  $20 \times 20 \times 2.74$   $\mu\text{m}$ . Rhopalia can be seen along the bell rim (purple arrows), and first oral arm bifurcation (black arrow) and an oral groove (white dashed circle) are clearly visible on the oral arms. (b) Tomographic cross section (B-scan) in the XZ plane through the bell, revealing the *in vivo* distribution of dense symbiont clusters underneath the subumbrella epidermis and diffusely spread deeper in the bell (white arrows), and large patches of white granules (purple dashed circles) underneath epidermis. A faint line of the exumbrella epidermis is visible at the bottom (green arrow). (c) Overview photo of the animal under OCT observation, the dashed white line indicates the B-scan presented in (b). Scale bar represents 1 mm. An animated 3D representation and the raw OCT file can be found in the supplementary information.

Externally, rhopalia were visible along the bell margin, and the first oral arm bifurcation and groves were clearly visible. Individual arms showed signs of vesicles forming apically, while digitata were not yet present (Muffett et al. 2022, e.g. Jordano et al. 2022) (Figure 18a). The bell-disk surface is not perfectly flat, but appears ridged in a radial pattern, possibly due to the musculature lining the subumbrella epidermis (Blanquet & Riordan 1981). Shading is apparent from oral arms and the marginal lobe reaching in over the bell disc, and the OCT generally did not manage to penetrate through the entire animal system from sub- to exumbrella epidermis due to multiple scattering effects degrading the contrast with depth. Internally, symbiont clusters and white granules were found in high densities near the subumbrella

epidermis (e.g., Estes et al. 2003, Lyndby et al. 2020b), and white granules can be seen extending further down into the exumbrella mesoglea along rhopalia canals (Figure 18b).

Changing to a higher magnification objective, we could zoom in on the above-mentioned structures to reveal more details, while also gaining more non-invasive information on the internal tissue organization of *Cassiopea*. We used both intact animals and cut-out tissue regions from multiple specimens of various sizes to scan a broad range of anatomical structures at different growth stages.

Rhopalia are specialized eyespots in Medusozoa that allow medusa to detect light and orientate themselves in the water column (Martin 2002, Kayal et al. 2018). *Cassiopea* have on average 16 rhopalia distributed along the bell margin (Bigelow 1900). Closeup scans with OCT showed that these eyespots are well nested between two marginal lappets along the rim (Figure 19a-c). Rhopalia canals are major canals of the gastric network extending from the center of the bell, out towards the rhopalia (Bigelow 1900) (Figure 19d, e). Cross sectional scans near one of the rhopalia showed that these major canals fork into two canals, each reaching out into a marginal lappet around the rhopalia (Figure 19d, e).

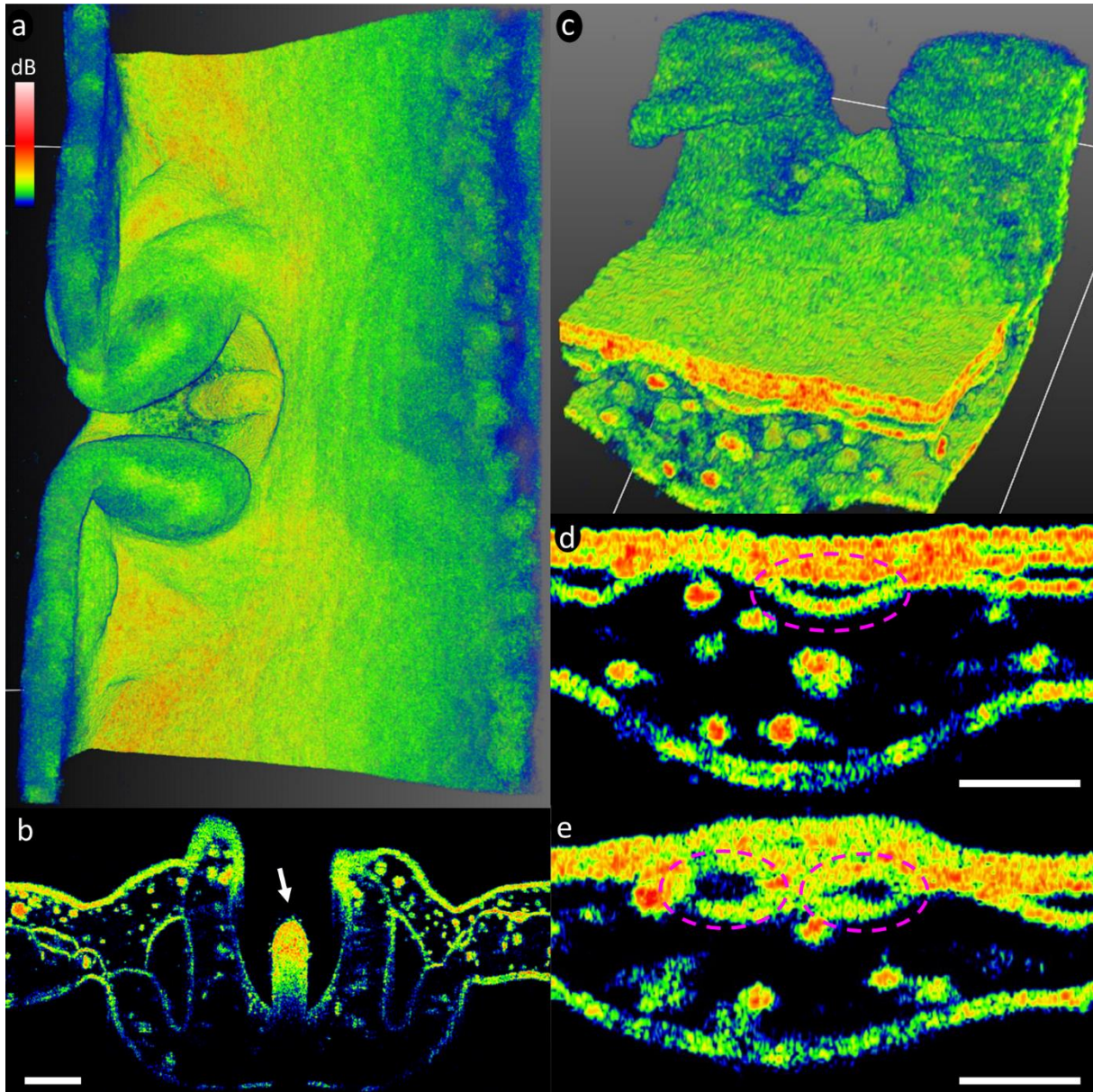


Figure 19 | Rhopalia, the eyespots of *Cassiopea* medusae of ~4 cm (a) and ~1 cm (c) in diameter. (b) The rhopalia were highly scattering of NIR light and appear almost solid (white arrow). (d) The rhopalia canal can be observed running out to the base of the rhopalia (purple dashed circles), before splitting into two canals that reach out into the marginal lappets on each side of the rhopalia (e). Throughout the scans, clusters of symbionts and white granules were diffusely spread out in the bell margin and marginal lappets along the rhopalia canal and into the bell margin. Scale bars represent 200  $\mu\text{m}$  in panel b, and 100  $\mu\text{m}$  in d-e. High resolution scans were performed with the LSM02 objective mounted on the OCT system.

Oral arms are highly branched at the center of the bell (Figure 20a). They typically occur in 4 pairs in *Cassiopea*, and each arm harbors secondary mouths and vesicular appendages. Vesicular appendages could be seen containing clusters of cassiosomes ready for deployment to catch prey (Ames et al. 2020) (Figure 20b). Cassiosomes are snared off from the vesicular epidermis in amorphous ‘popcorn’ shaped

tissue balls, with newly developing cassiosomes being formed underneath fully developed ones (Ames et al. 2020). However, it was not possible to confidently discern individual cassiosomes underneath the surface of the cluster, possibly due to the accumulated layers of dermis from each individual cassiosome, greatly lowering scan penetration depth (Figure 20b).

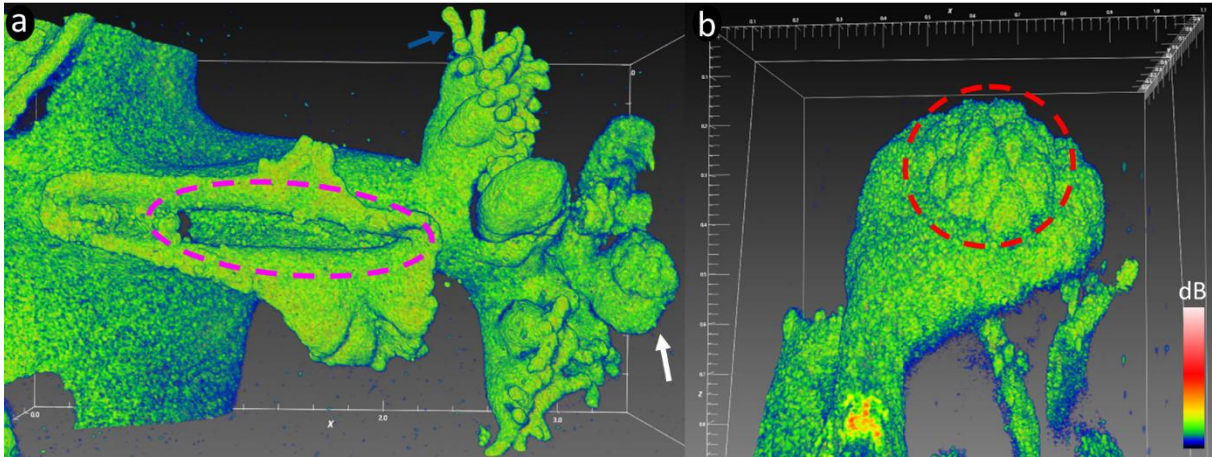


Figure 20 | (a) Oral arm with oral groove (purple dashed circle; ~10 mm in diameter). Sectional scans of the arm showed that the oral groove extended into the arm and further into the manubrium (not shown here). Oral vesicles (white arrow) were found apically on the arm, along with secondary mouths covered in frigid digitata (blue arrow). (b) closeup of vesicle with a developing cluster of cassiosomes (red dashed circle). Scale bars in mm.

### Improving depth penetration

During our OCT imaging work, we identified several factors that decreased the signal penetration. Host epidermal tissue, symbionts, and white granules all greatly scattered the NIR light from the OCT light source. To reduce the OCT signal loss at the upper tissue interface, we matched the refractive index of the surrounding medium to the epidermis in *Cassiopea*. Glycerol has a refractive index of 1.473, and submerging a piece of tissue in pure glycerol demonstrated that the *Cassiopea* epidermis has a very similar refractive index, thus improving OCT imaging (Figure 21a). Sectional scans of a vesicular lappet clearly showed the entire structure, and revealed a cavity in the center of the lappet (Figure 21b). Contrary to tissue scanned in water, where the endodermis/gastrodermis appeared thin or transparent, the endodermis of the lappet cavity appeared much clearer due to less backscattering in the epidermis. Individual symbiont clusters also became more distinctly visible throughout the lappet system when imaged in pure glycerol (Figure 21).



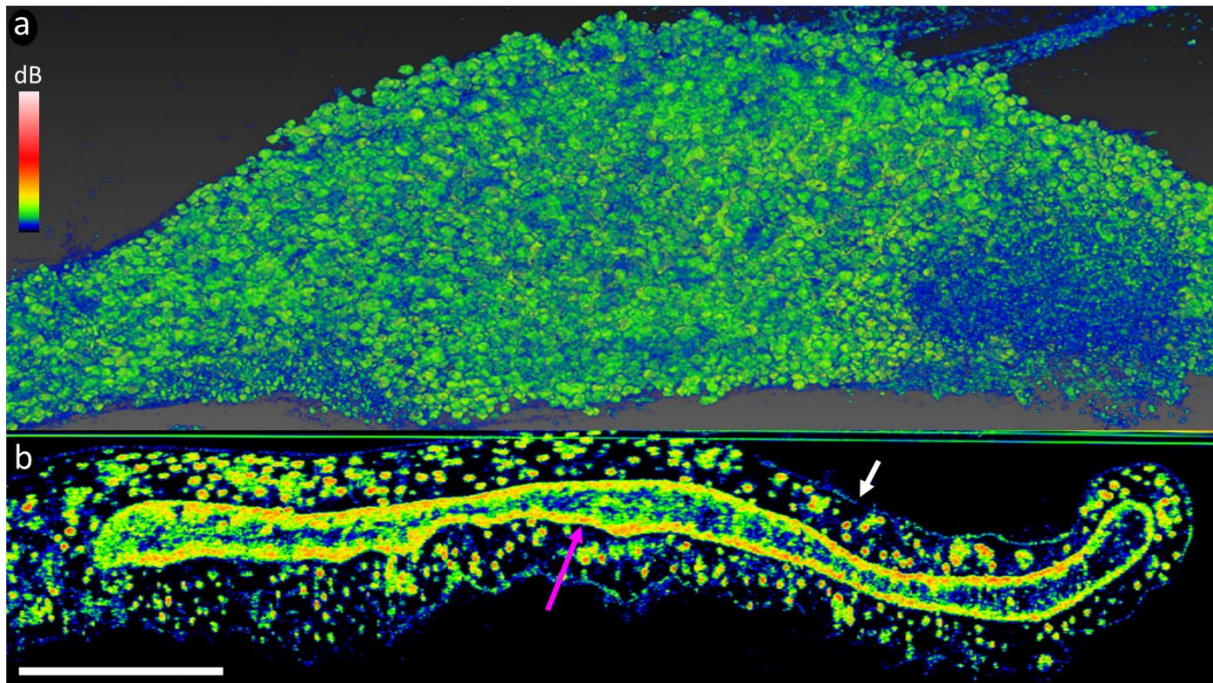


Figure 21 | (a) Overview of an intact vesicular lappet submerged in pure glycerol. The refractive index of glycerol and *Cassiopea* epidermis match closely, making the epidermis near-invisible and revealing underlying dispersed clusters of symbionts in the mesoglea. (b) Cross-sectional scan of the lappet. The epidermis was still faintly visible (white arrow). The endodermis (purple arrow) was much more distinct compared with images in water, due to the refractive mismatch between the endodermis and mesoglea in the lappet. The lappet clearly exhibits a closed cavity that does not extend back into the oral arm. What this cavity consists of, or if symbionts are present inside, remains to be studied in further detail. Scale bar represents 500  $\mu\text{m}$ .

While pure glycerol matches the refractive index of the epidermis well, the high viscosity of glycerol makes it difficult to image larger samples, and submerging intact medusae in glycerol did not improve depth penetration due to water and mucus sticking to the surface of the animal, which resulted in lower signal penetration and contrast.

To explore the deeper layers of the bell, we cut a piece of bell from a medusa and then carefully removed the subumbrella epidermis and mesoglea using a pair of fine tweezers. Removing the subumbrella epidermis greatly improved the OCT depth penetration, because the symbiont cell clusters and the epidermis were the main sources of light scattering in these anatomical structures (Figure 22a). When the tissue was cut, grabbing and ripping off the subumbrella epidermis proved easy, and even kept parts of the exumbrella gastrodermis from radial canals still visibly attached to the exumbrella mesoglea (Figure 22b).

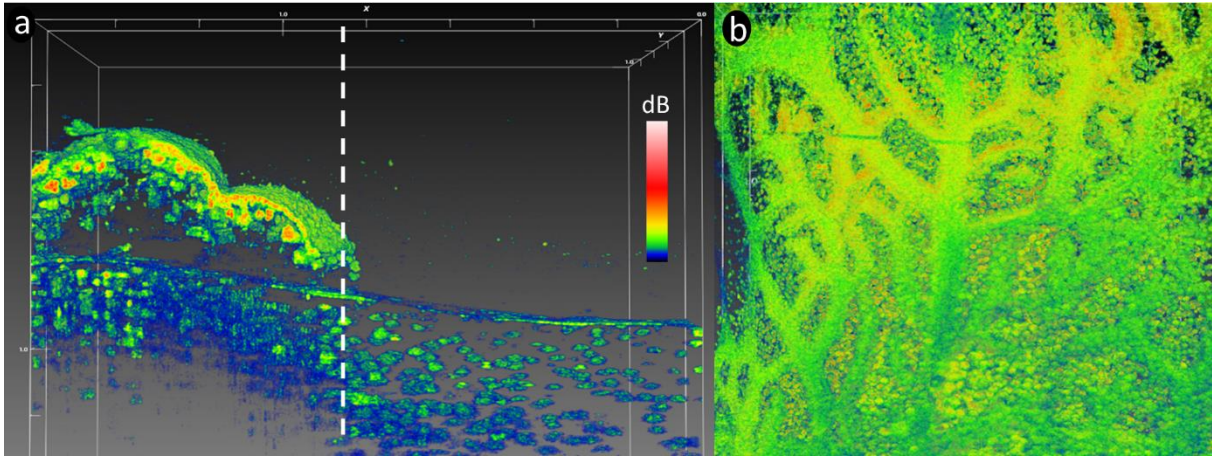


Figure 22 | (a) OCT scan of bell tissue with part of the subumbrella epidermis and mesoglea removed (right side of dashed line), improving scan penetration depth and clarity in this area. (b) Overview of bell tissue with subumbrella layer removed. The remaining gastrodermis from the radial canals was still attached to the exumbrella mesoglea showing how these canals branch out over the entire bell. A dense carpet of white granules was found in the exumbrella mesoglea underneath radial canals. Scale bars in mm.

Removing the subumbrella epidermis greatly improved visibility of symbiont clusters and white granules present in the exumbrella mesoglea. A side-by-side comparison of the exumbrella mesoglea, with half the scan covering the rhopalia canal full of white granules, and the other half covering anastomosing tissue only with symbiont clusters, revealed a major heterogeneity in the structure and content of the two tissue areas (Figure 23).

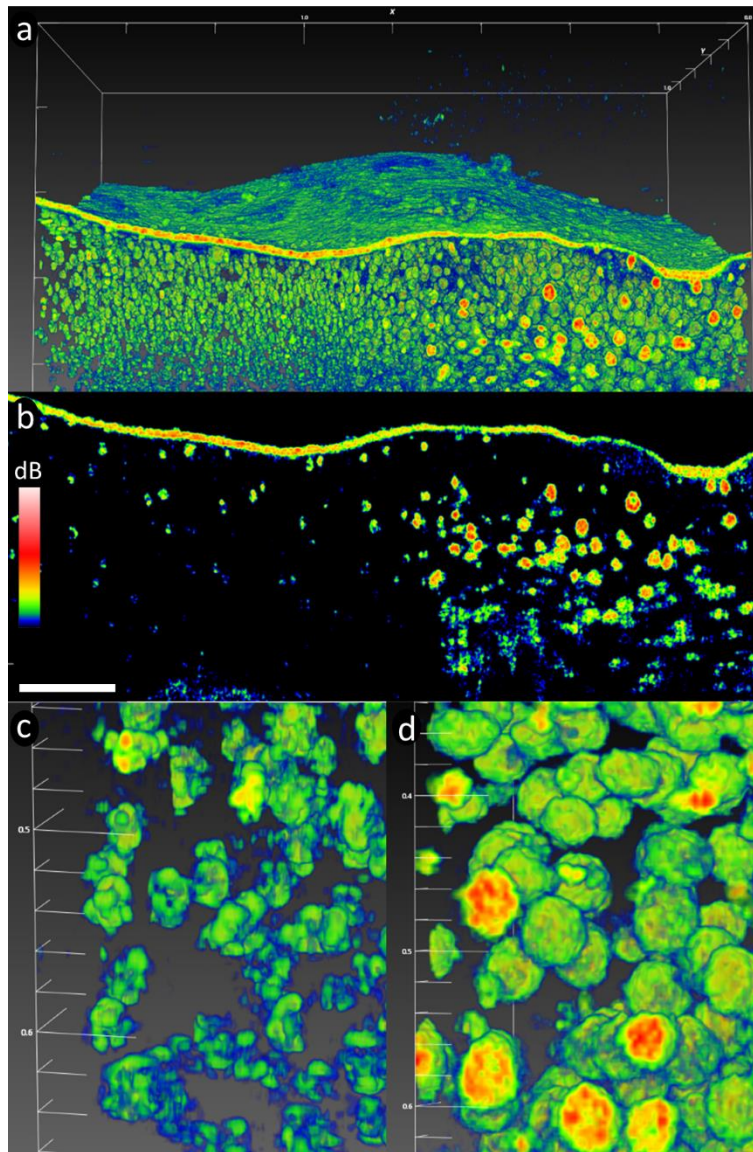


Figure 23 | (a) 3D scan of a rhopalia canal with the subumbrella layer removed, revealing the density of symbiont clusters in anastomosing tissue (left side) vs. white granules (right side). (b) A sectional scan showing that white granules appear much denser than symbiont clusters. White granules were mainly spherical in shape (up to 80  $\mu\text{m}$  in diameter), and appeared to be solid particles as judged from the OCT signal. (c) closeup-scan of symbiont clusters. (d) closeup-scan of white granules. Due to the density of granules it was not possible to discern symbiont clusters in this tissue region. Scale bars in panel a, c, and d in mm. Scale bar in panel b represent 200  $\mu\text{m}$ . An animated 3D representation of panel a can be found in the supplementary information.

### High-resolution scans

High-resolution scans with a voxel size of  $0.5 \times 0.5$  (Figure 23c) or  $1.0 \times 1.0$   $\mu\text{m}$  area (Figure 23d), and 2.7  $\mu\text{m}$  in height, were used for detailed scans of the spatial distribution of symbiont clusters and white granules. White granules were found in high density along the rhopalia canal, and appearing to be ‘solid’ spheres of roughly 80  $\mu\text{m}$  in diameter (Figure 23b). Symbiont clusters were also found in surprisingly high

density in the exumbrella epidermis, although more diffusely spread out compared to the white granules. Symbionts appeared to be positioned in elongated clusters, stretching up to 80  $\mu\text{m}$  across. Given that the average size of *Symbiodinium* cells *in hospite* with *Cassiopea* are normally around 10  $\mu\text{m}$  in diameter (Fitt 1985, Biquand et al. 2017), this indicates that amoebocytes can harbor more than 10 symbionts depending on clustering, as previously estimated (Lyndby et al. 2020b). Due to the high density of white granules near rhopalia canals, clusters of symbionts were hard to detect or distinguish from the granules in this region (Figure 23d). However, symbiont densities quantified from the two regions by cell counting were found to be equally distributed between the anastomosing- and rhopalia canal tissue (Figure 24a). We also found that the symbiont populations were more than 3-fold higher in the subumbrella side relative to the exumbrella side (Figure 24b). The data is in agreement with the larger OCT scans of intact tissue, which showed that symbiont population was much denser near the subumbrella epidermis compared to the rest of the *Cassiopea* medusa (Figure 18b).

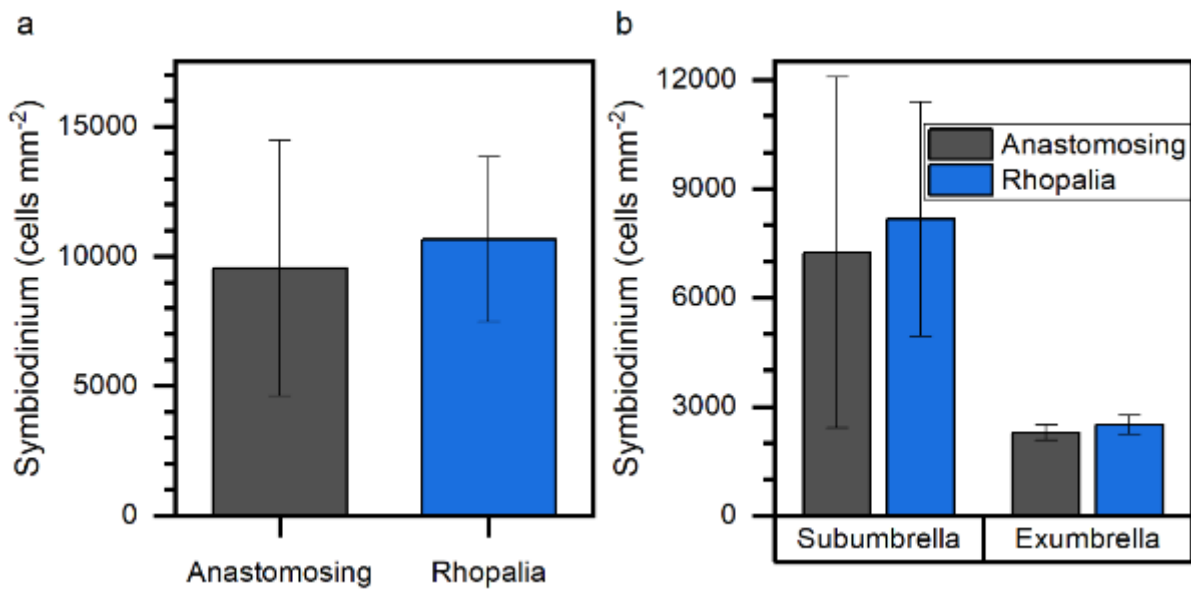


Figure 24 | (a) Symbiont densities in anastomosing tissue and rhopalia canals averaged over the entire depth of the bell. (b) Symbiont densities observed within the anastomosing tissue and rhopalia canals but distinguishing between the subumbrella and exumbrella side of the endodermis. Densities were averaged against the estimated surface area of tissue cut-outs (see methods). Data show means  $\pm$ SE ( $n = 3$  biological replicates).

### Optical properties of *Cassiopea* bell tissue

Studies of the optical properties of cnidarian tissue is an expanding field, yielding important information about how host tissue and symbionts modulate and interact with their light environment. Such information is also important for the development of models that simulate radiative transfer e.g. in

corals (e.g. Taylor Parkins et al. 2021). While the function of the white granules in *Cassiopea* remains unknown, other pigments in *Cassiopea* have been speculated to be either photoprotective or photo-enhancing (Blanquet & Phelan 1987, Phelan et al. 2006), similar to host pigments found in corals (Salih et al. 2000, e.g. Lyndby et al. 2016). The high density of the heterogeneously distributed light scattering white granules in the bell and oral arms suggests that the light microenvironment could be greatly altered in these tissue regions relative to tissue with no white granules. We estimated the optical properties of *Cassiopea* bell tissue with light scattering white granules using optical parameter extraction from OCT scans (Wangpraseurt et al. 2019).

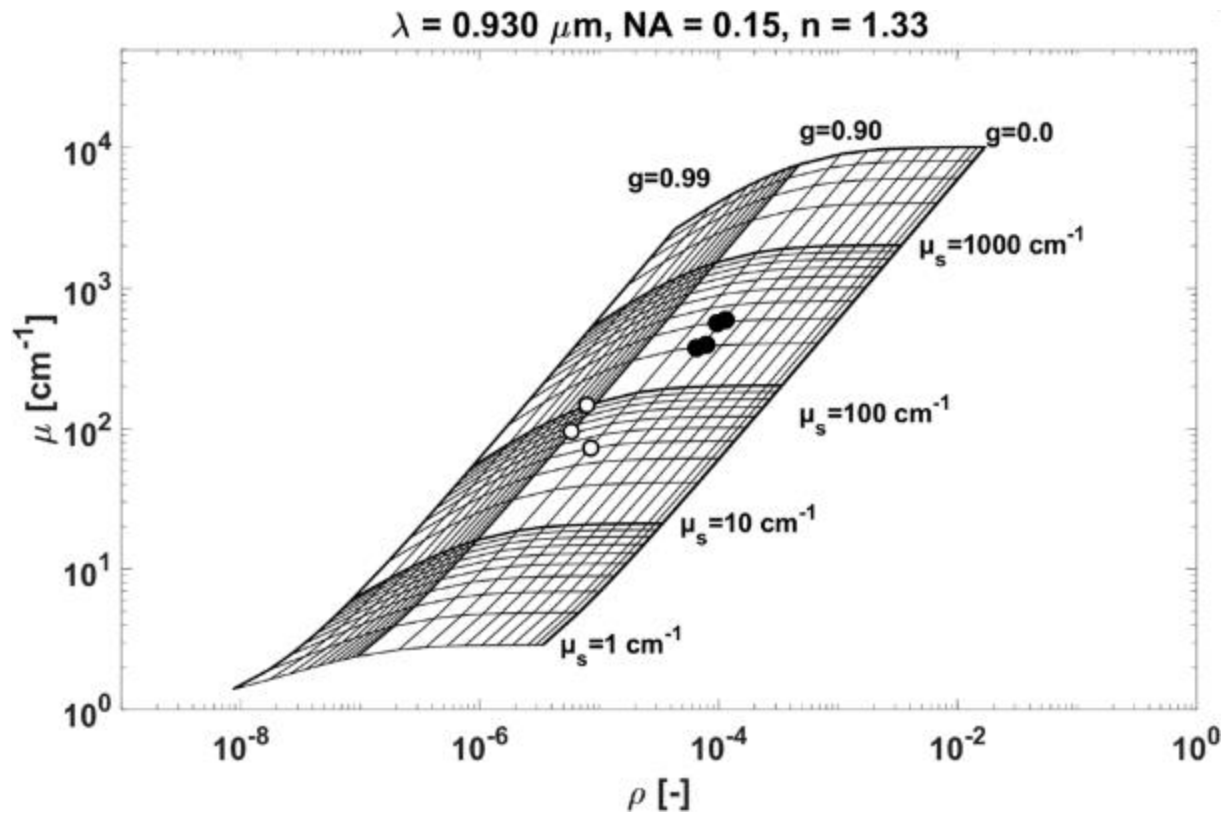


Figure 25 | The optical properties, i.e., scattering coefficient ( $\mu_s$ ), and anisotropy of scattering ( $g$ ), extracted from OCT scans of narrow regions targeting individual white granules (full circles) or large areas comprising of multiple granules (width of 10-20 granules per region; open circles) in rhopalia canal tissue with epidermis removed.

The optical properties of tissue with white granules near the rhopalia canals were vastly different from the anastomosing tissue (Figure 25). The scattering coefficient of tissue with white granules were estimated to be  $\mu_s = 200\text{-}300 \text{ cm}^{-1}$ , and with an anisotropy factor of  $g = 0.7$  for individual white granules (i.e., analyses targeting narrow regions with individual granules; Supplementary figure 1a). Estimates from larger areas of tissue (i.e., analyses averaged over large areas, comprising multiple granules with a width

of 10-20 granules; Supplementary figure 1b) indicated that  $g$  increased to 0.8-0.9 and the scattering coefficient dropped to  $\mu_s = 40-100 \text{ cm}^{-1}$ . This suggests that the arrangement of light scattering white granules in the tissue increases both the photon residence time and depth penetration, thereby enhancing the chance of absorption by symbionts near white granules, similar to reflective (and fluorescent) host pigments in corals (Lyndby et al. 2016, Wangpraseurt et al. 2019).

It was not possible to determine the optical properties of symbiont clusters in anastomosing tissue. Symbiont densities in the exumbrella mesoglea were on average 3-fold lower than in the subumbrella, with few clusters that were diffusely spread in the mesoglea, as judged from B-scans of this tissue region (Figure 23b, c). This prevented the extraction of meaningful optical properties and indicates that light travels through the exumbrella mesoglea in anastomosing tissue relatively unhindered. These differences suggest that symbionts in mesoglea with white granules might be more light-exposed based on an increased light scattering in this region, as compared to other tissue regions.

#### Photosynthetic performance in different *Cassiopea* tissue compartments

Given that the optical properties of light scattering white granules can drastically alter the local light microenvironment, a 6-hour isotopic labelling experiment was conducted in combination with NanoSIMS isotopic analyses (Pernice et al. 2012, Kopp et al. 2015, Krueger et al. 2017, Lyndby et al. 2020b). We used  $^{13}\text{C}$ -bicarbonate and  $^{15}\text{N}$ -ammonium incubations to investigate if carbon and nitrogen assimilation rates differed between symbiont algae in the subumbrella anastomosing tissue and rhopalia canals, and combined it with variable chlorophyll fluorescence imaging to investigate the photosynthetic performance and carbon assimilation of symbionts in the two tissue regions.

PAM chlorophyll fluorescence imaging showed no differences in  $F_v/F_m$  between symbionts found along rhopalia canals vs. anastomosing tissue in intact bell tissue (Figure 26a), and the effective quantum yield was also similar for the two regions, as measured with RLCs (Figure 26b). However, removing the subumbrella layer, and running RLCs on the sub- and exumbrella layers side-by-side showed that symbionts deeper in the bell had a drastically lower threshold for light saturation, and  $rETR$  saturated already around  $100-200 \mu\text{mol photons m}^{-2} \text{ s}^{-1}$  (Figure 26d), relative to the  $400-500 \mu\text{mol photons m}^{-2} \text{ s}^{-1}$  for symbionts in the subumbrella layer (Figure 26c, d). This stark contrast indicates that symbionts in the exumbrella epidermis are acclimated to lower light levels, suggesting that most light is absorbed at the subumbrella epidermis directly, or is backscattered by the white granules.

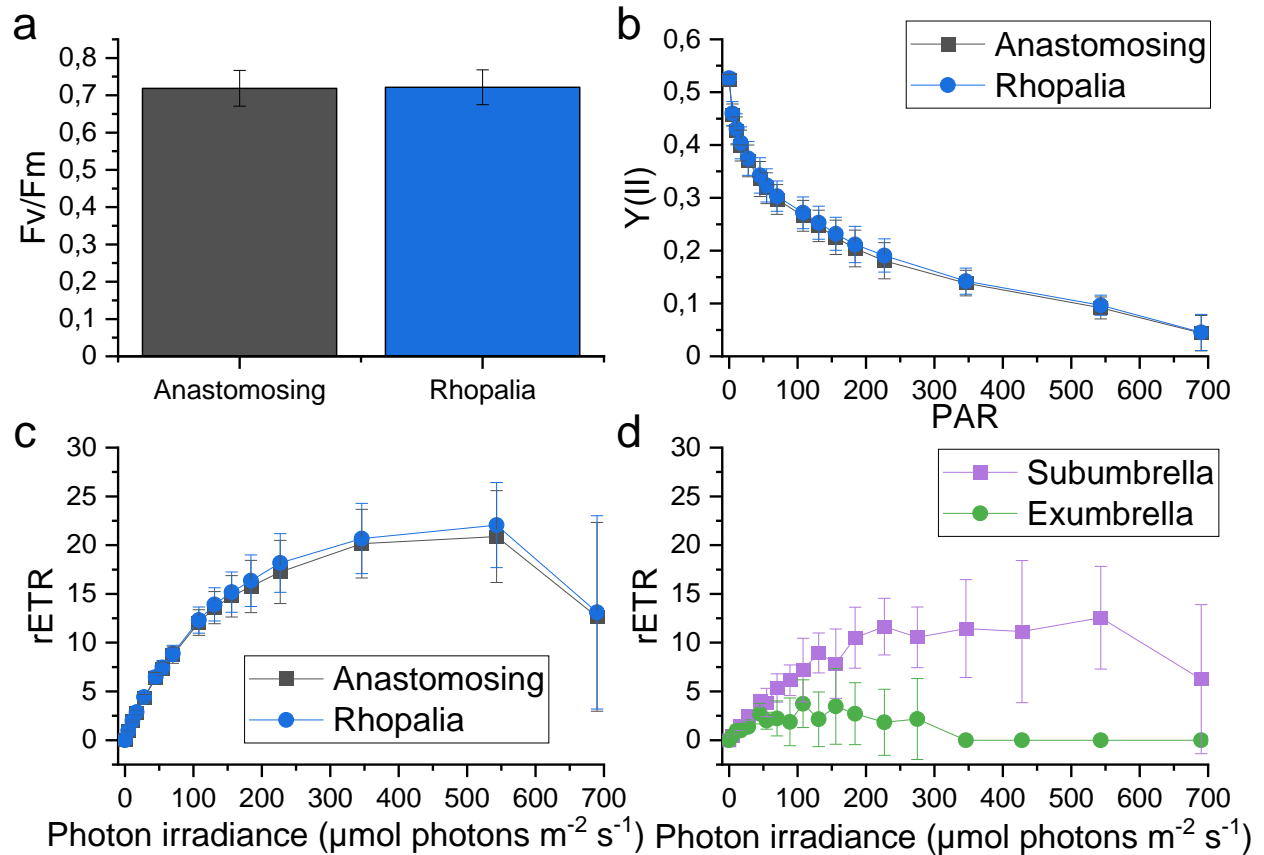


Figure 26 | Variable chlorophyll fluorescence imaging of anastomosing tissue and rhopalia canals. (a) Maximum quantum yield ( $F_v/F_m$ ) after 15 min dark adaptation, (b) effective PSII quantum yield [ $Y(II)$ ], (c) relative electron transport rate (rETR) of intact medusae, and (d) rETR measured on cut-out bell tissue (from different medusae) with subumbrella and exumbrella sides separated as a function of incident photon irradiance. Data show means  $\pm$  SEM ( $n = 3$  biological replicates for panel a-c, and  $n = 1$  biological replicate for panel d).

Stable isotope labelling of three sub-adult specimens of *Cassiopea* showed a significant difference in the  $^{13}\text{C}$  assimilation by symbiont algae near white granules, relative to symbionts found in anastomosing tissue (LMM,  $F_{1,4} = 8.8$ ,  $p = 0.041$ ; Figure 27a), suggesting that photosynthesis is locally enhanced by the light scattering from white granules. No differences in  $^{13}\text{C}$ -enrichment were observed in amoebocyte cells (LMM,  $F_{1,4} = 1.2$ ,  $p = 0.342$ ) or host epidermis (LMM,  $F_{1,4} = 0.5$ ,  $p = 0.508$ ). Finally, no differences in  $^{15}\text{N}$  uptake were found for symbionts (LMM,  $F_{1,4} = 0.04$ ,  $p = 0.854$ ), amoebocytes (LMM,  $F_{1,4} = 0.5$ ,  $p = 0.508$ ), or host epidermis (LMM,  $F_{1,4} = 0.2$ ,  $p = 0.649$ ), comparing between rhopalia canals and anastomosing tissue (Figure 27b), indicating that each region had equal access to nutrients during the labelling experiment.

Optical microniches in *Cassiopea* remains an unexplored field. Here, we provided evidence that the *Cassiopea* host directly alters the light microenvironment, benefitting nearby symbionts. White light scattering granules in *Cassiopea* provide a mean for the host to not only enhance photosynthetic performance of symbionts, but to guide light further down into the host tissue, potentially supporting symbiont populations present in shaded parts of the animal. While it remains unknown what triggers production of white light scattering granules in *Cassiopea*, it is possible that individuals living in overall more shaded environments, e.g., mangroves, would be more inclined to produce white light scattering granules to enhance photosynthesis of symbionts; this hypothesis could be rigorously tested.

Additionally, symbiont densities are typically found to be especially high near the subumbrella epidermis due to the high light availability here. However, the Mie scattering effect, guiding light through the *Cassiopea* tissue, might explain why roughly one quarter of the symbiont population is found deeper into the bell and exumbrella layers. Furthermore, light penetrating all the way through the animal to the substrate will potentially be backscattered up into the animal, additionally enhancing photon availability in the exumbrella.

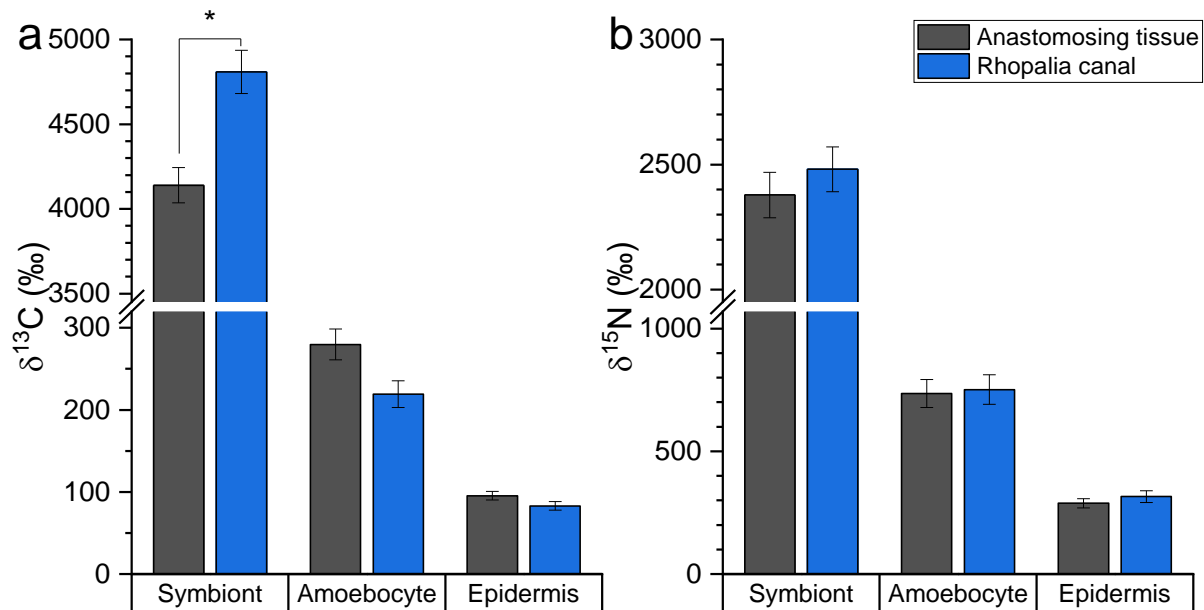


Figure 27 | Mean  $^{13}\text{C}$ - (a) and  $^{15}\text{N}$  enrichments (b) of symbiont algae, amoebocyte cells, and host epidermis in subumbrella tissue in 3 sub-adult *Cassiopea* medusae after a 6-hour pulse labelling incubation with  $^{13}\text{C}$ -bicarbonate and  $^{15}\text{N}$ -ammonium. \* indicates significant difference at the level  $p < 0.05$  between respective tissue/cell types from the two tissue regions. Error bars indicate  $\pm\text{SEM}$  ( $n = 3$  biological replicates). See supplementary information for complete dataset of all ROIs included.



## Conclusion

Optical coherence tomography can provide detailed scans of the *in vivo* tissue organization of intact *Cassiopea*, showing the distribution of symbiont clusters, white granules, and other structures at a high spatial resolution. The methods presented here enable detailed mapping of the distribution of entire symbiont populations or similar distinguishable objects in intact, living cnidarian systems, providing new means for non-invasive monitoring of the internal dynamics of symbiotic cnidarians, under both homeostasis and during stressful events. Additionally, we provided the first evidence on how light scattering granules in *Cassiopea* medusae can enhance the photosynthetic performance of their symbionts near these granules. Our observations support previous suggestions that white tissue regions with granules in *Cassiopea* play several roles in modulating the light microenvironment of *Cassiopea*, by enhancing light availability in the upper layer, while potentially minimizing it in the deeper tissue, thus displaying both photo-enhancing and photoprotective properties. The presented approach to study structure and function in *Cassiopea* is also applicable to other photosymbiotic cnidarians (e.g. cnidarian model systems such as *Exaiptasia* sp. and *Hydra* sp.), but we propose that OCT could find broad application for non-invasive monitoring of structure and morphology of particular tissues or whole specimens in many types of invertebrates.

## Acknowledgements

The authors thank the staff at the Electron Microscopy Facility at University of Lausanne for excellent support and assistance with processing samples for NanoSIMS analyses. This study was supported by an award from the Gordon and Betty Moore Foundation (MK; grant no. GBMF9206; <https://doi.org/10.37807/GBMF9206>), and the Swiss National Science Foundation (A.M.; grant no. 200021\_179092).

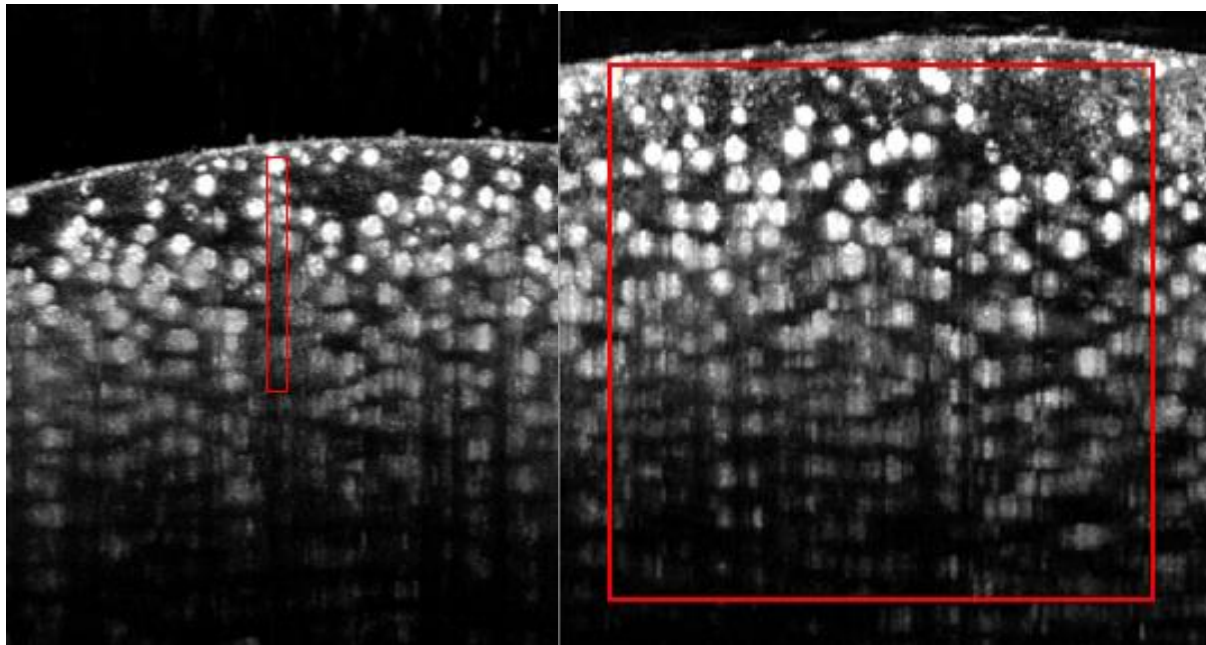
## Competing interests

The authors declare no competing interests.

## Supplementary information

Supplementary table 1 | NanoSIMS isotopic enrichment data summary. Treatment IDs correspond to the 2 bell regions detailed in the methods section of the main text. Delta values of  $^{13}\text{C}$  and  $^{15}\text{N}$  represent mean values  $\pm$ SEM calculated from all replicates of a given treatment/tissue area as described by equation 4 and 5 in the methods section.

Bell region	Tissue/cell type	Replicates	$\delta^{13}\text{C}$	$\delta^{15}\text{N}$
Anastomosing	Symbionts	218	$3798.3 \pm 122.9$	$2181.8 \pm 94.0$
Anastomosing	Amoebocytes	45	$236.2 \pm 22.0$	$621.4 \pm 62.4$
Anastomosing	Epidermis	39	$74.1 \pm 7.5$	$222.3 \pm 24.1$
Rhopalia canal	Symbionts	203	$4192.9 \pm 158.8$	$2163.3 \pm 97.4$
Rhopalia canal	Amoebocytes	45	$180.1 \pm 18.5$	$617.7 \pm 65.8$
Rhopalia canal	Epidermis	37	$64.4 \pm 7.2$	$246.8 \pm 28.6$



Supplementary figure 1 | Example of rhopalia canal tissue regions for inherent optical parameter extraction, showing the region for (a) individual white granules, and (b) large area with multiple granules (width of 10-20 granules).

## Chapter 4: Investigation of the O<sub>2</sub> dynamics in *Cassiopea* using O<sub>2</sub>-sensitive planar optodes

### I. Context

Chapter 4 presents work that has not yet been finalized for submission to a journal. In this chapter, we investigate the O<sub>2</sub> dynamics in greater detail by using O<sub>2</sub>-sensitive planar optodes to image the O<sub>2</sub> dynamics throughout the entire *Cassiopea* umbrella.

### Author contribution

NHL, MM, AM, and MK designed the experiment. NHL, MM, CP, and SLJ did the experiments. NHL and CP did the data extraction and analyses. NHL wrote the manuscript. All authors contributed equally to editing and comments on the writing process.

### II. Publication

# Imaging of O<sub>2</sub> dynamics in *Cassiopea* medusae using O<sub>2</sub>-sensitive planar optodes

Niclas Heidelberg Lyndby<sup>1</sup>, Maria Moßhammer<sup>2</sup>, Claudia Pogoreutz<sup>1</sup>, Sofie Lindegaard Jakobsen<sup>2</sup>, Anders Meibom<sup>1,3</sup>, Michael Kühl<sup>2</sup>

<sup>1</sup>Laboratory for Biological Geochemistry, School of Architecture, Civil and Environmental Engineering, Ecole Polytechnique Fédérale de Lausanne (EPFL), CH-1015 Lausanne, Switzerland.

<sup>2</sup>Marine Biological Section, Department of Biology, University of Copenhagen, DK-3000 Helsingør, Denmark.

<sup>3</sup>Center for Advanced Surface Analysis, Institute of Earth Sciences, University of Lausanne, CH-1015 Lausanne, Switzerland.

**Keywords:** *Optical sensing, chemical sensing, oxygen sensor, photosynthesis, jellyfish, symbiosis*

## Introduction

The symbiont-bearing jellyfish *Cassiopea* exhibits a benthic lifestyle in subtropical and tropical coastal habitats, positioning themselves upside down on the substrate (Bigelow 1900, Drew 1972, Hofmann et al. 1996) in order to autotrophically acquire carbon through their algal symbionts (Symbiodiniaceae), in a fashion similar to reef building corals (Hofmann & Kremer 1981, Welsh et al. 2009, Freeman et al. 2016, Lyndby et al. 2020b). Like other symbiont-bearing cnidarians, *Cassiopea* get their brown coloration from their photosymbionts (Lampert 2016), which are present in high densities near the subumbrella epidermis and in oral arms, and with a more dispersed occurrence near the exumbrella epidermis and in the mesoglea (Bigelow 1900, Lampert 2016, Lyndby et al. 2020b, 2022b). Unlike corals, however, the dinoflagellate photosymbionts in *Cassiopea* are mainly associated with specialized host cells, i.e., amoebocytes, which are motile cells responsible for transporting nutrients between the host and symbionts (Colley & Trench 1985, Estes et al. 2003, Lyndby et al. 2020b). Additionally, the bell and oral arm tissue can contain white granules, stretching in radial stripes across the bell and along the underside of the oral arms from base to apex (Bigelow 1900, Lyndby et al. 2022b). The white granules have been found to effectively scatter light (Lyndby et al. 2022b), and are speculated to have a photo-enhancing and/or photo-protecting function in *Cassiopea* by altering the light field and thus the photosynthetic performance of symbionts in near proximity of these granules (Hamaguchi et al. 2021, Lyndby et al. 2022b). Furthermore,  $O_2$  have been hypothesized to be buffered in the thick mesoglea of the medusae, providing a seemingly stable supply of  $O_2$  for symbionts and host tissue (e.g. musculature) during dark periods (Lyndby et al. 2022a). While both symbiont distribution, light fields and metabolic activity in *Cassiopea* thus exhibits spatial heterogeneity, spatial mapping of these parameters remains to be done.

Investigations of optical properties and photosynthetic performance of photosymbiotic cnidarians, such as reef building corals and jellyfish, have mostly focused on investigating photosynthesis on the colony or jellyfish-scale using closed chamber respirometry (e.g. Verde & McCloskey 1998, Hoogenboom et al. 2010, Mammone et al. 2021), or at the microscale (i.e. single polyps/point measurements) using microsensors (e.g., Kühl et al. 1995, Brodersen et al. 2014, Wangpraseurt et al. 2017a). However, previous studies have shown that photosynthesis can happen heterogeneously throughout coral colonies (de Beer et al. 2000, Al-Horani et al. 2005, Wangpraseurt et al. 2014b), potentially leading to an over/underestimation of actual oxygen ( $O_2$ ) production, and missing spatial information at either scale (Schrameyer et al. 2014, Lyndby et al. 2020a). More recent studies have used chemically sensitive optical dyes immobilized in  $O_2$ -, pH-, and temperature-sensitive planar optodes and nano/microparticles for

imaging 2D or 3D analyte distributions (Koren & Kühl 2018, Moßhammer et al. 2019). Imaging of sensor particles adds a new dimension to optical sensing, but their use involves the challenge of keeping them homogeneously distributed in a medium and/or sample. Nevertheless, chemically sensitive sensor micro- and nanoparticles directly coated on flow-exposed tissue surfaces have produced reliable results in several studies (Fabricius-Dyg et al. 2012, Koren et al. 2015, 2016, Brodersen et al. 2020).

Planar optodes are limited to sensing in one plane only, but offer a more straightforward way to map chemical dynamics in organisms or systems in 2D, provided that the region of interest can be pressed tightly onto the planar sensor foil (Santner et al. 2015). They are capable of delivering high spatial and temporal resolution of O<sub>2</sub> and pH dynamics in aquatic systems and organisms, and planar optodes have been used for visualizing photosynthetic activity in microbial biofilms, root systems, endolithic algal populations in corals and in the *Prochloron*-ascidian symbiosis (Glud et al. 1999, Jensen et al. 2005, Kühl et al. 2008, 2012, Larsen et al. 2011, Brodersen et al. 2017). In this study, we used O<sub>2</sub> sensitive planar optodes to investigate O<sub>2</sub> dynamics internally and on the surface of *Cassiopea andromeda* medusae. We combine information from variable chlorophyll *a* fluorescence imaging and hyperspectral imaging with O<sub>2</sub> dynamics for mapping the chemical dynamics and heterogeneous distribution of respiration and photosynthetic activity at high spatial resolution in the *C. andromeda* holobiont system.

## Methods

### Cassiopea specimens

Juvenile *Cassiopea andromeda* medusae (parents originally supplied by DeJong Marinelife, Netherlands; simply referred to as “*Cassiopea*” from this point on) were reared at an aquarium facility at the Institute of Earth Sciences, University of Lausanne, Switzerland. Detailed information on the molecular identification of animals is given in the supplementary information. A group of medusae with diameters between 10-50 mm were selected and transported to the aquarium facility at the Marine Biology Section (MBS), University of Copenhagen (Helsingør, Denmark) to a 50 L aquarium. Here, medusae were fed 5 times per week with recently hatched *Artemia* nauplii, and supplemented with AF Amino Mix (Aquaforest) 2-3 times per week. Medusae were kept in ASW (35 ‰ and 25 °C, pH of 8.2) under a programmable LED light source (Triton R2, Pacific Sun; Supplementary figure 2), running a 12/12-hour day/night cycle, provided a downwelling photon irradiance (400-700 nm) of ~350 μmol photons m<sup>-2</sup> s<sup>-1</sup> at the water surface.

## Planar optode O<sub>2</sub> imaging

### Preparing planar optodes

Planar O<sub>2</sub> sensitive sensor foils, i.e., planar optodes, were prepared by dissolving 3 mg of the red-emitting O<sub>2</sub>-sensitive dye Pt(II) meso-tetra(pentafluorophenyl)porphine (Frontier Scientific, USA), 3 mg of the green-emitting reference dye Macrolex Yellow, and 200 mg of polystyrene pellets (CAS# 3003-53-6) in 2 g of tetrahydrofuran (Glud et al. 1999). This sensor-cocktail was knife-coated onto a transparent, O<sub>2</sub>-impermeable PET foil using an applicator frame (80 mm wide, 90 µm gap, BYK-Gardner) to get an even sensor film after evaporation of the solvent. The optode foil was then cut out in pieces, and taped onto a microscope slide, with the O<sub>2</sub> sensitive surface facing away from the glass slide. The presence of O<sub>2</sub> reduces the luminescence intensity of the phosphorescent indicator dye, which can be read-out via ratiometric imaging with a regular SLR camera to correlate changes in the emission of the indicator dye with changing O<sub>2</sub> concentrations (see Koren and Kühl (2018) and Moßhammer (2019) for more details).

### Ratiometric camera system and setup for O<sub>2</sub> imaging

The imaging system is based on ratiometric luminescence imaging with a modified SLR camera (EOS 1000D, Canon, Japan) equipped with a macro lens (Macro 100 f2,8 D, Tokina, Japan), a 530 nm long-pass filter, and a yellow plastic filter in front to reduce background fluorescence (Larsen et al. 2011). Samples were illuminated using a 405 nm multichip LED (LedEngin Inc., UK) to excite the reference dye as well as the indicator dye in the planar optode during image acquisition. The software Look@RGB (imaging.fish-n-chips.de) was used for controlling both camera and light source during acquisition. The acquired images were automatically split into the red, green, and blue channels by the software, and were analyzed using the image processing package Fiji (2.9.0) for ImageJ (1.53q). Images of O<sub>2</sub> concentration were calculated by dividing the red image (O<sub>2</sub> sensitive emission) with the green image (reference emission).

Images were calibrated by obtaining a series of images with filtered ASW at known O<sub>2</sub> concentrations from 0-100 % air saturation, however, due to fitting, the range was extrapolated to higher concentrations allowing confident estimations of up to 250 % air saturation, albeit with greater error. The Stern-Volmer relationship was applied to plot the relative emission intensity against their respective O<sub>2</sub> concentrations as:

Eq. 1: 
$$\frac{I_f^0}{I_f} = \text{relative intensity}$$

where  $I_f^0$  is the intensity of fluorescence without O<sub>2</sub> present (0 % air saturation), and  $I_f$  is the intensity of fluorescence with O<sub>2</sub> at specific saturation levels (between 0-100 % air saturation). See supplementary

information for calibration curves. A simplified two site model was used to fit the data to extract  $\tau_0$ ,  $K_{SV}$ , and  $f$  (Carraway et al. 1991, Klimant et al. 1999), where  $\tau_0$  is the luminescence in absence of  $O_2$ ,  $K_{SV}$  is the operational quenching constant, and  $f$  is the quenchable fraction of the sensor material. Ratioed images (R/G) from *Cassiopea* samples were then calibrated by applying these values to the image stacks, and regions of interest (ROIs) were drawn in ImageJ over the images to extract  $O_2$  concentrations for further analysis (Supplementary figure 3).

The camera system was mounted on a tripod and positioned perpendicular above the sample. The 405 nm multichip LED light source for excitation of the sensor material illuminated the sensor foil from one side at an angle of  $30^\circ$  (relative to the horizontal plane imaged by the camera), while a fiber-optic white LED lamp (KL2500 LED, Schott AG) was illuminating the sample from the other side at a similar angle with a downwelling photon irradiance (400-700 nm) of  $200 \mu\text{mol photons m}^{-2} \text{ s}^{-1}$ , as measured with a cosine corrected mini quantum sensor (MQS-B, Walz), connected to a calibrated irradiance meter (ULM-500, Walz). Samples were positioned on a height-adjustable platform below the camera to keep the camera focal point and distance to the light sources constant while focusing on the sample (optode) surface. For planar optode imaging, the LED lamp was briefly turned off to avoid interference with the emission signal of the  $O_2$  sensitive dye.

#### Preparation of *Cassiopea* medusae for planar optode imaging

Medusae were prepared in two orientations for  $O_2$  imaging: 1) oral arms were removed with a razor and tweezers to image the subumbrella bell surface. The entire bell surface was spread out flat on the planar optode surface, and a 1 % solution of ultrapure low melting agarose (Thermo Fisher) in 35 ‰ filtered ASW (kept semi-liquid at  $\sim 30^\circ \text{C}$ ) was carefully dripped onto the animal to cover the entire bell. Finally, a plastic case or microscope slide would be pressed down on top of the bell and held in place until the agarose hardened (Figure 28); 2) medusae were cut into slices of  $\sim 2$  mm using a razor, typically with the cut running through the center of the bell to include oral arms. The slices were then placed on the planar optode, covered in the agarose solution, and the case or microscope slide pressed against it until the agarose hardened. In the event that tissues collapsed on the surface they were gently reorganized using thin tweezers entering from the side, to rearrange the tissue for a clear sideways view into the bell. All samples were immediately prepared in this manner, and encased in 1 % agarose, except for samples imaged with an I-PAM system (see description below). All  $O_2$  optode imaging was completed within 1-2 hours after this preparation.

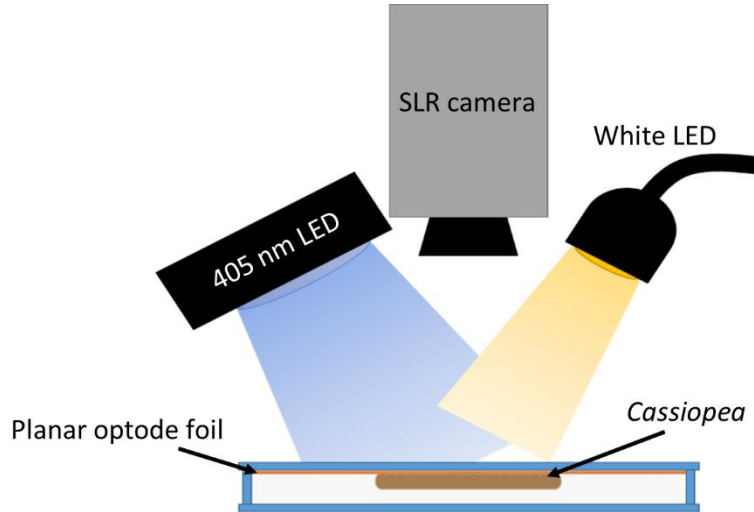


Figure 28 | Schematic overview of the planar optode setup. The SLR camera was mounted perpendicular from above via a tripod. Both the 405 nm LED and white light were mounted in 30 degrees relative to the horizontal plane. The *Cassiopea* sample, pressed tightly against the O<sub>2</sub> sensitive optode foil, and embedded in 1 % agarose in a case, was placed with the optode foil facing up towards the camera.

### Variable chlorophyll *a* fluorescence imaging

Absorptivity and PSII quantum yield were measured with focus on the newly exposed bell areas on each medusae using a variable chlorophyll fluorescence imaging system (I-PAM, IMAG MIN/B, Walz; Ralph et al. 2005, see also Lyndby et al. 2022b), providing weak, non-actinic measuring light pulses, strong saturating light pulses, as well as actinic light levels of known photon irradiance.

Medusae were dark acclimated individually for 15 min in a petri dish filled with ASW, and maximal PSII quantum yield ( $F_v/F_m$ ) was measured by applying a strong saturation pulse ( $> 3000 \mu\text{mol photons m}^{-2} \text{s}^{-1}$  for 0.8 s) using the I-PAM. Rapid light curves (RLCs), i.e., relative PSII electron transport as a function of photon irradiance, were subsequently run with photosynthetically active radiation (PAR, 400-700 nm) at intensities ranging 0-681  $\mu\text{mol photons m}^{-2} \text{s}^{-1}$  to measure the effective PSII quantum yield;  $Y(II)$ , and relative electron transport rate ( $rETR = Y(II) \times PAR$ ).

ROIs corresponding to the ROIs selected for the O<sub>2</sub> image analysis were carefully drawn on images of the bell surface and cross section samples for each medusa, and data extracted for further processing. All I-PAM measurements were performed, and ROIs drawn, in the software ImagingWin (v2.41a, Walz).

### Hyperspectral imaging

*Cassiopea* medusae were imaged with a hyperspectral camera (SNAPSCAN VNIR, imec) fitted with an anti-shading lens (Xenoplan 2.8/50, Schneider Optics Inc.). The hyperspectral unit was mounted above



a height-adjustable platform, and 4 halogen light spots were mounted around the camera to generate a homogenous light field over the imaging area. Samples were imaged with the hyperspectral unit after planar optode measurements. To do this, the planar optode was removed, and the sample, still encased in agarose, placed under the camera. In case of movement by bell contraction, a solution of 50 %  $MgCl_2$  in 35 ‰ filtered ASW was dripped onto the medusae until the animal stopped moving.

Similar imaging with a 95% diffuse reflectance standard (SG3151-20-alu, imec) was used to calibrate sample images in % reflectance. Both image acquisition and extraction of spectra were done using the system software (HSI studio v 1.2.1.0, imec). Spectra were extracted from ROIs drawn around rhopalia canal tissue with white granules visibly present, and anastomosing tissue with no white granules visible.

## Results

### Variable chlorophyll *a* fluorescence

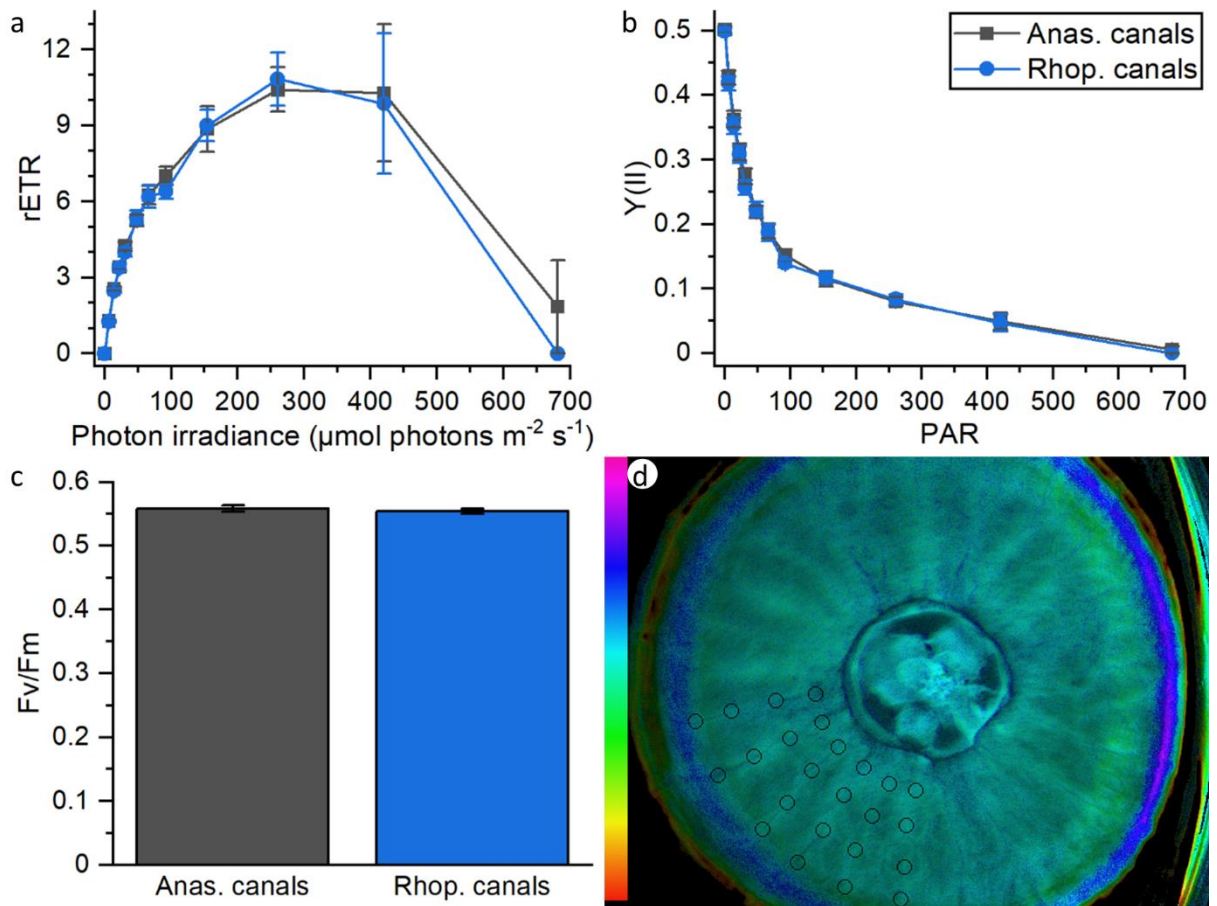


Figure 29 | Variable chlorophyll fluorescence data extracted from the subumbrella of a single individual. a) Relative electron transport rates (rETR). b) The effective quantum yield  $Y(II)$ . c) Maximal quantum yield

(Fv/Fm) after 15 min darkness. d) Subumbrella Fv/Fm measurement, with ROIs along rhopalia canals and anastomosing canals used for analysis. The shown ROIs reflect those used for planar optode analyses and hyperspectral imaging analyses. Note, due to the body plan of *Cassiopea* the bell rim folds up and is out of focus for the I-PAM camera and was thus avoided for analyses.

Variable chlorophyll *a* fluorescence imaging revealed no differences between fluorescence values (i.e., Y(II) and Fv/Fm) in ROIs along the anastomosing- and rhopalia canals. The maximal quantum yield was found to be ~0.55 for both tissue regions after oral arms had been removed, indicating the system was stressed from arms being removed (Figure 29c, d)(compare with Fv/Fm values from individuals with arms removed in chapter 3; Lyndby et al. 2022b). rETR showed that the photosystem saturated in both tissue regions around 250  $\mu\text{mol photons m}^{-2} \text{s}^{-1}$  and photosynthesis became photoinhibited after 400  $\mu\text{mol photons m}^{-2} \text{s}^{-1}$  (Figure 29a). The effective quantum yield revealed no differences in photosynthetic performance between the two tissue regions (Figure 29b).

## Planar optode imaging

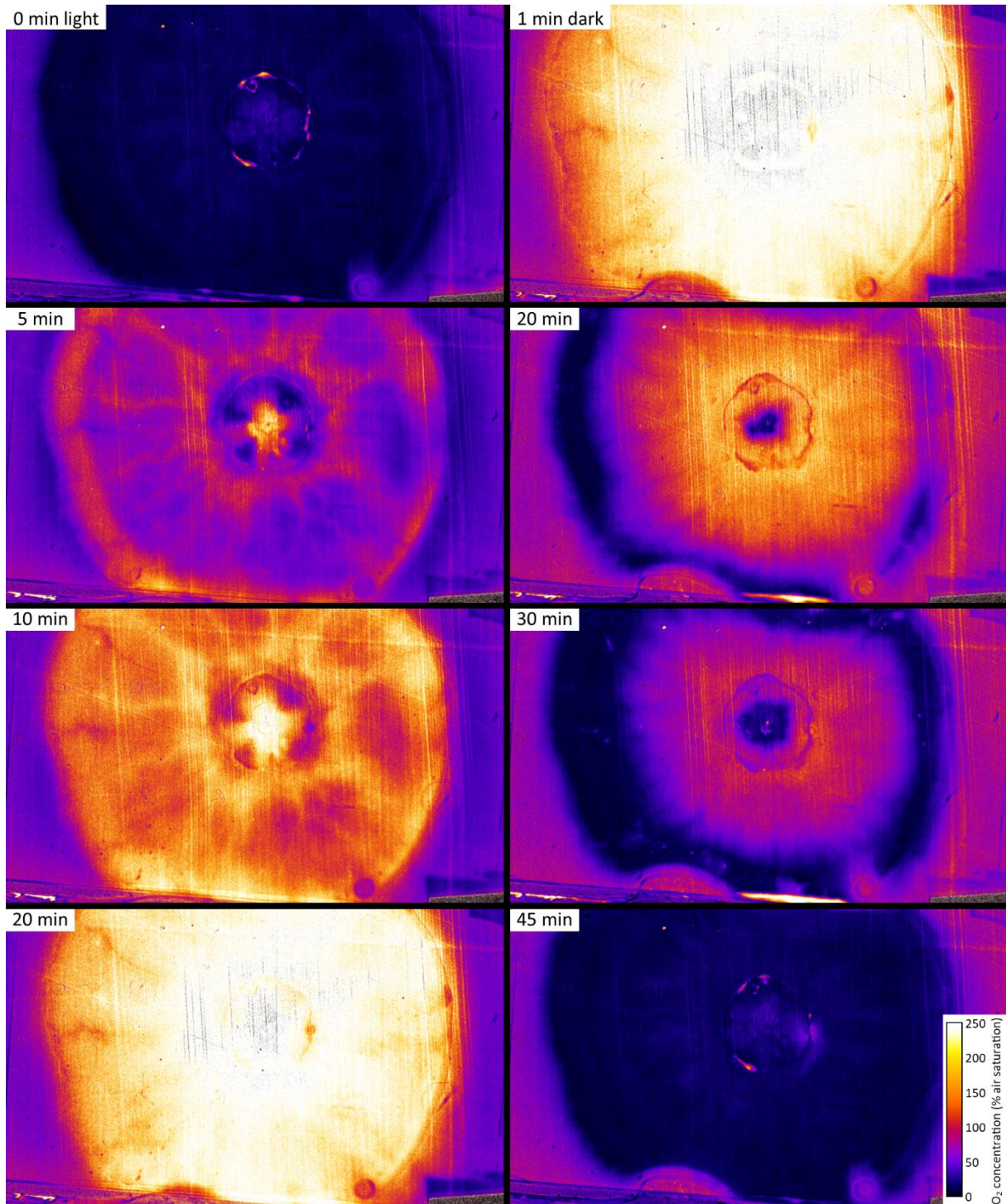


Figure 30 | Ratiometric imaging of O<sub>2</sub> dynamics in a *Cassiopea* medusae subumbrella (oral arms removed) pressed against an O<sub>2</sub> sensitive planar optode, and imaged during constant light for a total of 30 min (left column), or after onset of darkness for a total of 60 min (right column). Color bars represent 0-250 % air saturation. Note, due to the long photoperiod the bell became supersaturated in O<sub>2</sub>, and only the first 20 min of light exposure is shown due to most of the bell surface O<sub>2</sub> concentration exceeding the calibration

limit after this point. Animations of the observed O<sub>2</sub> production and consumption across the subumbrella can be found in the supplementary information.

The O<sub>2</sub> buildup was heterogeneous during the photoperiod, with the bell center, the bell rim, and several major radial canals showing a fast buildup to > 100 % air saturation within the first 5 min; and the entire bell surface had reached at least 200 % air saturation after 20 min of light exposure (Figure 30, left column). Conversely, during the dark period, O<sub>2</sub> was more uniformly depleted at the surface tissue, starting at the bell rim and at the very center of the bell where oral arms had been removed (Figure 30, right column). The O<sub>2</sub> depletion happened much slower compared to O<sub>2</sub> buildup, and the entire bell surface did not reach a pre-photoperiod O<sub>2</sub> concentration (~25 % air saturation) until after 45 min in darkness.

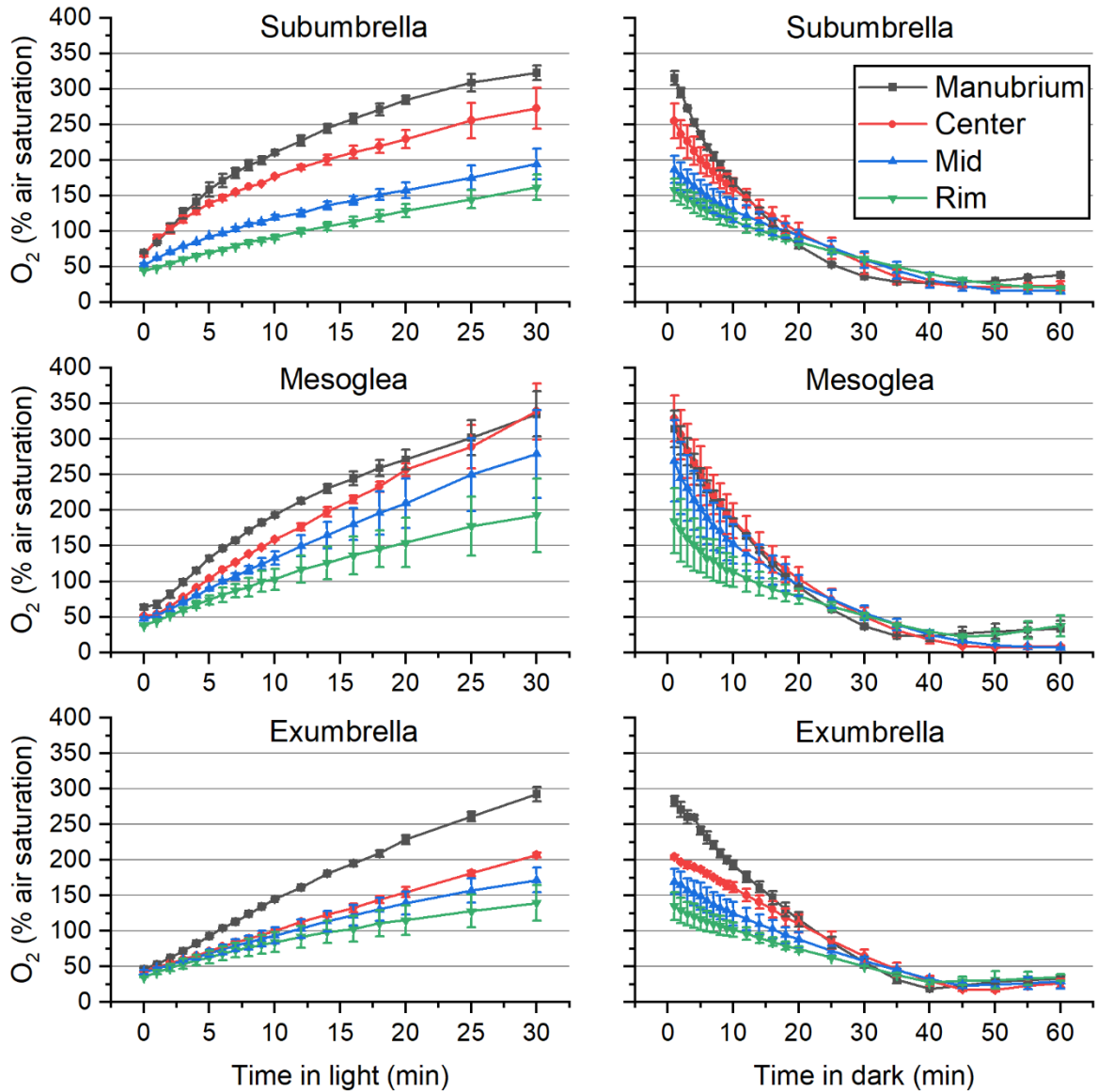


Figure 31 | Comparison of O<sub>2</sub> evolution in subumbrella epidermis (top row), mesoglea (middle row), and exumbrella epidermis (bottom row), as seen from a cross section, at 200 μmol photons m<sup>-2</sup> s<sup>-1</sup> downwelling irradiance (left column) and darkness (right column). Data presented as mean values ±SEM (n = 2, technical replicates). Animations of observed O<sub>2</sub> production and consumption in the cross section can be found in the supplementary information. Note, data in Figure 30 and Figure 31 is obtained from different individuals.

Cross sectional comparisons of O<sub>2</sub> evolution in the tissue revealed the subumbrella epidermis to be the most productive tissue in the system, with all but the outermost subumbrella (near the bell rim) reaching 100 % air saturation within the first 5 minutes (Figure 31, top row). Both subumbrella and exumbrella epidermis continued to build up O<sub>2</sub> to a maximum of 100-300 % air saturation, with the subumbrella and exumbrella epidermis at the manubrium site reaching the highest concentrations, and

the exumbrella closest to the bell rim reaching the lowest of ~140 % concentration after a 30 min photoperiod. Additionally, the mesoglea would continue to build up O<sub>2</sub> to higher concentrations than the surrounding tissue, for all sites except the manubrium, reaching between 200-340 % air saturation (Figure 31, top row). During the dark period, the manubrium was again the site with the highest activity, depleting most of the stored O<sub>2</sub> within the first 30 min, while sites further out towards the bell rim would deplete their storage down to a minimum only after 40-45 min. All sites would reach a minimum of 15-20 % air saturation, before showing a minute increase towards the end of the measurement (still in darkness; Figure 31, bottom row).

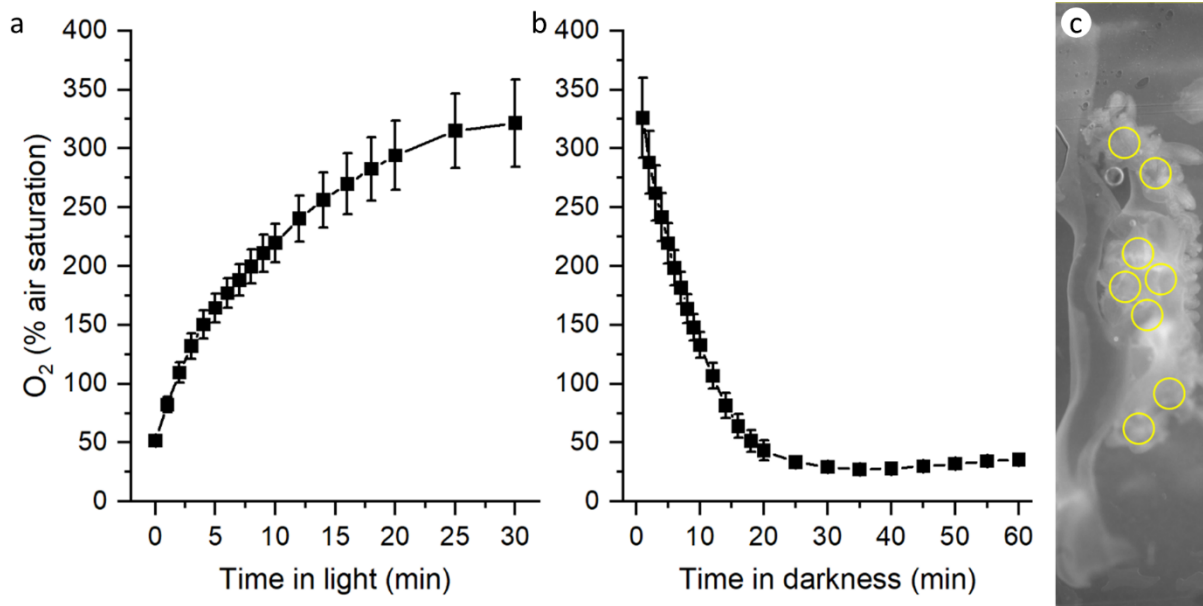


Figure 32 | O<sub>2</sub> evolution of the center of the *Cassiopea* medusa bell imaged with the ratiometric imaging system using planar optodes on the oral arms and associated external growth. a) Arms were subjected to a 30 min photoperiod (200  $\mu\text{mol photons m}^{-2} \text{s}^{-1}$ ), b) followed by 60 min of darkness. Data show mean  $\pm$ SEM, and ROIs are shown in panel c.

O<sub>2</sub> concentrations reached > 100 % air saturation in the oral arms within the first few minutes. O<sub>2</sub> continued to build up in and near the arms to a maximum of 300 % after 30 min of light (Figure 32a). O<sub>2</sub> quickly depleted in the oral arms, reaching a minimum of 25 % air saturation within 30 min of darkness (Figure 32b).

## Hyperspectral imaging

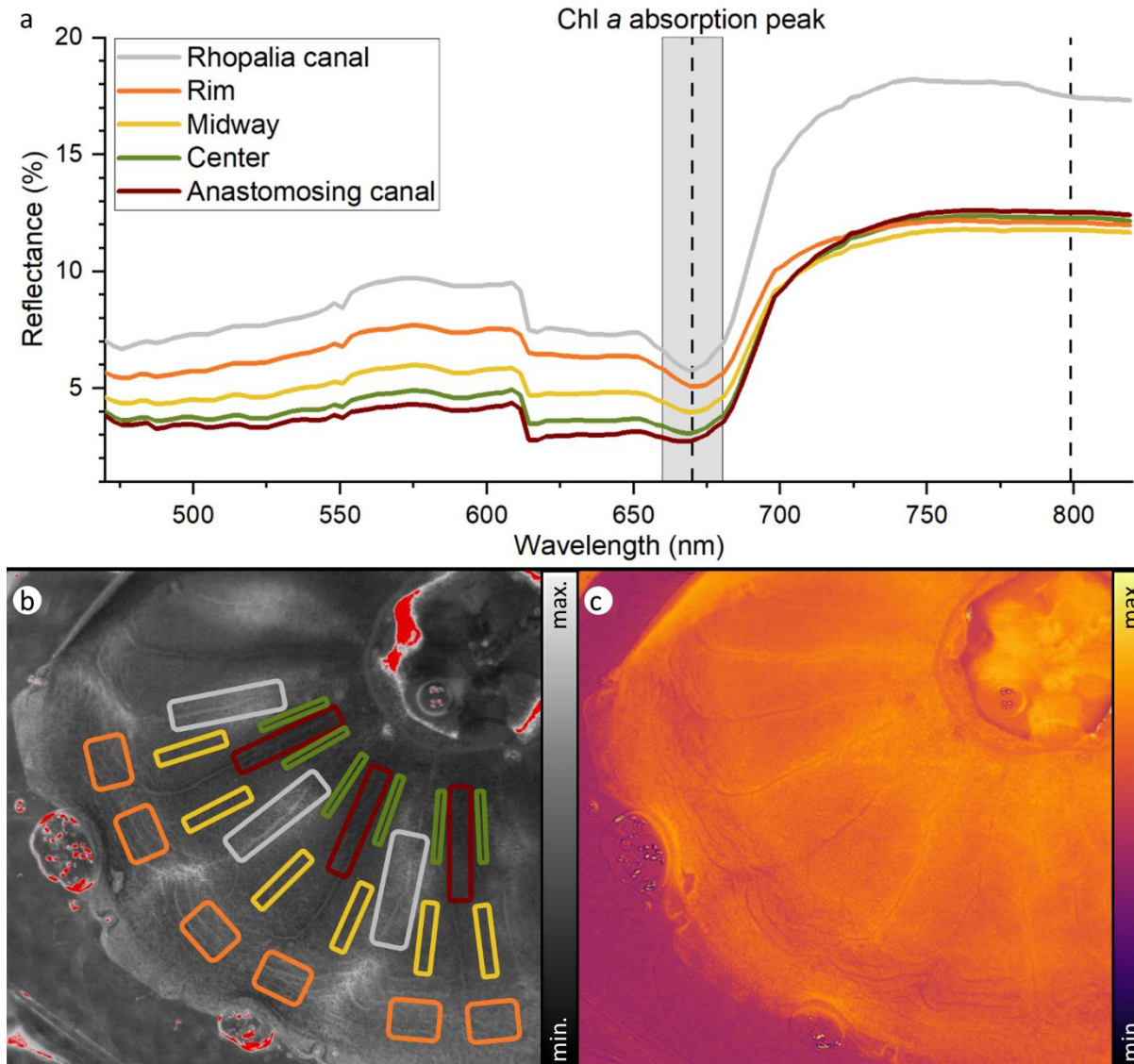


Figure 33 | Hyperspectral imaging of reflectance of *Cassiopea* bell tissue, a) comparing rhopalia canals (with white granules) vs. anastomosing tissue canals (without white granules), and anastomosing tissue near the center of the bell, midway between rim and center, and bell rim. Color codes in plot match the shown ROIs in panel b. b) Image showing calibrated reflectance across the bell at 669 nm (calibrated against a 95 % white diffusing standard). Areas marked in red in b) indicate oversaturation and are not included in the analysis. c) NDVI extracted from the HIS Studio software, using wavelength 669 and 799 nm (indicated by dashed lines in panel a). Due to a misalignment in the hyperspectral camera there is a drop in the spectrum around 630 nm, but this does not interfere with the data extracted.

Hyperspectral imaging showed that tissue with white granules on average reflects photons two-fold compared to areas without white granules (Figure 33a). Additionally, the spectra clearly show the presence of chlorophyll *a* (indicated by a major dip in reflectance around 660-680 nm). Normalized difference vegetation index (NDVI) comparing the Chl *a* absorption peak from symbionts at 669 nm with

799 nm (Tucker 1979), across the whole bell, indicate higher concentrations of symbionts found in anastomosing tissue, with the major radial canals showing overall highest values (Figure 33c).

## Discussion

We present the first application of O<sub>2</sub> imaging on medusae of the symbiotic jellyfish, *Cassiopea andromeda*, using O<sub>2</sub> sensitive planar optodes to map their O<sub>2</sub> dynamics under light and dark conditions at high spatial resolution. We found that O<sub>2</sub> buildup and depletion is highly heterogenous at the bell surface and within the bell system, where the mesoglea exhibits the slowest dynamics. Furthermore, hyperspectral imaging showed that symbiont densities are focused around the bell center and along major radial canals of adult medusa. Symbiont densities alone however did not correlate with O<sub>2</sub> buildup observed across the bell surface.

### O<sub>2</sub> dynamics in *Cassiopea* bell tissue

The O<sub>2</sub> production was heterogeneous throughout the bell surface in large medusae during photoperiods, where O<sub>2</sub> production primarily took place at the center and rim of the bell. Additionally, several major radial canals, both of rhopalia canals and anastomosing tissue canals, exhibited signs of high O<sub>2</sub> buildup, and thus high photosynthetic performance, near the bell surface (Figure 30). *Cassiopea* medusae are known to harbor the majority of their symbionts directly under the subumbrella epidermis (Estes et al. 2003, Lampert 2016, Lyndby et al. 2022b). A previous study working on animals of the same origin as in the present study found no significant difference in symbiont densities at the subumbrella epidermis when comparing between rhopalia canals and anastomosing tissue (Lyndby et al. 2020b). In the current study, I-PAM data showed no difference in photosynthetic efficiency comparing the two types of tissue (Figure 29). However, hyperspectral imaging of the bell surface revealed distinct differences in the overall reflectance comparing canals and regions of immediately adjacent tissue near the bell center and rim (Figure 33). Focusing on the 669 nm waveband (close to the *in vivo* absorption peak of Chl *a*), the bell showed clear signs of symbionts being heterogeneously distributed, with higher densities found near the bell center and radial canals in anastomosing tissue (Figure 33b), thus explaining the fast O<sub>2</sub> buildup observed here (Figure 30, left column). However, bell surface O<sub>2</sub> buildup appeared equally fast near the bell rim relative to the center, while hyperspectral data suggested symbiont densities being the lowest towards this area of the bell (Figure 33). Previous work has shown that the mesoglea can buffer O<sub>2</sub> supply in medusae when experiencing hypoxic conditions, and *Cassiopea* medusae are able to build up their own O<sub>2</sub> storage in the mesoglea during photoperiods which seem proportional to the thickness of the mesoglea



layer (Thuesen et al. 2005, Lyndby et al. 2022a). Our cross section O<sub>2</sub> imaging supports this finding, as mesoglea near the thick center of the bell appeared to store higher concentrations of O<sub>2</sub>, while gradually reaching lower concentrations towards the bell rim (Figure 31). As such, it is likely that the thin mesoglea at the bell rim will not store much of the produced O<sub>2</sub>, but instead show a combined effect of sub- and exumbrella symbiont photosynthesis as the cause of fast O<sub>2</sub> buildup in this tissue region (Figure 30).

White granules in *Cassiopea* tissue are typically found along rhopalia canals, giving the medusa a distinct white striated pattern reaching from the manubrium to the bell rim (Bigelow 1900). These white granules have been shown to enhance the local scattering of light, benefiting carbon assimilation in symbionts in close proximity (Lyndby et al. 2022b). In accordance, our hyperspectral data of the bell surface showed more light reflected near the granule-rich areas in our medusae (Figure 33). However, O<sub>2</sub> buildup at the bell surface was not found to be related to the presence of white granules in our medusae. On the contrary, radial canals in anastomosing tissue had, on average, a slightly faster O<sub>2</sub> buildup than rhopalia canal tissue (Figure 30 and Supplementary figure 4). The Mie scattering effect caused by the white granules, effectively scattering light deeper into the tissue in areas with white light scattering granules (Lyndby et al. 2022b), potentially play a role in the observed differences in O<sub>2</sub> buildup in the two regions, as light will be spread out more throughout the entire tissue column in the rhopalia canal region, while most light will be absorbed by the symbionts near the surface in anastomosing tissue. However, whether our result is due to differences in symbiont densities and presence of white granules, or other (unaccounted) internal processes such as O<sub>2</sub> transport through the gastric network, remains to be determined.

#### Light-dependent O<sub>2</sub> buildup and dark respiration

Unlike the heterogeneous O<sub>2</sub> buildup, O<sub>2</sub> depletion at the bell surface appeared much more uniform, with the very center of the manubrium (where oral arms had been removed) and the bell rim being the first parts depleted of O<sub>2</sub> (Figure 30). As previously mentioned, the buffering capacity of the mesoglea is proportional to its thickness. This effect can be observed in the medusa during the dark period as the O<sub>2</sub> concentration reduces to pre-photoperiod levels at the rim first, and then gradually depleting towards the thick center of the bell over 45 min (Figure 30). Interestingly however, the very center of the manubrium where the oral arms were removed revealed the highest activity in both O<sub>2</sub> buildup and depletion of the bell (Figure 30). Within 3 min, O<sub>2</sub> concentrations at the center went from < 50 % air saturation to > 100 % air saturation, and O<sub>2</sub> was again rapidly depleted here during the dark period. Furthermore, this area always appears to contain slightly more O<sub>2</sub> relative to the surrounding tissue. The center of the bell is

known to harbor important organs like the main stomach and gonads of the medusa (Bigelow 1900), and muscle bands line the epidermis for bell contraction (Blanquet & Riordan 1981). It is likely that such vital organs have a higher physiological demand for O<sub>2</sub>, and as such O<sub>2</sub> might not just be stored in this area but potentially directed there by unknown internal transport mechanisms (e.g. pumping through radial canals). Finally, removing the oral arms no doubt caused stress to the animal (as observed from the Fv/Fm data; Figure 29c), and wound regeneration requires O<sub>2</sub> and other metabolites for fast recovery (Henry & Hart 2005, Ostendarp et al. 2022). As such, directing excess O<sub>2</sub> towards the wounded site might explain some of the observed O<sub>2</sub> dynamics observed at the bell center during light- and dark periods.

### *Cassiopea* oral arm contribution to O<sub>2</sub> production

*Cassiopea* oral arms are considered a major contributor to photosynthesis in the medusae system due to high densities of symbionts present (e.g., Arossa et al. 2021) and our planar optode imaging of intact oral arms supports this notion (Figure 32). The O<sub>2</sub> level in and around oral arms quickly went from ~50 % to > 100 % air saturation within the first few minutes, and continued to increase to ~300 % within 30 min of light. Additionally, arms quickly depleted O<sub>2</sub> around them, reaching pre-photosynthesis levels within 20 min of darkness (Figure 32). The oral arms reached pre-photosynthesis levels faster than the bell surface and cross section analyses of the bell, suggesting that the arms are not only a major source of O<sub>2</sub> during photoperiods, but also have a high demand of O<sub>2</sub> similar to the bell center (Arossa et al. 2021). Such high O<sub>2</sub> demand might be explained by muscular movement of oral arms and the secondary mouths constantly searching for food around them. Interestingly, the high O<sub>2</sub> productivity in the oral arms did not seem to affect O<sub>2</sub> levels in the mesoglea below them, suggesting that O<sub>2</sub> is not delivered to the bell for storage, but is instead lost to the surroundings and potentially removed by water moving over the oral arms as the bell pulsates (Hamlet et al. 2011, Santhanakrishnan et al. 2012, Battista et al. 2022). To further understand this exchange, the combination of chemically sensitive dyes with particle image velocimetry would be required (e.g., Ahmerkamp et al. 2022).

### Conclusion

The *Cassiopea*-dinoflagellate holobiont is known as a highly productive photosynthetic unit. Here, we have shown that O<sub>2</sub> production happens heterogeneously throughout the *Cassiopea* system, illustrating the need for applying techniques that cover whole areas of photosynthetic organisms to correctly assess their productivity. O<sub>2</sub> dynamics across the bell surface of *Cassiopea* were found to only partially correlate to symbiont density and the presence of light scattering white granules. We speculate that unaccounted internal transport mechanisms beyond that of the mesoglea, (e.g., using radial canals

for circulation of O<sub>2</sub> rich water; see chapter 3; Lyndby et al. 2022b) might play an important role in transportation of O<sub>2</sub> to parts of the *Cassiopea* system where it is needed. Additionally, O<sub>2</sub> buffering of the mesoglea was illustrated, and we show that buffering occurs in individuals even when light levels do not stimulate photosynthesis to reach supersaturating O<sub>2</sub> concentrations in the bell system. However, oral arms that are typically associated with high production in *Cassiopea* due to a high density of symbionts, did not visibly contribute to buffering of O<sub>2</sub> in the bell manubrium. We hypothesize that excess O<sub>2</sub> is instead lost due to gas exchange and continuous pulsation that drives water across the oral arms, removing excess O<sub>2</sub>. However, such dynamics remain to be identified.

## Acknowledgements

This study was supported by an award from the Gordon and Betty Moore Foundation (MK; grant no. GBMF9206; <https://doi.org/10.37807/GBMF9206>), and the Swiss National Science Foundation (A.M.; grant no. 200021\_179092).

## Supplementary information

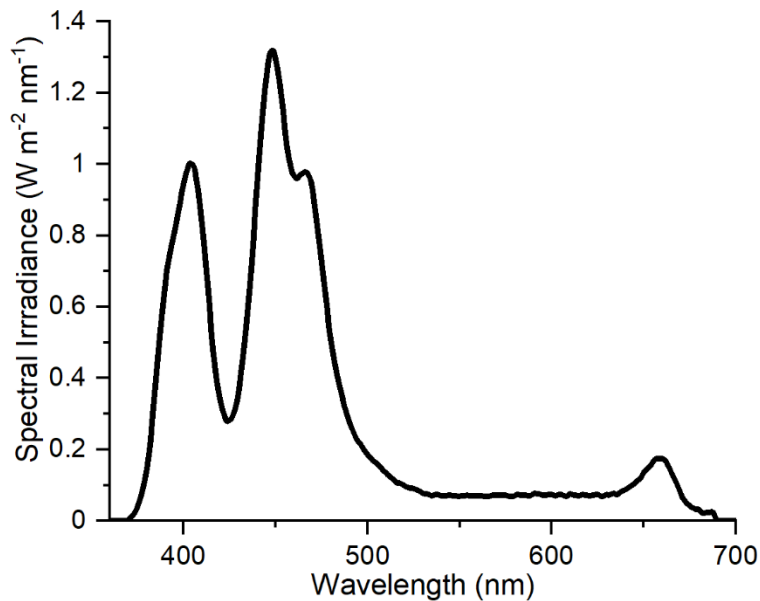
### Molecular identification

Pieces of tentacles (~250 mg) were collected from three individual jellyfish and homogenized for 30 s at full speed in 800 µL of CD1 buffer (PowerSoil Pro DNA extraction kit; Qiagen, Germany) using a Polytron Immersion Disperser (Kinematica, Switzerland). The resulting homogenate was stored at -20 °C until further processing. For DNA extraction, samples were gently thawed on ice. The homogenate was then added to PowerBead Pro Tubes supplied with the PowerSoil Pro kit, and bead beaten at 90 Hz three times for 30 s. Samples were then loaded into the QIAcube Connect DNA extraction platform (Qiagen, Germany) and DNA was extracted using the PowerSoil Pro DNA extraction kit following the manufacturer's instructions. The purified DNA was eluted in 100 µL of solution C6. Quality and quantity of purified DNA was assessed using a NanoDrop 2000C spectrophotometer and Qubit fluorometer, respectively (both Thermo Fisher Scientific, US). Purified DNA was stored at -20 °C until further use.

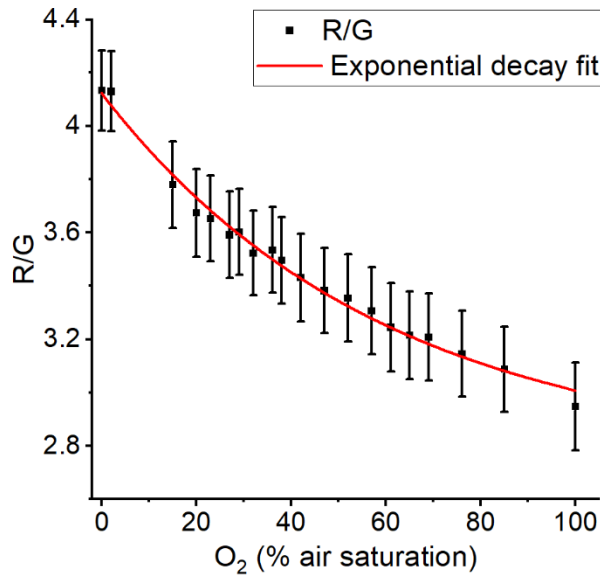
For species identification, a fragment of the mitochondrial cytochrome oxidase (COI) subunit was amplified using the primer pair CasF (5'-GGTCTTCTCCACCAACCACAARGAYATHGG-3') and CasR (5'-ATTCTATCHGTTARYAACATTGTRAT-3') (Maggio et al. 2019). Each PCR reaction was performed in duplicate in total reaction volumes of 10 µL and consisted of 5 µL Qiagen Multiplex Mix (Qiagen, Germany)

with 1  $\mu\text{L}$  DNA input (normalized to a concentration of 10  $\text{ng}/\mu\text{L}$ ) and a total primer concentration of 1  $\mu\text{M}$ . The PCR conditions were as follows: Initial denaturation at 95  $^{\circ}\text{C}$  for 15 min, followed by 30 cycles of denaturation at 94  $^{\circ}\text{C}$  for 30 s, annealing at 48  $^{\circ}\text{C}$  for 30 s, and extension at 72  $^{\circ}\text{C}$  for 30 s, and a final extension at 72  $^{\circ}\text{C}$  for 7 min. In addition, a null template (no DNA input) ‘negative’ control reaction was run to assess for PCR reagent contamination. After confirmation of a specific PCR product in the expected size range in electrophoresis (1 % TAE agarose gel stained with GelRed Nucleic Acid Gel Stain; Biotium, USA), post-PCR clean-up was performed by adding 2.5  $\mu\text{L}$  of Illustra ExpProStar 1-Step to 12.5  $\mu\text{L}$  of PCR product and following the manufacturer’s instructions (GE Healthcare Life Sciences, Germany). Purified PCR products were sent to Fasteris (Genesupport SA, Switzerland) for Sanger sequencing services on an Applied Biosystems 96-capillary 3730xl platform. The obtained sequences were quality trimmed in CodonCode Aligner (CodonCode Corporation, USA) and queried against the Nucleotide Collection on NCBI using the BLASTN tool, which confirmed a percentage similarity of >99 % to the species *Cassiopea andromeda*.

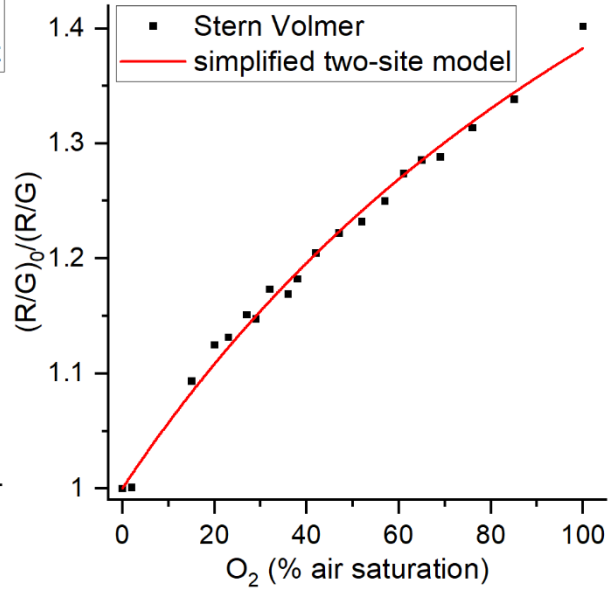
#### Supplementary figures



Supplementary figure 2 | Spectrum of light provided by the programmable LED light (Triton R2, Pacific Sun) illuminating the *Cassiopea* holding tank, providing  $\sim 350 \mu\text{mol photons m}^{-2} \text{ s}^{-1}$  on a 12/12-hour schedule.

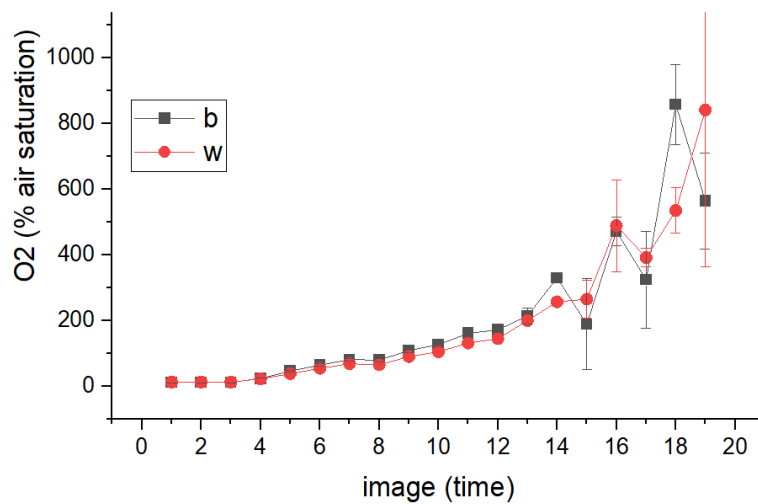


Model	ExpDec1
Equation	$y = A1 \cdot \exp(-x/t1) + y0$
Plot	Mean
y0	$2.75436 \pm 0.0747$
A1	$1.36886 \pm 0.06675$
t1	$59.29911 \pm 6.20634$
Reduced Chi-Sqr	0.00108
R-Square (COD)	0.99007
Adj. R-Square	0.9889



Model	O22site (User)
Equation	$1/((f/(1+x \cdot Ksv)) + (1-f))$
Plot	Stern Volmer
Ksv	$0.0118 \pm 9.92346E-4$
f	$0.51123 \pm 0.02474$
Reduced Chi-Sqr	$9.11086E-5$
R-Square (COD)	0.99204
Adj. R-Square	0.9916

Supplementary figure 3 | calibration curves for O<sub>2</sub>-sensitive planar optode. Relative intensity of ratioed images of the red and green channel (R/G) plotted against their respective O<sub>2</sub> concentrations (left), and the Stern Volmer relationship applied to relative intensities (right). A two-site model was fitted against the Stern Volmer plot to extract K<sub>sv</sub>, f, and τ<sub>0</sub>.



Supplementary figure 4 | O<sub>2</sub> concentrations measured along major radial canals of anastomosing tissue (b) and rhopalia canals (w). Data represent mean  $\pm$ SEM, and n = 4 (technical replicates) for each tissue type. Note, calibration range is 0-100 % air saturation, thus measured values above this is extrapolated from original range and source of uncertainty.

## General discussion

In this thesis, the symbiotic model system *Cassiopea* was used to investigate metabolic host-symbiont interactions and relate this interplay to the photobiology of the system. The first chapter addressed the basic metabolism of *Cassiopea*, with stable isotope labelling experiments in combination with correlated SEM and NanoSIMS analyses, to lay the foundation for understanding the exchange of metabolites between the animal host and its algal symbionts. The second chapter sought to map the internal light field in the host, and investigate photosynthetic activity and chemical dynamics of the *Cassiopea* bell tissue using microsensors. The third chapter built upon the previous two, by investigating the (*in hospite*) micromorphology of *Cassiopea* with non-invasive optical coherence tomography to generate 3D reconstructions of the holobiont system with spatial resolution sufficient to distinguish symbiont algal cells. Additionally, chapter three further combined knowledge acquired from the previous two chapters to investigate the optical properties of white granules in *Cassiopea* bell tissue and their potential role for enhancing the photosynthetic performance of adjacent algal symbionts, as quantified with  $^{13}\text{C}$ -bicarbonate labeling and NanoSIMS imaging. Finally, the fourth chapter explored the photosynthetic performance across the entire bell and the  $\text{O}_2$  buildup in different layers of the bell, specifically the sub- and exumbrella epidermis and the mesoglea. While each chapter represents a standalone project, the experiments were designed to supplement each other. The results are put into context and discussed in the following.

### Inorganic nutrient assimilation in *Cassiopea* and the role of amoebocytes

The *Cassiopea*-Symbiodiniaceae symbiosis is distinct from other symbiotic cnidarians in that *Cassiopea* predominantly harbor their symbionts in amoebocytes, diffusely distributed in the vast mesoglea of the host. This adds an extra layer of complexity to the translocation pathways and the exchange of nutrients, as the mesoglea represents a significant spatial barrier between the host tissue and the symbiont cell. While the first chapter corroborates previous reports that nutrients are indeed actively transferred between *Cassiopea* and its symbionts, the high resolution of NanoSIMS isotopic analyses improved our spatio-temporal understanding of this exchange, as correlated SEM-NanoSIMS analyses clearly provided new evidence of photosynthate translocation in *Cassiopea*.

The amoebocytes have already been identified to play an important role during symbiosis establishment in *Cassiopea* (Colley & Trench 1985) and studies on other scyphozoans revealed amoebocytes to be involved in tissue maintenance (Shaposhnikova et al. 2005). Here, we further illustrate how amoebocytes are important for *Cassiopea* by facilitating nutrient translocation between host and

symbionts, suggesting they are key actors in nutrient cycling in the medusa. Previous work focused on bulk uptake in symbionts cells and host tissue (e.g. Welsh et al. 2009, Freeman et al. 2016), while the dynamics of underlying nutrient exchange were not resolved. By using a correlated imaging approach in combination with stable isotope labeling, we revealed anabolically incorporated photosynthates inside respective holobiont compartments (i.e., the symbiont cell, amoebocytes, and host dermis). This allowed us to infer a natural order of translocation as follow: Dinoflagellates fix carbon and subsequently translocate photosynthates to their host amoebocytes. Amoebocytes then move close to host tissue and release carbon substrates (e.g. lipids) to other compartments of the holobiont, such as the epidermis. However, exact pathways and underlying mechanisms of such exchange between the respective cells, including stimuli for amoebocyte movement, remain to be identified.

### Nitrogen species and assimilation in *Cassiopea*

Nitrogen assimilation mechanisms in *Cassiopea* mirror those observed in corals (Pernice et al. 2012). The *Cassiopea* holobiont has previously been found to assimilate nitrogen in the form of  $\text{NH}_4^+$ ,  $\text{NO}_2^-$ , and  $\text{NO}_3^-$ . While the host animal is only able to sequester  $\text{NH}_4^+$ , the algal symbionts cells are capable of reducing  $\text{NO}_x$  (i.e.,  $\text{NO}_2^- + \text{NO}_3^-$ ) into more bioavailable  $\text{NH}_4^+$ , which can then be incorporated into both symbiont and host tissue. However, our study comparing the uptake of  $\text{NO}_3^-$  and  $\text{NH}_4^+$  in *Cassiopea* found that only  $^{15}\text{NH}_4^+$  was readily taken up, while isotopic enrichment from incubation experiments using  $^{15}\text{NO}_3^-$  could not be detected in NanoSIMS images.

Previous studies have investigated the uptake of nitrogen in *Cassiopea* by measuring the relative removal of  $\text{NO}_x$  in incubated water (i.e., measuring the disappearance of nitrogen species from incubation water) and accredited the measured difference to assimilation in the holobiont. While such experiments are relatively straightforward, they do not account for the fate of  $\text{NO}_x$  within the *Cassiopea* system, and studies have suggested that the presence of non-photosynthetic, nitrate-sequestering microbes associated with *Cassiopea* can be partially responsible for nitrogen removal (e.g. Freeman et al. 2016). Furthermore,  $\text{NO}_3^-$  assimilation has been shown to reduce the carbon translocation from symbionts to host, as the symbionts require more energy to reduce acquired  $\text{NO}_3^-$ ; indeed corals relying on  $\text{NO}_3^-$  have shown increased susceptibility to bleaching during stress (Wiedenmann et al. 2012, Ezzat et al. 2015). Finally, previous work on corals has suggested that enzymatic pathways for the uptake of  $\text{NO}_3^-$  get downregulated when *in hospite*  $\text{NH}_4^+$  levels get high (Grover et al. 2003). The same assumptions can be made for *Cassiopea*, given the phylogenetic similarities shared with corals, and that symbionts are of the



same family (Symbiodiniaceae), thus suggesting that  $\text{NH}_4^+$  is the preferred nitrogen species for *Cassiopea*. Taken together, these studies suggest *Cassiopea* avoids uptake of  $\text{NO}_3^-$ , potentially as a trophic strategy to enhance their resilience to environmental stressors, and maximize photosynthate delivery from symbionts, as long as  $\text{NH}_4^+$  is readily available from internal and external sources.

### Mesoglea buffers the chemical environment of symbionts

Autotrophic assimilation of inorganic carbon through photosynthesis has primarily been studied via isotope labelling experiments with bulk analyses of tissue enrichment or through closed chamber measurements investigating the evolution of  $\text{O}_2$  or  $\text{CO}_2$  in the chamber. While these techniques can give a good estimate of the primary production and respiration of the entire holobiont, they typically fail to identify any granularity/heterogeneity, e.g. niche areas for high production/consumption, that might be present in the system. Point measurements with microsensors investigating photosynthesis have shown that coral respiration/photosynthesis can be highly heterogenous and dynamic throughout a colony (e.g. Wangpraseurt et al. 2014b).

Microsensors are fragile and proper setup and careful handling is required when applying these tools on stony corals where tips may easily break. Gelatinous animals like *Cassiopea*, however, present another unique challenge, in that the rather large medusa constantly pulse to move water. This motion potentially makes measurements imprecise and could damage the sensor. As such, using microsensors on *Cassiopea* is not straightforward, and only one previous study used this approach prior to this thesis by investigating the microenvironment in dissected oral arms (Arossa et al. 2021). In this thesis, the first microsensor measurements on intact *Cassiopea* medusae are presented in Chapter 2.

We found that the  $\text{O}_2$  dynamics of the *Cassiopea* system seem to resemble those observed in corals. The bell, even with pulsing behavior, exhibits a boundary layer across the bell surface, and the holobiont changes from a net source of  $\text{O}_2$  during photosynthesis, to a net sink during darkness. Measurements inside the bell proved that  $\text{O}_2$  concentrations can increase dramatically during photoperiods, reaching  $\text{O}_2$  levels much higher than the surrounding water. Previous studies have shown that non-symbiotic jellyfish like *Aurelia labiata* exhibit a similar  $\text{O}_2$ -absorbing mechanism (i.e., passive accumulation of  $\text{O}_2$  in the mesoglea) in the bell (Thuesen et al. 2005), and the same was recently shown in the oral arms of *Cassiopea* (Arossa et al. 2021). However, unlike the oral arms of *Cassiopea* and the non-symbiotic *A. labiata* bell, the thick mesoglea in *Cassiopea* proved to accumulate  $\text{O}_2$  to a much higher degree. This confirms that the bell

mesoglea acts as an important storage compartment buffering changes of O<sub>2</sub> in the holobiont and suggests that the presence of endosymbionts in *Cassiopea* enhances this ability during photoperiods.

While O<sub>2</sub> buffering in the bell first became evident with depth profiles revealing supersaturated concentrations of O<sub>2</sub> deep in the bell, light-driven dynamics of O<sub>2</sub> and pH provided further evidence for this mechanism. Light-dark shifts performed on small and large individuals showed significant changes in the O<sub>2</sub> dynamics within the mesoglea. While small medusae exhibited O<sub>2</sub> dynamics similar to that observed in corals (i.e., immediate responses in O<sub>2</sub> evolution and pH changes caused by the change in light), the large medusae showed a slower response. The slow response meant a continued buildup/consumption of O<sub>2</sub> deep in the mesoglea for several minutes after light had been turned off/on, respectively. Similarly, pH would continue to increase/decrease for 5-10 minutes after light was turned off/on, respectively. Based on the results provided in chapter 2, we hypothesized that the *Cassiopea* bell mesoglea provides a very stable and buffered environment for their symbionts. As such, this buffering capacity may enable *Cassiopea* to cope with the pronounced environmental fluctuations associated with a benthic lifestyle and potentially explains their broad environmental resilience. However, further studies are required to fully understand the buffering capacity of the *Cassiopea* mesoglea, and its effect on *Cassiopea* resilience to environmental stressors.

### Light scattering in *Cassiopea*

Light availability in the host is a key factor for efficient photosymbiosis. The host morphology, host and symbiont pigmentation, and symbiont density can affect scattering and absorption of light in symbiotic cnidarians and generate optical micro-niches in the system. Light modulation and photosynthesis at the microscale have already been thoroughly studied in reef building corals (e.g. Enríquez et al. 2005, D'Angelo et al. 2008, Wangpraseurt et al. 2014b), however, to our knowledge only one other study on microscale O<sub>2</sub> dynamics has been done for *Cassiopea* (Arossa et al. 2021), despite it representing a model system for symbiosis and photosynthesis.

The structural complexity of *Cassiopea* no doubt gives rise to the possibility of optical micro-niches for the hosted symbionts. In chapter 2 we showed the presence of a heterogenous light field across the medusa with the oral side and apical parts (i.e., oral arms/the manubrium) having the overall highest photon flux relative to the remaining bell (Lyndby et al. 2022a). The bell itself also revealed interesting heterogeneity, as white granules along rhopalia canals in the bell were found to enhance light scattering and reflectance near the white granules. As such, the results provided in chapter 2 lead to the speculation

that the white granules play a role similar to the light scattering skeleton in reef building corals (Enrriquez et al. 2017). The optical properties of the white granules and the overall structure of *Cassiopea* medusa were further investigated in chapter 3, using Optical Coherence Tomography (OCT).

The chemical composition of the granules is currently not known. We were unable to determine if these granules are due to a mineral aggregation or crystal formation, or purely organic in composition (see also Hamaguchi et al. 2021). However, these granules are typically found in high density along the rhopalia canals and in oral arms. While their exact purpose remains to be determined, the optical properties of tissue regions with abundant white granules revealed that they have strong light scattering properties, suggesting they play a role in photoprotection and/or photo enhancement of symbionts in close proximity. Higher densities of white granules lead to higher scattering locally, resulting in an increased chance of photon absorption by symbionts in close proximity. Unfortunately, the optical properties of the host epidermis were not possible to characterize with the tools available, but OCT data indicate that photons travel relatively unhindered through the mesoglea, once they have passed the epidermis and the dense symbiont population in the subumbrella.

#### **Investigating micromorphology and organization of symbionts in *Cassiopea* medusae**

In general, studies of morphology and ultrastructure of organisms provide important information on how these organisms function. Conventional observations typically include various types of microscopy, which often requires sample preparation steps that introduce tissue artifacts. This is especially true in *Cassiopea*, as their tissues have high water content and are prone to distortion of the morphology and displacement of constituents. The clear spatial segregation of symbionts into mobile amoebocytes situated in the mesoglea, i.e., spatially separated from the medusa gastro- and endodermis, raises intriguing questions about the inner workings of this holobiont, but also represents an extra observational challenge. The non-invasive imaging tool OCT elegantly overcomes issues related to sample preparation and furthermore provides 3D spatial information (chapter 3) (Wangpraseurt et al. 2017b). OCT scans were achieved at a resolution high enough to identify microstructures, such as amoebocyte clusters and light scattering white granules in the umbrella. While individual symbiont cells could not be distinguished within individual amoebocyte clusters, these clusters were typically observed as elongated spheres, up to 100  $\mu\text{m}$  long, suggesting that they have the capacity to harbor much more than 10 dinoflagellate cells per cluster. The OCT observations thus radically change the estimate of dinoflagellates-per-amoebocyte obtained with more conventional observations, such as TEM or histological sectioning; cf. chapter 2 (Lyndby et al. 2020b). While the algal symbionts in *Cassiopea* are highly efficient in

assimilating inorganic nutrients, it is also known (i.e., from corals; Jokiel et al. 1994, Dubinsky & Berman-Frank 2001) that – at high density – the algal symbionts begin to compete for nutrients, although photosynthate release to host remains unchanged regardless of competition pressure (Krueger et al. 2020). Given the high density of symbionts in the subumbrella and the local high density of symbionts that can be found within individual amoebocytes (> 10 per cluster; cf. chapter 3), it is likely that such competition occurs in *Cassiopea* as well. Quantitative data to prove or disprove this hypothesis are still not available, but given that host-mediated nutrient limitation is believed to stimulate release of photosynthates in corals (Dubinsky & Berman-Frank 2001) similar mechanisms are likely at play in *Cassiopea*.

OCT investigations of deeper bell mesoglea revealed that symbiont clusters were also present but more diffusely scattered deep inside the bell. Based on histological sections (chapter 1) the deeper mesoglea layers appeared mostly empty with few amoebocyte-clusters dotted across the entire bell (see figure 2b in Lyndby et al. 2020b). However, the OCT scans showed clusters of symbionts across the entire bell. As described in chapter 1, the motile amoebocytes clearly play a role in facilitating efficient nutrient translocation between the host and its symbionts. However, amoebocytes with clusters of symbionts several mm deep into the bell seem unlikely to serve the function of exchanging nutrients with the host epidermis, and measurements of PSII-related relative electron transport rate (as a proxy for photosynthetic activity) with an imaging PAM revealed that symbionts deep in the mesoglea quickly reached supersaturation, thus limiting photosynthesis. At this point, it is unknown to what extent these deep-dwelling symbionts contribute to the host metabolism, but several possibilities should be considered. The symbionts might act as a reserve population to replenish the subumbrella region in case of symbiont loss (e.g. through bleaching). Alternatively, the deep-dwelling symbionts represent a different strain of symbionts, or simply a sub-population optimized for the darker environment experienced there. However, more studies are needed to identify the role of these seemingly shade-acclimated symbionts deep in *Cassiopea* mesoglea.

### **Photosynthesis and nutrient assimilation across the bell**

Point measurements and depth profiles of photosynthetic performance for algal symbionts near the subumbrella epidermis (chapter 2) focused on the anastomosing tissue based on the visibly high density of symbionts in this region. In chapters 2 and 3, distinct optical microniches of the bell were identified, primarily through light scattering by the white granules located in the rhopalia canals. The optical properties of the white granules determined from the OCT observations/data are such that they

permit very efficient scattering of light and larger densities of white granules locally enhance such scattering, thereby increasing the chance of photon absorption by adjacent algal symbionts. Stable isotope labelling experiment combined with NanoSIMS imaging showed that symbionts near white granules have significantly higher rates of  $^{13}\text{C}$ -bicarbonate assimilation into starch and lipids relative to symbionts found in anastomosing tissue without (visible) white granules (chapter 3), demonstrating that the environment for photosynthesis is very heterogeneous across the bell. This aspect of *Cassiopea* physiology was explored in greater detail in chapter 4 through the use of  $\text{O}_2$ -sensitive planar optodes to image  $\text{O}_2$  production across the entire bell surface with a sufficient lateral resolution to distinguish major radial canals in the bell.

In the studied animals (roughly 4 cm in diameter),  $\text{O}_2$  imaging across the subumbrella bell surface suggested that photosynthetic activity is highest near the bell center and along the rim. However, symbiont density resolved via hyperspectral imaging as relative absorption by major chlorophyll *a* absorption peak (669 nm wavelength) also indicated that these were found in higher density along radial canals in anastomosing tissue and towards the center, while the tissue near the rim exhibited the lowest algal density. The thickness of the bell varies substantially from the center and manubrium region (thick bell) to the rim, where the bell is several times thinner. As such, it is likely that the  $\text{O}_2$  buffering effect of the mesoglea is negligible near the rim, and that observed  $\text{O}_2$  buildup in the bell-rim represents an accumulation with contributions from the entire symbiont population between sub- to exumbrella, possibly explaining the relatively high production observed in thin tissue, similar to previous studies on photosynthesis in oral arms (Arossa et al. 2021). Several major radial canals also showed signs of high  $\text{O}_2$  buildup but were not correlated to either symbiont density nor to the presence of light scattering granules, which were otherwise shown to enhance the carbon assimilation (chapter 3). Radial canals act as the main passage ways for distribution of food/nutrients and uptake of symbionts in *Cassiopea* medusae, and water flow is facilitated through cilia beating. It is therefore likely that radial canals also provide a mean for internal gas exchange with the mesoglea (across the gastroderm), and as such  $\text{O}_2$  buildup during photoperiods might be more actively re-distributed internally than first assumed. However, further studies are required to understand the potential role of the gastric network for internal gas transport and exchange in *Cassiopea*.

## Concluding remarks and future perspective

In this thesis work, I have explored the photobiology and metabolic interactions between the *Cassiopea* medusa and its dinoflagellate symbionts. The work has revealed new aspects of the *Cassiopea* physiology, such as the fate of autotrophically assimilated carbon that is efficiently transferred between symbiont and host via the motile amoebocytes. The physico-chemical microenvironment of *Cassiopea* bell mesoglea showed that mesoglea effectively buffers the environment of the symbionts by storing O<sub>2</sub> and alleviating dramatic changes in pH. I investigated the micromorphology of *Cassiopea* using non-invasive 3D imaging, and provided a new perspective on the organization and distribution of symbionts and white granules across the umbrella system. Optical parameters extracted from light scattering white granules provided evidence of enhancement of carbon assimilation in nearby symbionts and support the hypothesis that white granules serve as a photo-enhancing mechanism similar to what is known from coral host pigments and skeleton. Finally, I showed that photosynthetic activity across the bell is much more heterogeneous than previously assumed. These results expand our knowledge of how the *Cassiopea* holobiont functions, and open up for new –higher level– questions for scientists to answer.

Given the results at hand, a number of future research objectives immediately present themselves: The amoebocytes play a key role in the exchange of autotrophically acquired carbon between symbiont and host tissue. However, the extent and regulation of their motility remains unknown. Future research should explore what triggers amoebocytes to move, and to what extent they move around in the mesoglea. In the same vein, amoebocytes harboring algal symbionts is a unique trait of symbiotic scyphozoans like *Cassiopea*. It remains unknown, whether this trait enables dynamic relocation of symbionts inside *Cassiopea*, and whether active redistribution of symbionts can happen towards damaged or bleached tissue areas for repopulation?

The buffering capacity of the bell mesoglea appears to be an extraordinary preadaptation to survive in a more ‘extreme’ environment (relative to corals), e.g. under hypoxic conditions or other environmental extremes in shallow coastal habitats. The extent of this buffering effect should be explored in greater detail, to understand the limits to the buffering capacity for O<sub>2</sub> and pH. Does this buffering capacity truly offer a more stable environment for symbionts when the host is stressed (e.g. from excessive heating or salinity)? Does the buffering capacity extend beyond O<sub>2</sub> and pH, and could mesoglea act as a storage for (in)organic nutrients like nitrogen, phosphorus, and even species of carbon other than CO<sub>2</sub> /HCO<sub>3</sub><sup>-</sup>?

Finally, the usage of O<sub>2</sub> sensitive planar optodes proved to be a very powerful approach to explore the photosynthesis and O<sub>2</sub> dynamics in *Cassiopea*. However, the results provided here only showed a glimpse of the activity in *Cassiopea*. While the planar optode method should be improved, it should also be considered in combination with suspended O<sub>2</sub> sensitive nanoparticles for a more complete overview of the photosynthetic activity in 3D, to investigate O<sub>2</sub> dynamics under various feeding- and environmental scenarios.

In summary, the results of this thesis advance our understanding of the photobiology of *Cassiopea* and offer exciting new research venues for the future investigations of this symbiosis model system.

## References

- Ahmerkamp S, Jalaluddin FM, Cui Y, Brumley DR, Pacherres CO, Berg JS, Stocker R, Kuypers MMM, Koren K, Behrendt L (2022) Simultaneous visualization of flow fields and oxygen concentrations to unravel transport and metabolic processes in biological systems. *Cell Rep Methods* 2:100216.
- Al-Horani FA, Ferdelman T, Al-Moghrabi SM, de Beer D (2005) Spatial distribution of calcification and photosynthesis in the scleractinian coral *Galaxea fascicularis*. *Coral Reefs* 24:173–180.
- Aljbour SM, Al-Horani FA, Kunzmann A (2018) Metabolic and oxidative stress responses of the jellyfish *Cassiopea* to pollution in the Gulf of Aqaba, Jordan. *Mar Pollut Bull* 130:271–278.
- Aljbour SM, Zimmer M, Al-Horani FA, Kunzmann A (2019) Metabolic and oxidative stress responses of the jellyfish *Cassiopea* sp. to changes in seawater temperature. *J Sea Res* 145:1–7.
- Aljbour SM, Zimmer M, Kunzmann A (2017) Cellular respiration, oxygen consumption, and trade-offs of the jellyfish *Cassiopea* sp. in response to temperature change. *J Sea Res* 128:92–97.
- Allemand D, Furla P (2018) How does an animal behave like a plant? Physiological and molecular adaptations of zooxanthellae and their hosts to symbiosis. *C R Biol* 341:276–280.
- Al-Moghrabi S, Goiran C, Allemand D, Speziale N, Jaubert J (1996) Inorganic carbon uptake for photosynthesis by the symbiotic coral-dinoflagellate association II. Mechanisms for bicarbonate uptake. *J Exp Mar Bio Ecol* 199:227–248.
- Ames CL, Klompen AML, Badhiwala K, Muffett K, Reft AJ, Kumar M, Janssen JD, Schultzhous JN, Field LD, Muroski ME, Bezio N, Robinson JT, Leary DH, Cartwright P, Collins AG, Vora GJ (2020) Cassiosomes are stinging-cell structures in the mucus of the upside-down jellyfish *Cassiopea xamachana*. *Commun Biol* 3:67.
- Anthony KRN, Hoegh-Guldberg O (2003) Variation in coral photosynthesis, respiration and growth characteristics in contrasting light microhabitats: an analogue to plants in forest gaps and understoreys? *Funct Ecol* 17:246–259.
- Arai MN (2001) Pelagic coelenterates and eutrophication: a review. *Hydrobiologia* 451:69–87.
- Arai Y, Gotoh RO, Yokoyama J, Sato C, Okuizumi K, Hanzawa N (2017) Phylogenetic relationships and morphological variations of upside-down jellyfishes, *Cassiopea* spp. inhabiting Palau Island. *Biogeography* 19:133–141.
- Arossa S, Barozzi A, Callegari M, Klein SG, Parry AJ, Hung S-H, Steckbauer A, Aranda M, Daffonchio D, Duarte CM (2021) The Internal Microenvironment of the Symbiotic Jellyfish *Cassiopea* sp. From the Red Sea. *Frontiers in Marine Science* 8.
- Avian M, Mancini L, Voltolini M, Bonnet D, Dreossi D, Macaluso V, Pillepich N, Prieto L, Ramšak A, Terlizzi A, Motta G (2022) A novel endocast technique providing a 3D quantitative analysis of the gastrovascular system in *Rhizostoma pulmo*: An unexpected through-gut in cnidaria. *PLoS One* 17:e0272023.
- Baker AC (2003) Flexibility and Specificity in Coral-Algal Symbiosis: Diversity, Ecology, and Biogeography of Symbiodinium. *Annu Rev Ecol Evol Syst* 34:661–689.
- Banha TNS, Mies M, Güth AZ, Pomory CM, Sumida PYG (2020) Juvenile *Cassiopea andromeda* medusae are resistant to multiple thermal stress events. *Mar Biol* 167:173.
- Battista N, Gaddam MG, Hamlet CL, Hoover AP, Miller LA, Santhanakrishnan A (2022) The Presence of a Substrate Strengthens The Jet Generated by Upside-Down Jellyfish. *Frontiers in Marine Science* 9.
- Bayha KM, Dawson MN, Collins AG, Barbeitos MS, Haddock SHD (2010) Evolutionary Relationships Among Scyphozoan Jellyfish Families Based on Complete Taxon Sampling and Phylogenetic Analyses of 18S and 28S Ribosomal DNA. *Integr Comp Biol* 50:436–455.
- de Beer D, Kühl M, Stambler N, Vaki L (2000) A microsensor study of light enhanced  $Ca^{2+}$  uptake and photosynthesis in the reef-building hermatypic coral *Favia* sp. *Mar Ecol Prog Ser* 194:75–85.



- Berkelmans R, van Oppen MJH (2006) The role of zooxanthellae in the thermal tolerance of corals: a “nugget of hope” for coral reefs in an era of climate change. *Proc Biol Sci* 273:2305–2312.
- Béziat P, Kunzmann A (2022) Under pressure: *Cassiopea andromeda* jellyfish exposed to increasing water temperature or lead, cadmium and anthropogenic gadolinium contamination. *Mar Biol Res*:1–16.
- Bigelow Robert Payne (1900) The anatomy and development of *Cassiopea xamachana*. Boston, Pub. by the Boston Society of Natural History, Boston.
- Biquand E, Okubo N, Aihara Y, Rolland V, Hayward DC, Hatta M, Minagawa J, Maruyama T, Takahashi S (2017) Acceptable symbiont cell size differs among cnidarian species and may limit symbiont diversity. *ISME J* 11:1702–1712.
- Blanquet RS, Phelan MA (1987) An unusual blue mesogleal protein from the mangrove jellyfish *Cassiopea xamachana*. *Mar Biol* 94:423–430.
- Blanquet RS, Riordan GP (1981) An ultrastructural study of the subumbrellar musculature and desmosomal complexes of *Cassiopea xamachana* (Cnidaria: Scyphozoa). *Trans Am Microsc Soc* 100:109–119.
- Bollati E, Lyndby NH, D’Angelo C, Kühl M, Wiedenmann J, Wangpraseurt D (2022) Green fluorescent protein-like pigments optimise the internal light environment in symbiotic reef-building corals. *eLife* 11:e73521.
- Bourne DG, Garren M, Work TM, Rosenberg E, Smith GW, Harvell CD (2009) Microbial disease and the coral holobiont. *Trends Microbiol* 17:554–562.
- Boxer SG, Kraft ML, Weber PK (2009) Advances in imaging secondary ion mass spectrometry for biological samples. *Annu Rev Biophys* 38:53–74.
- Brafield AE, Chapman G (1983) Diffusion of Oxygen through the Mesogloea of the Sea Anemone *Calliactis Parasitica*. *J Exp Biol* 107:181–187.
- Brodersen KE, Koren K, Moßhammer M, Ralph PJ, Kühl M, Santner J (2017) Seagrass-Mediated Phosphorus and Iron Solubilization in Tropical Sediments. *Environ Sci Technol* 51:14155–14163.
- Brodersen KE, Kühl M, Trampe E, Koren K (2020) Imaging O<sub>2</sub> dynamics and microenvironments in the seagrass leaf phyllosphere with magnetic optical sensor nanoparticles. *Plant J* 104:1504–1519.
- Brodersen KE, Lichtenberg M, Ralph PJ, Kühl M, Wangpraseurt D (2014) Radiative energy budget reveals high photosynthetic efficiency in symbiont-bearing corals. *J R Soc Interface* 11:20130997.
- Brown BE (1997) Coral bleaching: causes and consequences. *Coral Reefs* 16:S129–S138.
- Carraway ER, Demas JN, DeGraff BA, Bacon JR (1991) Photophysics and photochemistry of oxygen sensors based on luminescent transition-metal complexes. *Anal Chem* 63:337–342.
- Çevik C (2006) A new record of an alien jellyfish from the Levantine coast of Turkey - *Cassiopea andromeda* (Forsskål, 1775) (Cnidaria: Scyphozoa:Rhizostomea). *Aquat Invasions* 1:196–197.
- Chan NCS, Wangpraseurt D, Kühl M, Connolly SR (2016) Flow and coral morphology control coral surface pH: Implications for the effects of ocean acidification. *Frontiers in Marine Science* 3:10.
- Chapman DM (1999) Microanatomy of the bell rim of *Aurelia aurita* (Cnidaria: Scyphozoa). *Can J Zool* 77:34–46.
- Clode PL, Stern RA, Marshall AT (2007) Subcellular imaging of isotopically labeled carbon compounds in a biological sample by ion microprobe (NanoSIMS). *Microsc Res Tech* 70:220–229.
- Cohen SK, Aschtgen M-S, Lynch JB, Koehler S, Chen F, Escrig S, Daraspe J, Ruby EG, Meibom A, McFall-Ngai M (2020) Tracking the cargo of extracellular symbionts into host tissues with correlated electron microscopy and nanoscale secondary ion mass spectrometry imaging. *Cell Microbiol* 22:e13177.
- Colley NJ, Trench RK (1985) Cellular events in the reestablishment of a symbiosis between a marine dinoflagellate and a coelenterate. *Cell Tissue Res* 239:93–103.

- Colley NJ, Trench RK (1983) Selectivity in phagocytosis and persistence of symbiotic algae by the scyphistoma stage of the jellyfish *Cassiopeia xamachana*. *Proceedings of the Royal Society of London Series B Biological Sciences* 219:61–82.
- Cruz S, LeKieffre C, Cartaxana P, Hubas C, Thiney N, Jakobsen S, Escrig S, Jesus B, Kühl M, Calado R, Meibom A (2020) Functional kleptoplasts intermediate incorporation of carbon and nitrogen in cells of the Sacoglossa sea slug *Elysia viridis*. *Sci Rep* 10:10548.
- Curtis SK, Cowden RR (1974) Some Aspects of Regeneration in the Scyphistoma of *Cassiopea* (Class Scyphozoa) as Revealed by the Use of Antimetabolites and Microspectrophotometry. *Integr Comp Biol* 14:851–866.
- D'Angelo C, Denzel A, Vogt A, Matz MV, Oswald F, Salih A, Nienhaus GU, Wiedenmann J (2008) Blue light regulation of host pigment in reef-building corals. *Mar Ecol Prog Ser* 364:97–106.
- Davy SK, Allemand D, Weis VM (2012) Cell Biology of Cnidarian-Dinoflagellate Symbiosis. *Microbiol Mol Biol Rev* 76:229–261.
- Dekkers JF, Alieva M, Wellens LM, Ariese HCR, Jamieson PR, Vonk AM, Amatngalim GD, Hu H, Oost KC, Snippert HJG, Beekman JM, Wehrens EJ, Visvader JE, Clevers H, Rios AC (2019) High-resolution 3D imaging of fixed and cleared organoids. *Nat Protoc* 14:1756–1771.
- Depetris A, Peter H, Bordoloi AD, Bernard H, Niayifar A, Kühl M, de Anna P, Battin TJ (2021) Morphogenesis and oxygen dynamics in phototrophic biofilms growing across a gradient of hydraulic conditions. *iScience* 24:102067.
- Djehri N, Pondaven P, Stibor H, Dawson MN (2019) Review of the diversity, traits, and ecology of zooxanthellate jellyfishes. *Mar Biol* 166:19.
- Djehri N, Stibor H, Lebeau O, Pondaven P (2020)  $\Delta^{13}C$ ,  $\delta^{15}N$ , and C:N ratios as nutrition indicators of zooxanthellate jellyfishes: insights from an experimental approach. *J Exp Mar Bio Ecol* 522:151257.
- Dove SG, Hoegh-Guldberg O, Ranganathan S (2001) Major colour patterns of reef-building corals are due to a family of GFP-like proteins. *Coral Reefs* 19:197–204.
- Dove SG, Lovell C, Fine M, Deckenback J, Hoegh-Guldberg O, Iglesias-Prieto R, Anthony KRN (2008) Host pigments: potential facilitators of photosynthesis in coral symbioses. *Plant Cell Environ* 31:1523–1533.
- Drew EA (1972) The biology and physiology of alga-invertebrate symbioses. I. Carbon fixation in *Cassiopea* sp. at aldraba atoll. *J Exp Mar Bio Ecol* 9:65–69.
- Dubinsky Z, Berman-Frank I (2001) Uncoupling primary production from population growth in photosynthesizing organisms in aquatic ecosystems. *Aquat Sci* 63:4–17.
- Edmunds PJ, Davies PS (1986) An energy budget for *Porites porites* (Scleractinia). *Mar Biol* 92:339–347.
- Enríquez S, Méndez ER, Hoegh-Guldberg O, Iglesias-Prieto R (2017) Key functional role of the optical properties of coral skeletons in coral ecology and evolution. *Proc Biol Sci* 284.
- Enríquez S, Méndez ER, -Prieto RI (2005) Multiple scattering on coral skeletons enhances light absorption by symbiotic algae. *Limnol Oceanogr* 50:1025–1032.
- Estes AM, Kempf SC, Henry RP (2003) Localization and quantification of carbonic anhydrase activity in the symbiotic Scyphozoan *Cassiopea xamachana*. *Biol Bull* 204:278–289.
- Ezzat L, Maguer J-F, Grover R, Ferrier-Pagès C (2015) New insights into carbon acquisition and exchanges within the coral-dinoflagellate symbiosis under  $NH_4^+$  and  $NO_3^-$  supply. *Proc Biol Sci* 282:20150610.
- Fabricius-Dyg J, Mistlberger G, Staal M, Borisov SM, Klimant I, Kühl M (2012) Imaging of surface  $O_2$  dynamics in corals with magnetic micro optode particles. *Mar Biol* 159:1621–1631.
- Falkowski PG, Dubinsky Z, Muscatine L, Porter JW (1984) Light and the bioenergetics of a symbiotic coral. *Bioscience* 34:705–709.

- Fercher AF, Drexler W, Hitzemberger CK, Lasser T (2003) Optical coherence tomography - principles and applications. *Rep Prog Phys* 66:239–303.
- Fitt WK (1985) Effect of different strains of the zooxanthella *Symbiodinium microadriaticum* on growth and survival of their coelenterate and molluscan hosts.
- Fitt WK, Costley K (1998) The role of temperature in survival of the polyp stage of the tropical rhizostome jellyfish *Cassiopea xamachana*. *J Exp Mar Bio Ecol* 222:79–91.
- Fitt WK, Hofmann DK, Kemp DW, Ohdera AH (2021) Different Physiology in the Jellyfish *Cassiopea xamachana* and *C. frondosa* in Florida Bay. *J Geophys Res C: Oceans* 2:811–821.
- Fitt WK, Trench RK (1983) Endocytosis of the symbiotic dinoflagellate *Symbiodinium microadriaticum* Freudenthal by endodermal cells of the scyphistomae of *Cassiopeia xamachana* and resistance of the algae to host digestion. *J Cell Sci* 64:195–212.
- Fleck J, Fitt WK (1999) Degrading mangrove leaves of *Rhizophora mangle* Linne provide a natural cue for settlement and metamorphosis of the upside down jellyfish *Cassiopea xamachana* Bigelow. *J Exp Mar Bio Ecol* 234:83–94.
- Fleck J, Fitt WK, Hahn MG (1999) A proline-rich peptide originating from decomposing mangrove leaves is one natural metamorphic cue of the tropical jellyfish *Cassiopea xamachana*. *Mar Ecol Prog Ser* 183:115–124.
- Floss C, Stadermann FJ, Bradley JP, Dai ZR, Bajt S, Graham G, Lea AS (2006) Identification of isotopically primitive interplanetary dust particles: A NanoSIMS isotopic imaging study. *Geochim Cosmochim Acta* 70:2371–2399.
- Flynn KJ, Mitra A, Anestis K, Anschütz AA, Calbet A, Ferreira GD, Gypens N, Hansen PJ, John U, Martin JL, Mansour JS, Maselli M, Medić N, Norlin A, Not F, Pitta P, Romano F, Saiz E, Schneider LK, Stolte W, Traboni C (2019) Mixotrophic protists and a new paradigm for marine ecology: where does plankton research go now? *J Plankton Res* 41:375–391.
- Forsskål P, Niebuhr C (1775) *Descriptiones animalium, avium, amphibiorum, piscium, insectorum, vermium. ex officina Mölleri, Hauniæ* :
- Freeman CJ, Stoner EW, Easson CG, Matterson KO, Baker DM (2016) Symbiont carbon and nitrogen assimilation in the *Cassiopea–Symbiodinium* mutualism. *Mar Ecol Prog Ser* 544:281–286.
- Freudenthal (1959) Observations on the algal cells (zooxanthellae) inhabiting the anemone *Cassiopeia* sp. *J At Mol Phys*.
- Freudenthal HD (1962) *Symbiodinium* Gen Nov and *Symbiodinium Microadriaticum* Sp Nov, a Zooxanthella - Taxonomy, Life Cycle, and Morphology. *J Protozool* 9:45-.
- Fujimoto JG, Pitris C, Boppart SA, Brezinski ME (2000) Optical coherence tomography: an emerging technology for biomedical imaging and optical biopsy. *Neoplasia* 2:9–25.
- Gibbin E, Banc-Prandi G, Fine M, Comment A, Meibom A (2020) A method to disentangle and quantify host anabolic turnover in photosymbiotic holobionts with subcellular resolution. *Communications Biology* 3:14.
- Gibbin EM, Krueger T, Putnam HM, Barott KL, Bodin J, Gates RD, Meibom A (2018) Short-term thermal acclimation modifies the metabolic condition of the coral holobiont. *Frontiers in Marine Science* 5:1–11.
- Gibbin EM, Putnam HM, Davy SK, Gates RD (2014) Intracellular pH and its response to CO<sub>2</sub>-driven seawater acidification in symbiotic versus non-symbiotic coral cells. *Journal of Experimental Biology* 217:1963–1969.
- Glud RN, Kühl M, Kohls O, Ramsing NB (1999) Heterogeneity of oxygen production and consumption in a photosynthetic microbial mat as studied by planar optodes. *J Phycol* 35:270–279.
- Glynn PW (1996) Coral reef bleaching: Facts, hypotheses and implications. *Glob Chang Biol* 2:495–509.

- Gold DA, Jacobs DK (2013) Stem cell dynamics in Cnidaria: are there unifying principles? *Dev Genes Evol* 223:53–66.
- Goldfarb AJ (1914) Changes in salinity and their effects upon the regeneration of *Cassiopea xamachana*. In: *Papers from the Tortugas Laboratory of the Carnegie Institution of Washington*. Carnegie Institution of Washington, Washington, D.C, p 83–94
- Grignon N, Halpern S, Jeusset J, Briançon C, Fragu P (1997) Localization of chemical elements and isotopes in the leaf of soybean (*Glycine max*) by secondary ion mass spectrometry microscopy: critical choice of sample preparation procedure. *J Microsc* 186:51–66.
- Grovenor CRM, Smart KE, Kilburn MR, Shore B, Dilworth JR, Martin B, Hawes C, Rickaby REM (2006) Specimen preparation for NanoSIMS analysis of biological materials. *Appl Surf Sci* 252:6917–6924.
- Grover R, Maguer JF, Allemand D, Ferrier-Pages C (2003) Nitrate uptake in the scleractinian coral *Stylophora pistillata*. *Limnol Oceanogr* 48:2266–2274.
- Grover R, Maguer JF, Allemand D, Ferrier-Pages C (2008) Uptake of dissolved free amino acids by the scleractinian coral *Stylophora pistillata*. *J Exp Biol* 211:860–865.
- Hamaguchi Y, Iida A, Nishikawa J, Hirose E (2021) Umbrella of *Mastigias papua* (Scyphozoa: Rhizostomeae: Mastigiidae): Hardness and cytomorphology with remarks on colors. *Plankton Benthos Res* 16:221–227.
- Hamlet C, Santhanakrishnan A, Miller LA (2011) A numerical study of the effects of bell pulsation dynamics and oral arms on the exchange currents generated by the upside-down jellyfish *Cassiopea xamachana*. *J Exp Biol* 214:1911.
- Hartenstein V (2006) Blood Cells and Blood Cell Development in the Animal Kingdom. *Annu Rev Cell Dev Biol* 22:677–712.
- Hatcher BG (1990) Coral reef primary productivity. A hierarchy of pattern and process. *Trends Ecol Evol* 5:149–155.
- Henry L-A, Hart M (2005) Regeneration from injury and resource allocation in sponges and corals - a review. *Int Rev Hydrobiol* 90:125–158.
- Hettinger JW, de la Peña Mattozzi M, Myers WR, Williams ME, Reeves A, Parsons RL, Haskell RC, Petersen DC, Wang R, Medford JI (2000) Optical coherence microscopy. A technology for rapid, *in vivo*, non-destructive visualization of plants and plant cells. *Plant Physiol* 123:3–16.
- Hoegh-Guldberg O, Jacob D, Taylor M, Guillén Bolaños T, Bindi M, Brown S, Camilloni IA, Diedhiou A, Djalante R, Ebi K, Engelbrecht F, Guiot J, Hijioka Y, Mehrotra S, Hope CW, Payne AJ, Pörtner H-O, Seneviratne SI, Thomas A, Warren R, Zhou G (2019) The human imperative of stabilizing global climate change at 1.5°C. *Science* 365:eaaw6974.
- Hofmann DK, Fitt WK, Fleck J (1996) Checkpoints in the life-cycle of *Cassiopea* spp.: Control of metagenesis and metamorphosis in a tropical jellyfish. *Int J Dev Biol* 40:331–338.
- Hofmann DK, Hadfield MG (2002) Hermaphroditism, gonochorism, and asexual reproduction in *Cassiopea* sp.—an immigrant in the islands of Hawai'i. *Invertebr Reprod Dev* 41:215–221.
- Hofmann DK, Kremer BP (1981) Carbon metabolism and strobilation in *Cassiopea andromeda* (Cnidaria: Scyphozoa): Significance of endosymbiotic dinoflagellates. *Mar Biol* 65:25–33.
- Hofmann DK, Neumann R, Henne K (1978) Strobilation, budding and initiation of scyphistoma morphogenesis in the rhizostome *Cassiopea andromeda* (Cnidaria: Scyphozoa). *Mar Biol* 47:161–176.
- Holland BS, Dawson MN, Crow GL, Hofmann DK (2004) Global phylogeography of *Cassiopea* (Scyphozoa: Rhizostomeae): molecular evidence for cryptic species and multiple invasions of the Hawaiian Islands. *Mar Biol* 145:1119–1128.

- Hoogenboom M, Beraud E, Ferrier-Pagès C (2010) Relationship between symbiont density and photosynthetic carbon acquisition in the temperate coral *Cladocora caespitosa*. *Coral Reefs* 29:21–29.
- Hoppe P (2006) NanoSIMS: A new tool in cosmochemistry. *Appl Surf Sci* 252:7102–7106.
- Hoppe P, Cohen S, Meibom A (2013) NanoSIMS: Technical aspects and applications in cosmochemistry and biological geochemistry. *Geostand Geoanal Res* 37:111–154.
- Huang D, Swanson EA, Lin CP, Schuman JS, Stinson WG, Chang W, Hee MR, Flotte T, Gregory K, Puliafito CA (1991) Optical coherence tomography. *Science* 254:1178–1181.
- Hudspith M, Rix L, Achlatis M, Bougoure J, Guagliardo P, Clode PL, Webster NS, Muyzer G, Pernice M, De Goeij JM (2021) Subcellular view of host–microbiome nutrient exchange in sponges: insights into the ecological success of an early metazoan–microbe symbiosis. *Microbiome* 9.
- Huebinger J, Spindler J, Holl KJ, Koos B (2018) Quantification of protein mobility and associated reshuffling of cytoplasm during chemical fixation. *Sci Rep* 8:17756.
- Hughes TP, Baird AH, Bellwood DR, Card M, Connolly SR, Folke C, Grosberg R, Hoegh-Guldberg O, Jackson JB, Kleypas J, Lough JM, Marshall P, Nystrom M, Palumbi SR, Pandolfi JM, Rosen B, Roughgarden J (2003) Climate change, human impacts, and the resilience of coral reefs. *Science* 301:929–933.
- Hughes TP, Kerry JT, Alvarez-Noriega M, Alvarez-Romero JG, Anderson KD, Baird AH, Babcock RC, Beger M, Bellwood DR, Berkelmans R, Bridge TC, Butler IR, Byrne M, Cantin NE, Comeau S, Connolly SR, Cumming GS, Dalton SJ, Diaz-Pulido G, Eakin CM, Figueira WF, Gilmour JP, Harrison HB, Heron SF, Hoey AS, Hobbs JA, Hoogenboom MO, Kennedy EV, Kuo CY, Lough JM, Lowe RJ, Liu G, McCulloch MT, Malcolm HA, McWilliam MJ, Pandolfi JM, Pears RJ, Pratchett MS, Schoepf V, Simpson T, Skirving WJ, Sommer B, Torda G, Wachenfeld DR, Willis BL, Wilson SK (2017) Global warming and recurrent mass bleaching of corals. *Nature* 543:373–377.
- Jacques SL, Wangpraseurt D, Kühl M (2019) Optical properties of living corals determined with diffuse reflectance spectroscopy. *Frontiers in Marine Science* 6.
- Jantzen C, Wild C, Rasheed M, El-Zibdah M, Richter C (2010) Enhanced pore-water nutrient fluxes by the upside-down jellyfish *Cassiopea* sp. in a Red Sea coral reef. *Mar Ecol Prog Ser* 411:117–125.
- Jarms G, Morandini AC (2019) *World Atlas of Jellyfish: Scyphozoa Except Stauromedusae*. Dölling und Galitz Verlag.
- Jensen SI, Kühl M, Glud RN, Jørgensen LB, Priemé A (2005) Oxidic microzones and radial oxygen loss from roots of *Zostera marina*. *Mar Ecol Prog Ser* 293:49–58.
- Jimenez IM, Kühl M, Larkum AWD, Ralph PJ (2008) Heat budget and thermal microenvironment of shallow-water corals: Do massive corals get warmer than branching corals? *Limnol Oceanogr* 53:1548–1561.
- Jimenez IM, Larkum AWD, Ralph PJ, Kühl M (2012) Thermal effects of tissue optics in symbiont-bearing reef-building corals. *Limnol Oceanogr* 57:1816–1825.
- Jokiel PL, Dubinsky Z, Stambler N (1994) Results of the 1991 United States-Israel Workshop, "Nutrient Limitation in the Symbiotic Association between Zooxanthellae and Reef-building Corals". *Pac Sci* 48:215–218.
- Jordano M de A, Miyake H, Nagata RM, Morandini AC (2022) Patterns of morphological development in Scyphozoa ephyrae (Cnidaria, Medusozoa). *Mar Biodivers* 52:31.
- Kayal E, Bentlage B, Collins AG, Kayal M, Pirro S, Lavrov DV (2012) Evolution of linear mitochondrial genomes in medusozoan cnidarians. *Genome Biol Evol* 4:1–12.
- Kayal E, Bentlage B, Sabrina Pankey M, Ohdera AH, Medina M, Plachetzki DC, Collins AG, Ryan JF (2018) Phylogenomics provides a robust topology of the major cnidarian lineages and insights on the origins of key organismal traits. *BMC Evol Biol* 18:68.
- Keilin D, Mann T (1939) Carbonic Anhydrase. *Nature* 144:442–443.

- Klein SG, Pitt KA, Lucas CH, Hung S-H, Schmidt-Roach S, Aranda M, Duarte CM (2019) Night-time temperature reprieves enhance the thermal tolerance of a symbiotic cnidarian. *Frontiers in Marine Science* 6.
- Klein SG, Pitt KA, Nitschke MR, Goyen S, Welsh DT, Suggett DJ, Carroll AR (2017a) *Symbiodinium* mitigate the combined effects of hypoxia and acidification on a noncalcifying cnidarian. *Glob Chang Biol* 23:3690–3703.
- Klein SG, Pitt KA, Nitschke MR, Goyen S, Welsh DT, Suggett DJ, Carroll AR (2017b) *Symbiodinium* mitigate the combined effects of hypoxia and acidification on a noncalcifying cnidarian. *Glob Chang Biol* 23:3690–3703.
- Klimant I, Ruckruh F, Liebsch G, Stangelmayer A, Wolfbeis OS (1999) Fast Response Oxygen Micro-Optodes Based on Novel Soluble Ormosil Glasses. *Microchim Acta* 131:35–46.
- Kopp C, Domart-Coulon I, Barthelemy D, Meibom A (2016) Nutritional input from dinoflagellate symbionts in reef-building corals is minimal during planula larval life stage. *Science Advances* 2:e1500681.
- Kopp C, Domart-Coulon I, Escrig S, Humbel BM, Hignette M, Meibom A (2015) Subcellular investigation of photosynthesis-driven carbon and nitrogen assimilation and utilization in the symbiotic reef coral *Pocillopora damicornis*. *MBio* 6:1–9.
- Koren K, Brodersen KE, Jakobsen SL, Kühl M (2015) Optical sensor nanoparticles in artificial sediments—a new tool to visualize O<sub>2</sub> dynamics around the rhizome and roots of seagrasses. *Environ Sci Technol* 49:2286–2292.
- Koren K, Jakobsen SL, Kühl M (2016) In-vivo imaging of O<sub>2</sub> dynamics on coral surfaces spray-painted with sensor nanoparticles. *Sens Actuators B Chem* 237:1095–1101.
- Koren K, Kühl M (2018) CHAPTER 7:Optical O<sub>2</sub> Sensing in Aquatic Systems and Organisms. In: *Quenched-phosphorescence Detection of Molecular Oxygen*. Detection Science, Papkovsky DB, Dmitriev RI (eds) p 145–174
- Kramer N, Tamir R, Ben-Zvi O, Jacques SL, Loya Y, Wangpraseurt D (2021) Efficient light-harvesting of mesophotic corals is facilitated by coral optical traits. *Funct Ecol* 36:406–418.
- Kremer P, Costello J, Kremer J, Canino M (1990) Significance of Photosynthetic Endosymbionts to the Carbon Budget of the Scyphomedusa *Linuche unguiculata*. *Limnol Oceanogr* 35:609–624.
- Krueger T, Horwitz N, Bodin J, Giovani M-E, Escrig S, Fine M, Meibom A (2020) Intracellular competition for nitrogen controls dinoflagellate population density in corals. *Proc Biol Sci* 287:20200049.
- Krueger T, Horwitz N, Bodin J, Giovani M-E, Escrig S, Meibom A, Fine M (2017) Common reef-building coral in the Northern Red Sea resistant to elevated temperature and acidification. *Royal Society Open Science* 4:170038.
- Kühl M (2005) Optical microsensors for analysis of microbial communities. In: *Methods in Enzymology*. Academic Press, p 166–199
- Kühl M, Behrendt L, Trampe E, Qvortrup K, Schreiber U, Borisov SM, Klimant I, Larkum AWD (2012) Microenvironmental Ecology of the Chlorophyll b-Containing Symbiotic Cyanobacterium *Prochloron* in the Didemnid Ascidian *Lissoclinum patella*. *Front Microbiol* 3:402.
- Kühl M, Cohen Y, Dalsgaard T, Jørgensen BB, Revsbech NP (1995) Microenvironment and photosynthesis of zooxanthellae in scleractinian corals studied with microsensors for O<sub>2</sub>, pH and light. *Mar Ecol Prog Ser* 117:159–172.
- Kühl M, Holst G, Larkum AWD, Ralph PJ (2008) Imaging of oxygen dynamics within the endolithic algal community of the massive coral *Porites lobata*. *J Phycol* 44:541–550.
- Ladouceur EEB, Garner MM, Wynne J, Fish S, Adams L (2013) Ulcerative Umbrellar Lesions in Captive Moon Jelly (*Aurelia aurita*) Medusae. *Vet Pathol* 50:434–442.

- LaJeunesse TC (2001) Investigating the biodiversity, ecology, and phylogeny of endosymbiotic dinoflagellates in the genus *Symbiodinium* using the ITS region: In search of a “species” level marker. *J Phycol* 37:866–880.
- LaJeunesse TC, Parkinson JE, Gabrielson PW, Jeong HJ, Reimer JD, Voolstra CR, Santos SR (2018) Systematic Revision of Symbiodiniaceae Highlights the Antiquity and Diversity of Coral Endosymbionts. *Curr Biol* 28:2570–2580 e6.
- Lampert KP (2016) Cassiopea and its zooxanthellae. In: *The Cnidaria, Past, Present and Future: The world of Medusa and her sisters*. Goffredo S, Dubinsky Z (eds) Springer International Publishing, Cham, p 415–423
- Lampert KP, Bürger P, Striewski S, Tollrian R (2012) Lack of association between color morphs of the jellyfish *Cassiopea andromeda* and zooxanthella clade. *Mar Ecol* 33:364–369.
- Larsen M, Borisov SM, Grunwald B, Klimant I, Glud RN (2011) A simple and inexpensive high resolution color ratiometric planar optode imaging approach: application to oxygen and pH sensing. *Limnol Oceanogr Methods* 9:348–360.
- Lawley JW, Carroll AR, McDougall C (2021) Rhizostomins: A novel pigment family from rhizostome jellyfish (Cnidaria, Scyphozoa). *Front Mar Sci* 8.
- Lechene C, Hillion F, McMahon G, Benson D, Kleinfeld AM, Kampf JP, Distel D, Luyten Y, Bonventre J, Hentschel D, Park KM, Ito S, Schwartz M, Benichou G, Slodzian G (2006) High-resolution quantitative imaging of mammalian and bacterial cells using stable isotope mass spectrometry. *J Biol* 5:20.
- Leggat W, Hoegh-Guldberg O, Dove S, Yellowlees D (2007) Analysis of an EST library from the dinoflagellate (*Symbiodinium* sp.) symbiont of reef-building corals. *J Phycol* 43:1010–1021.
- Lekieffre C, Spero HJ, Fehrenbacher JS, Russell AD, Ren H, Geslin E, Meibom A (2020) Ammonium is the preferred source of nitrogen for planktonic foraminifer and their dinoflagellate symbionts. *Proceedings of the Royal Society B: Biological Sciences* 287:20200620.
- Lesser MP, Farrell JH (2004) Exposure to solar radiation increases damage to both host tissues and algal symbionts of corals during thermal stress. *Coral Reefs* 23:367–377.
- Levitz D, Hinds MT, Choudhury N, Tran NT, Hanson SR, Jacques SL (2010) Quantitative characterization of developing collagen gels using optical coherence tomography. *J Biomed Opt* 15:026019.
- Levitz D, Thrane L, Frosz M, Andersen P, Andersen C, Andersson-Engels S, Valanciunaite J, Swartling J, Hansen P (2004) Determination of optical scattering properties of highly-scattering media in optical coherence tomography images. *Opt Express* 12:249–259.
- Lewis Ames C (2018) *Medusa: A Review of an Ancient Cnidarian Body Form*. Springer International Publishing, p 105–136
- Loussert-Fonta C, Toullec G, Paraecattil AA, Jeangros Q, Krueger T, Escrig S, Meibom A (2020) Correlation of fluorescence microscopy, electron microscopy, and NanoSIMS stable isotope imaging on a single tissue section. *Communications Biology* 3:362.
- Lyndby NH, Holm JB, Wangpraseurt D, Ferrier-Pagès C, Kühl M (2019) Bio-optical properties and radiative energy budgets in fed and unfed scleractinian corals (*Pocillopora* sp.) during thermal bleaching. *Marine Ecology Progress Series* 629:1–17.
- Lyndby NH, Holm JB, Wangpraseurt D, Grover R, Rottier C, Kühl M, Ferrier-Pagès C (2020a) Effect of temperature and feeding on carbon budgets and O<sub>2</sub> dynamics in *Pocillopora damicornis*. *Mar Ecol Prog Ser* 652:49–62.
- Lyndby NH, Kühl M, Wangpraseurt D (2016) Heat generation and light scattering of green fluorescent protein-like pigments in coral tissue. *Sci Rep* 6:26599.

- Lyndby NH, Murray MC, Trampe E, Meibom A, Kühl M (2022a) The mesoglea buffers the physico-chemical microenvironment of photosymbionts in the upside-down jellyfish *Cassiopea* sp. bioRxiv:2022.10.06.511124.
- Lyndby NH, Murthy S, Bessette S, Jakobsen SL, Meibom A, Kühl M (2022b) Non-invasive investigation of the morphology and optical properties of the upside-down jellyfish *Cassiopea* with optical coherence tomography.
- Lyndby NH, Radecker N, Bessette S, Jensen LHS, Escrig S, Trampe E, Kühl M, Meibom A (2020b) Amoebocytes facilitate efficient carbon and nitrogen assimilation in the *Cassiopea*-Symbiodiniaceae symbiosis. *Proceedings of the Royal Society B* 287.
- Lyndby NH, Radecker N, Bessette S, Sjøgaard Jensen LH, Escrig S, Trampe E, Kühl M, Meibom A (2020c) Amoebocytes facilitate efficient carbon and nitrogen assimilation in the *Cassiopea*-Symbiodiniaceae symbiosis. *Proc Biol Sci* 287:20202393.
- Madshus IH (1988) Regulation of intracellular pH in eukaryotic cells. *Biochem J* 250:1–8.
- Maggio T, Allegra A, Bosch-Belmar M, Cillari T, Cuttitta A, Falautano M, Milisenda G, Nicosia A, Perzia P, Sinopoli M, Castriota L (2019) Molecular identity of the non-indigenous *Cassiopea* sp. from Palermo Harbour (central Mediterranean Sea). *J Mar Biol Assoc U K* 99:1765–1773.
- Mammone M, Ferrier-Pagés C, Lavorano S, Rizzo L, Piraino S, Rossi S (2021) High photosynthetic plasticity may reinforce invasiveness of upside-down zooxanthellate jellyfish in Mediterranean coastal waters. *PLoS One* 16:e0248814.
- Marcelino LA, Westneat MW, Stoyneva V, Henss J, Rogers JD, Radosevich A, Turzhitsky V, Siple M, Fang A, Swain TD, Fung J, Backman V (2013) Modulation of light-enhancement to symbiotic algae by light-scattering in corals and evolutionary trends in bleaching. *PLoS One* 8:e61492.
- Martin VJ (2002) Photoreceptors of cnidarians. *Can J Zool* 80:1703–1722.
- Mayer AG (1910) *Medusae of the world: Volume III The Scyphomedusae*. Carnegie institution of Washington, Washington, DC.
- McCloskey LR, Muscatine L, Wilkerson FP (1994) Daily photosynthesis, respiration, and carbon budgets in a tropical marine jellyfish (*Mastigias* sp.). *Mar Biol* 119:13–22.
- McFall-Ngai M, Hadfield MG, Bosch TCG, Carey HV, Domazet-Lošo T, Douglas AE, Dubilier N, Eberl G, Fukami T, Gilbert SF, Hentschel U, King N, Kjelleberg S, Knoll AH, Kremer N, Mazmanian SK, Metcalf JL, Neelson K, Pierce NE, Rawls JF, Reid A, Ruby EG, Rumpho M, Sanders JG, Tautz D, Wernegreen JJ (2013) Animals in a bacterial world, a new imperative for the life sciences. *Proceedings of the National Academy of Sciences* 110:3229–3236.
- McGill CJ, Pomory CM (2008) Effects of bleaching and nutrient supplementation on wet weight in the jellyfish *Cassiopea xamachana* (Bigelow) (Cnidaria: Scyphozoa). *Mar Freshw Behav Physiol* 41:179–189.
- Medina M, Sharp V, Ohdera A, Bellantuono A, Dalrymple J, Gamero-Mora E, Steinworth B, Hofmann DK, Martindale MQ, Morandini AC, Degennaro M, Fitt WK (2021) The upside-down jellyfish *Cassiopea xamachana* as an emerging model system to study cnidarian–algal symbiosis. In: *Handbook of Marine Model Organisms in Experimental Biology*. CRC Press, Boca Raton, p 149–171
- Mellas RE, McIlroy SE, Fitt WK, Coffroth MA (2014) Variation in symbiont uptake in the early ontogeny of the upside-down jellyfish, *Cassiopea* spp. *J Exp Mar Bio Ecol* 459:38–44.
- Miller DJ, Yellowlees D (1989) Inorganic nitrogen uptake by symbiotic marine cnidarians: a critical review. *Proc R Soc Lond* 237:109–125.
- Mills CE (2001) Jellyfish blooms: are populations increasing globally in response to changing ocean conditions? *Hydrobiologia* 451:55–68.



- Morandini AC, Stampar SN, Maronna MM, Da Silveira FL (2017) All non-indigenous species were introduced recently? The case study of *Cassiopea* (Cnidaria: Scyphozoa) in Brazilian waters. *J Mar Biol Assoc U K* 97:321–328.
- Moßhammer M, Brodersen KE, Kühl M, Koren K (2019) Nanoparticle- and microparticle-based luminescence imaging of chemical species and temperature in aquatic systems: a review. *Mikrochim Acta* 186:126.
- Muffett KM, Aulgur J, Miglietta MP (2022) Impacts of light and food availability on early development of *Cassiopea medusae*. *Front Mar Sci* 8.
- Muscatine L, McCloskey LR, Marian RE (1981) Estimating the daily contribution of carbon from zooxanthellae to coral animal respiration. *Limnol Oceanogr* 26:601–611.
- Newkirk CR, Frazer TK, Martindale MQ (2018) Acquisition and proliferation of algal symbionts in bleached polyps of the upside-down jellyfish, *Cassiopea xamachana*. *J Exp Mar Bio Ecol* 508:44–51.
- Newkirk CR, Frazer TK, Martindale MQ, Schnitzler CE (2020) Adaptation to Bleaching: Are Thermotolerant Symbiodiniaceae Strains More Successful Than Other Strains Under Elevated Temperatures in a Model Symbiotic Cnidarian? *Front Microbiol* 11.
- Niggli W, Wild C (2010) Spatial distribution of the upside-down jellyfish *Cassiopea* sp. within fringing coral reef environments of the Northern Red Sea: implications for its life cycle. *Helgol Mar Res* 64:281–287.
- Nomaki H, Bernhard JM, Ishida A, Tsuchiya M, Uematsu K, Tame A, Kitahashi T, Takahata N, Sano Y, Toyofuku T (2016) Intracellular Isotope Localization in *Ammonia* sp. (Foraminifera) of Oxygen-Depleted Environments: Results of Nitrate and Sulfate Labeling Experiments. *Front Microbiol* 7:163.
- Nuñez J, Renslow R, Cliff III JB, Anderton CR (2018) NanoSIMS for biological applications: Current practices and analyses. *Biointerphases* 13:03B301.
- Ohdera AH, Abrams MJ, Ames CL, Baker DM, Suescún-Bolívar LP, Collins AG, Freeman CJ, Gamero-Mora E, Goulet TL, Hofmann DK, Jaimes-Becerra A, Long PF, Marques AC, Miller LA, Mydlarz LD, Morandini AC, Newkirk CR, Putri SP, Samson JE, Stampar SN, Steinworth B, Templeman M, Thomé PE, Vlok M, Woodley CM, Wong JCY, Martindale MQ, Fitt WK, Medina M (2018) Upside-down but headed in the right direction: Review of the highly versatile *Cassiopea xamachana* system. *Frontiers in Ecology and Evolution* 6.
- Ostendarp M, Plewka J, Flathmann J, Tilstra A, El-Khaled YC, Wild C (2022) Complete and rapid regeneration of fragments from the upside-down jellyfish *Cassiopea*. *Frontiers in Marine Science* 9.
- Palmer DA, Van Eldik R (1983) The chemistry of metal carbonate and carbon dioxide complexes. *Chem Rev* 83:651–731.
- Passarelli MK, Ewing AG, Winograd N (2013) Single-cell lipidomics: characterizing and imaging lipids on the surface of individual *Aplysia californica* neurons with cluster secondary ion mass spectrometry. *Anal Chem* 85:2231–2238.
- Pernice M, Dunn SR, Tonk L, Dove S, Domart-Coulon I, Hoppe P, Schintlmeister A, Wagner M, Meibom A (2015) A nanoscale secondary ion mass spectrometry study of dinoflagellate functional diversity in reef-building corals. *Environ Microbiol* 17:3570–3580.
- Pernice M, Meibom A, Van Den Heuvel A, Kopp C, Domart-Coulon I, Hoegh-Guldberg O, Dove S (2012) A single-cell view of ammonium assimilation in coral-dinoflagellate symbiosis. *ISME J* 6:1314–1324.
- Phelan MA, Matta JL, Reyes YM, Fernando R, Boykins RA, Blanquet RS (2006) Associations between metals and the blue mesogleal protein of *Cassiopea xamachana*. *Mar Biol* 149:307–312.

- Pitt KA, Koop K, Rissik D (2005) Contrasting contributions to inorganic nutrient recycling by the co-occurring jellyfishes, *Catostylus mosaicus* and *Phyllorhiza punctata* (Scyphozoa, Rhizostomeae). *J Exp Mar Bio Ecol* 315:71–86.
- Pitt KA, Welsh DT, Condon RH (2009) Influence of jellyfish blooms on carbon, nitrogen and phosphorus cycling and plankton production. *Hydrobiologia* 616:133–149.
- Popa R, Weber PK, Pett-Ridge J, Finzi JA, Fallon SJ, Hutcheon ID, Neelson KH, Capone DG (2007) Carbon and nitrogen fixation and metabolite exchange in and between individual cells of *Anabaena oscillarioides*. *ISME J* 1:354–360.
- Purcell J, Uye S, Lo W (2007) Anthropogenic causes of jellyfish blooms and their direct consequences for humans: a review. *Mar Ecol Prog Ser* 350:153–174.
- Rädecker N, Pogoreutz C, Wild C, Voolstra CR (2017) Stimulated Respiration and Net Photosynthesis in *Cassiopeia* sp. during Glucose Enrichment Suggests in hospite CO<sub>2</sub> Limitation of Algal Endosymbionts. *Frontiers in Marine Science* 4.
- Rahat M, Adar O (1980) Effect of Symbiotic Zooxanthellae and Temperature on Budding and Strobilation in *Cassiopeia andromeda* (Eschscholz). *Biol Bull* 159:394–401.
- Ralph PJ, Gademann R (2005) Rapid light curves: A powerful tool to assess photosynthetic activity. *Aquat Bot* 82:222–237.
- Ralph PJ, Schreiber U, Gademann R, Kühl M, Larkum AWD (2005) Coral photobiology studied with a new imaging pulse amplitude modulated fluorometer. *J Phycol* 41:335–342.
- Rickelt LF, Lichtenberg M, Trampe ECL, Kühl M (2016) Fiber-optic probes for small-scale measurements of scalar irradiance. *Photochem Photobiol* 92:331–342.
- Rohwer F, Seguritan V, Azam F, Knowlton N (2002) Diversity and distribution of coral-associated bacteria. *Mar Ecol Prog Ser* 243:1–10.
- Rosenberg E, Koren O, Reshef L, Efrony R, Zilber-Rosenberg I (2007) The role of microorganisms in coral health, disease and evolution. *Nature Reviews Microbiology* 5:355–362.
- Roth MS (2014) The engine of the reef: photobiology of the coral-algal symbiosis. *Front Microbiol* 5:422.
- Röthig T, Puntin G, Wong JCY, Burian A, McLeod W, Baker DM (2021) Holobiont nitrogen control and its potential for eutrophication resistance in an obligate photosymbiotic jellyfish. *Microbiome* 9.
- Rowen DJ, Templeman MA, Kingsford MJ (2017) Herbicide effects on the growth and photosynthetic efficiency of *Cassiopea maretens*. *Chemosphere* 182:143–148.
- Ruppert EE, Fox RS, Barnes RD (2004) *Invertebrate Zoology: A Functional Evolutionary Approach*. Thomson-Brooks/Cole.
- Sachs JL, Wilcox TP (2006) A shift to parasitism in the jellyfish symbiont *Symbiodinium microadriaticum*. *Proc Biol Sci* 273:425–429.
- Salih A (2012) Screening reef corals for novel GFP-type fluorescent proteins by confocal imaging. In: *In Vivo Cellular Imaging Using Fluorescent Proteins: Methods and Protocols*. Hoffman RM (ed) Humana Press, Totowa, NJ, p 217–233
- Salih A, Larkum A, Cox G, Kühl M, Hoegh-Guldberg O (2000) Fluorescent pigments in corals are photoprotective. *Nature* 408:850–853.
- Samatham R, Jacques SL, Campagnola P (2008) Optical properties of mutant versus wild-type mouse skin measured by reflectance-mode confocal scanning laser microscopy (rCSLM). *J Biomed Opt* 13:041309.
- Santhanakrishnan A, Dollinger M, Hamlet CL, Colin SP, Miller LA (2012) Flow structure and transport characteristics of feeding and exchange currents generated by upside-down *Cassiopea* jellyfish. *J Exp Biol* 215:2369.
- Santner J, Larsen M, Kreuzeder A, Glud RN (2015) Two decades of chemical imaging of solutes in sediments and soils--a review. *Anal Chim Acta* 878:9–42.

- Schembri PJ, Deidun A, Vella PJ (2010) First record of *Cassiopea andromeda* (Scyphozoa: Rhizostomeae: Cassiopeidae) from the central Mediterranean Sea. *Mar Biodivers Rec* 3.
- Schiariti A, Morandini AC, Jarms G, von Glehn Paes R, Franke S, Mianzan H (2014) Asexual reproduction strategies and blooming potential in Scyphozoa. *Mar Ecol Prog Ser* 510:241–253.
- Schmitt JM (1999) Optical coherence tomography (OCT): a review. *IEEE J Sel Top Quantum Electron* 5:1205–1215.
- Schoenberg DA, Trench RK (1980) Genetic Variation in *Symbiodinium* (=Gymnodinium) *microadriaticum* Freudenthal, and Specificity in its Symbiosis with Marine Invertebrates. II. Morphological Variation in *Symbiodinium microadriaticum*. *Proceedings of the Royal Society of London Series B, Biological Sciences* 207:429–444.
- Schrameyer V, Wangpraseurt D, Hill R, Kühl M, Larkum AWD, Ralph PJ (2014) Light respiratory processes and gross photosynthesis in two scleractinian corals. *PLoS One* 9:e110814.
- Shapiro OH, Kramarsky-Winter E, Gavish AR, Stocker R, Vardi A (2016) A coral-on-a-chip microfluidic platform enabling live-imaging microscopy of reef-building corals. *Nat Commun* 7:10860.
- Shaposhnikova T, Matveev I, Napara T, Podgornaya O (2005) Mesogleal cells of the jellyfish *Aurelia aurita* are involved in the formation of mesogleal fibres. *Cell Biol Int* 29:952–958.
- Sivaguru M, Fried GA, Miller CAH, Fouke BW (2014) Multimodal optical microscopy methods reveal polyp tissue morphology and structure in Caribbean reef building corals. *J Vis Exp*:e51824.
- Smith FA, Raven JA (1979) Intracellular pH and its regulation. *Annu Rev Plant Physiol* 30:289–311.
- Smith VJ (2016) Immunology of Invertebrates: Cellular. In: *eLS*. Wiley, p 1–13
- Speiser DI, Gagnon YL, Chhetri RK, Oldenburg AL, Johnsen S (2016) Examining the effects of chromatic aberration, object distance, and eye shape on image-formation in the mirror-based eyes of the bay scallop *Argopecten irradians*. *Integr Comp Biol* 56:796–808.
- Spicer GLC, Eid A, Wangpraseurt D, Swain TD, Winkelmann JA, Yi J, Kühl M, Marcelino LA, Backman V (2019) Measuring light scattering and absorption in corals with Inverse Spectroscopic Optical Coherence Tomography (ISOCT): a new tool for non-invasive monitoring. *Sci Rep* 9:14148.
- Stern RA, Fletcher IR, Rasmussen B, McNaughton NJ, Griffin BJ (2005) Ion microprobe (NanoSIMS 50) Pb-isotope geochronology at <5 µm scale. *Int J Mass Spectrom* 244:125–134.
- Stoecker DK, Hansen PJ, Caron DA, Mitra A (2017) Mixotrophy in the Marine Plankton. *Ann Rev Mar Sci* 9:311–335.
- Stoner EW, Layman CA, Yeager LA, Hassett HM (2011) Effects of anthropogenic disturbance on the abundance and size of epibenthic jellyfish *Cassiopea* spp. *Mar Pollut Bull* 62:1109–1114.
- Swain TD, DuBois E, Gomes A, Stoyneva VP, Radosevich AJ, Henss J, Wagner ME, Derbas J, Grooms HW, Velazquez EM, Traub J, Kennedy BJ, Grigorescu AA, Westneat MW, Sanborn K, Levine S, Schick M, Parsons G, Biggs BC, Rogers JD, Backman V, Marcelino LA (2016) Skeletal light-scattering accelerates bleaching response in reef-building corals. *BMC Ecol* 16:10.
- Taylor Parkins SK, Murthy S, Picioreanu C, Kühl M (2021) Multiphysics modelling of photon, mass and heat transfer in coral microenvironments. *J R Soc Interface* 18:20210532.
- Terán E, Méndez ER, Enríquez S, Iglesias-Prieto R (2010) Multiple light scattering and absorption in reef-building corals. *Appl Opt* 49:5032–5042.
- Thé J, Barroso H de S, Mammone M, Viana M, Batista Melo CS, Mies M, Banha TNS, Morandini AC, Rossi S, Soares M de O (2020) Aquaculture facilities promote populational stability throughout seasons and increase medusae size for the invasive jellyfish *Cassiopea andromeda*. *Mar Environ Res* 162:105161.
- Thompson AW, Foster RA, Krupke A, Carter BJ, Musat N, Vaultot D, Kuypers MMM, Zehr JP (2012) Unicellular cyanobacterium symbiotic with a single-celled eukaryotic alga. *Science* 337:1546–1550.

- Thornhill DJ, Daniel MW, LaJeunesse TC, Schmidt GW, Fitt WK (2006) Natural infections of aposymbiotic *Cassiopea xamachana* scyphistomae from environmental pools of Symbiodinium. *J Exp Mar Bio Ecol* 338:50–56.
- Thrane L, Frosz MH, Levitz D, Jorgensen TM, Andersen CB, Hansen PR, Valanciunaite J, Swartling J, Andersson-Engels S, Tycho A, Yura HT, Andersen PE (2005) Extraction of tissue optical properties from optical coherence tomography images for diagnostic purposes. In: *Saratov Fall Meeting 2004: Optical Technologies in Biophysics and Medicine VI*. SPIE, p 139–150
- Thuesen EV, Rutherford LD, Brommer PL, Garrison K, Gutowska MA, Towanda T (2005) Intragel oxygen promotes hypoxia tolerance of scyphomedusae. *J Exp Biol* 208:2475.
- Todd BD, Thornhill DJ, Fitt WK (2006) Patterns of inorganic phosphate uptake in *Cassiopea xamachana*: A bioindicator species. *Mar Pollut Bull* 52:515–521.
- Trench RK (1971) The Physiology and Biochemistry of Zooxanthellae Symbiotic with Marine Coelenterates. III. The Effect of Homogenates of Host Tissues on the Excretion of Photosynthetic Products in vitro by Zooxanthellae from Two Marine Coelenterates. *Proc R Soc Lond B Biol Sci* 177:251–264.
- Tucker CJ (1979) Red and photographic infrared linear combinations for monitoring vegetation. *Remote Sens Environ* 8:127–150.
- Uchida T (1970) Occurrence of a Rhizostome Medusa, *Cassiopea mertensii* BRANDT from the Hawaiian Islands.
- Valle N, Drillet J, Pic A, Migeon H-N (2011) Nano-SIMS investigation of boron distribution in steels. *Surf Interface Anal* 43:573–575.
- Van Lieshout JS, Martin VJ (1992) Development of Planuloid Buds of *Cassiopea xamachana* (Cnidaria: Scyphozoa). *Trans Am Microsc Soc* 111:89–110.
- Veal CJ, Carmi M, Dishon G, Sharon Y, Michael K, Tchernov D, Hoegh-Guldberg O, Fine M (2010) Shallow-water wave lensing in coral reefs: a physical and biological case study. *J Exp Biol* 213:4304–4312.
- Verde EA, McCloskey LR (1998) Production, respiration, and photophysiology of the mangrove jellyfish *Cassiopea xamachana* symbiotic with zooxanthellae: effect of jellyfish size and season. *Mar Ecol Prog Ser* 168:147–162.
- Wacey D, Saunders M, Brasier MD, Kilburn MR (2011) Earliest microbially mediated pyrite oxidation in ~3.4 billion-year-old sediments. *Earth Planet Sci Lett* 301:393–402.
- Wagner M, Taherzadeh D, Haisch C, Horn H (2010) Investigation of the mesoscale structure and volumetric features of biofilms using optical coherence tomography. *Biotechnol Bioeng* 107:844–853.
- Wangpraseurt D, Holm JB, Larkum AWD, Pernice M, Ralph PJ, Suggett DJ, Kühl M (2017a) In vivo Microscale Measurements of Light and Photosynthesis during Coral Bleaching: Evidence for the Optical Feedback Loop? *Frontiers in Microbiology* 8:59.
- Wangpraseurt D, Jacques S, Lyndby N, Holm JB, Pages CF, Kühl M (2019) Microscale light management and inherent optical properties of intact corals studied with optical coherence tomography. *J R Soc Interface* 16:20180567.
- Wangpraseurt D, Larkum AWD, Franklin J, Szabó M, Ralph PJ, Kühl M (2014a) Lateral light transfer ensures efficient resource distribution in symbiont-bearing corals. *J Exp Biol* 217:489–498.
- Wangpraseurt D, Larkum AWD, Ralph PJ, Kühl M (2012) Light gradients and optical microniches in coral tissues. *Front Microbiol* 3:316.
- Wangpraseurt D, Pernice M, Guagliardo P, Kilburn MR, Clode PL, Polerecky L, Kühl M (2016) Light microenvironment and single-cell gradients of carbon fixation in tissues of symbiont-bearing corals. *ISME J* 10:788–792.
- Wangpraseurt D, Polerecky L, Larkum AWD, Ralph PJ, Nielsen DA, Pernice M, Kühl M (2014b) The *in situ* light microenvironment of corals. *Limnol Oceanogr* 59:917–926.

- Wangpraseurt D, Wentzel C, Jacques SL, Wagner M, Kühl M (2017b) *In vivo* imaging of coral tissue and skeleton with optical coherence tomography. *J R Soc Interface* 14:20161003.
- Weis VM (2008) Cellular mechanisms of Cnidarian bleaching: stress causes the collapse of symbiosis. *J Exp Biol* 211:3059–3066.
- Weis VM, Smith GJ, Muscatine L (1989) A “CO<sub>2</sub> supply” mechanism in zooxanthellate cnidarians: role of carbonic anhydrase. *Mar Biol* 100:195–202.
- Welsh DT, Dunn RJK, Meziane T (2009) Oxygen and nutrient dynamics of the upside down jellyfish (*Cassiopea* sp.) and its influence on benthic nutrient exchanges and primary production. *Hydrobiologia* 635:351–362.
- Wiedenmann J, D’Angelo C, Smith EG, Hunt AN, Legiret F-E, Postle AD, Achterberg EP (2012) Nutrient enrichment can increase the susceptibility of reef corals to bleaching. *Nat Clim Chang* 3:160–164.
- Wilkerson, Kremer (1992) DIN, DON and PO<sub>4</sub> flux by a medusa with algal symbionts. *Mar Ecol Prog Ser* 90:237–250.
- Yamashita H, Suzuki G, Hayashibara T, Koike K (2011) Do corals select zooxanthellae by alternative discharge? *Mar Biol* 158:87–100.
- Yellowlees D, Rees TAV, Leggat W (2008) Metabolic interactions between algal symbionts and invertebrate hosts. *Plant Cell Environ* 31:679–694.
- van der Zande RM, Achlatis M, Bender-Champ D, Kubicek A, Dove S, Hoegh-Guldberg O (2020) Paradise lost: End-of-century warming and acidification under business-as-usual emissions have severe consequences for symbiotic corals. *Glob Chang Biol* n/a.
- Zarnoch CB, Hossain N, Fusco E, Alldred M, Hoellein TJ, Perdikaris S (2020) Size and density of upside-down jellyfish, *Cassiopea* sp., and their impact on benthic fluxes in a Caribbean lagoon. *Mar Environ Res* 154:104845.
- Zumholz K, Hansteen T, Hillion F, Horreard F, Piatkowski U (2007) Elemental distribution in cephalopod statoliths: NanoSIMS provides new insights into nano-scale structure. *Rev Fish Biol Fish* 17:487–491.

## Curriculum Vitae

**Name:** Niclas Heidelberg Lyndby  
**Address:** La Ruelle 17, 1302 Vufflens-la-Ville, Vaud, Switzerland  
**Mobile:** +45 2030 0640  
**E-mail:** [niclas.lyndby@epfl.ch](mailto:niclas.lyndby@epfl.ch) | [nhlyndby@gmail.com](mailto:nhlyndby@gmail.com)  
**Date of birth:** May 6, 1991  
**Nationality:** Danish  
**Languages:** Danish (mother tongue), English (fluent)



ORCID: <https://orcid.org/0000-0003-0533-9663>

ResearchGate: [https://www.researchgate.net/profile/Niclas\\_Lyndby](https://www.researchgate.net/profile/Niclas_Lyndby)

Google Scholar: <https://scholar.google.com/citations?user=5rUNqQgAAAAJ&hl=en&oi=ao>

### Education

2018 - 2022: Swiss Federal Institute of Technology Lausanne (EPFL), Laboratory for Biological Geochemistry, PhD candidate. *Photobiology and metabolic interactions in the symbiotic jellyfish Cassiopea*.

Acquired skills: Working with stable isotope incubations, classical sample preparation with resin infiltration, microtomy of resin samples, scanning electron microscopy imaging, nanoscale secondary ion mass spectrometry (NanoSIMS), cultivation and completing lifecycle of *Cassiopea andromeda* in laboratory setting.

2015 – 2017: University of Copenhagen, Department of Biology, M.Sc. in Biological Science.

Master's thesis (awarded the top grade, 12): *Effects of feeding on the bleaching response of the scleractinian coral Pocillopora damicornis: Light and radiative energy budgets*. I was part of a two-part project about thermal stress in fed and starved corals of the species *Pocillopora damicornis*. The experimental part was primarily done at the Scientifique Centre of Monaco in Monaco, with a one week stay three months in advance to setup up everything, and subsequently one month of measurements at the facility. My part of the project (my thesis) was covering radiative energy budgets in the corals before and during thermal stress, calculating how much of the incident light is conserved as photosynthesis and how much is dissipated as heat or backscattered. The second part covered carbon energy budgets of the same corals, investigating how the stressed corals utilize the carbon available when fed and starved. The work is currently prepared for submission as 2 back-to-back papers in *Marine Ecology Progress Series*.

Acquired skills: During my M.Sc. I have primarily taken marine biology courses, giving me a broad and more in depth understanding of marine environments, marine ecology, macro ecology, and marine microbiology and virology. In addition, I have carried out two projects, one about marine algae and their ecophysiology (Title: *Ecophysiological studies of Pseudochatonella verruculosa – Effects of temperature, salinity, and pH on growth rate*), the other about coral cilia and their function, as well as developing a new method for studying oxygen dynamics in small coral fragments under well-defined conditions (Title: *Coral cilia and the effect on oxygen uptake*).

2010 – 2015: University of Copenhagen, Department of Biology, B.Sc. in Biological Science.

Bachelor's thesis (awarded the top grade, 12): *The role of green fluorescent pigments for the optical and thermal properties of corals* (Lyndby et al. 2016). I worked with a broad range of electrochemical and optical microsensors and imaging techniques to study the optical and thermal properties of the surface tissue of the coral *Dipsastraea* sp. During my thesis I was 3 months in Australia; one week on Heron Island in the Great Barrier Reef to gather coral samples, and subsequently at the University of Technology, Sydney, to do measurements and write on my thesis. The thesis led to a publication in *Scientific Reports* with me as lead author.

Acquired skills: Throughout my B.Sc. I have acquired a broad understanding of basic biology and field work along with biologically oriented chemistry, math, and statistics (fundamental courses). In addition, I have worked with applied marine biology, biological assessments of freshwater ecosystems, macroscopic anatomy and classification of Danish fauna, extended statistical methods and experimental design, as well as to learn to plan and carry out own experimental research (Title: *Detritus Recyclers in Terrestrial Ecosystems*).

### **Peer-reviewed publications**

Lyndby NH, Kühl M, Wangpraseurt D (2016) Heat generation and light scattering of green fluorescent protein-like pigments in coral tissue. *Scientific Reports* 6:14. DOI: 10.1038/srep26599

Ordoñez A, Wangpraseurt D, Lyndby NH, Kühl M, Diaz-Pulido G (2019) Elevated CO<sub>2</sub> Leads to Enhanced Photosynthesis but Decreased Growth in Early Life Stages of Reef Building Coralline Algae. *Frontiers in Marine Science* 5. DOI: 10.3389/fmars.2018.00495

Wangpraseurt D, Jacques S, Lyndby NH, Holm JB, Ferrier-Pagès C, Kühl M (2019) Microscale light management and inherent optical properties of intact corals studied with optical coherence tomography. *Journal of The Royal Society Interface* 16:20180567. DOI: 10.1098/rsif.2018.0567

Lyndby NH, Holm JB, Wangpraseurt D, Ferrier-Pagès C, Kühl M (2019) Bio-optical properties and radiative energy budgets in fed and unfed scleractinian corals (*Pocillopora* sp.) during thermal bleaching. *Marine Ecology Progress Series* 629:1–17. DOI: 10.3354/meps13146

Lyndby NH, Holm JB, Wangpraseurt D, Grover R, Rottier C, Kühl M, Ferrier-Pagès C (2020) Effect of temperature and feeding on carbon budgets and O<sub>2</sub> dynamics in *Pocillopora damicornis*. *Marine Ecology Progress Series* 652:49–62. DOI: 10.3354/meps13474

Lyndby NH, Rådecker N, Bessette S, Søgaaard Jensen LH, Escrig S, Trampe E, Kühl M, Meibom A (2020) Amoebocytes facilitate efficient carbon and nitrogen assimilation in the *Cassiopea*-Symbiodiniaceae symbiosis. *Proceedings Biological sciences / The Royal Society* 287:20202393. DOI: 10.1098/rspb.2020.2393

Bollati E, Lyndby NH, D'Angelo C, Kühl M, Wiedenmann J, Wangpraseurt D (2022) Green fluorescent protein-like pigments optimise the internal light environment in symbiotic reef-building corals. *eLife* 11:e73521. DOI: 10.7554/eLife.73521

### **Work in progress manuscripts**

Lyndby NH, Murray MC, Trampe E, Meibom A, Kühl M (2022) The mesoglea buffers the physico-chemical microenvironment of photosymbionts in the upside-down jellyfish *Cassiopea* sp. bioRxiv:2022.10.06.511124. (submitted)

Lyndby NH, Murthy S, Bessette S, Jakobsen SL, Meibom A, Kühl M. Non-invasive investigation of the morphology and optical properties of the upside-down jellyfish *Cassiopea* with optical coherence tomography

Lyndby NH, Moßhammer M, Pogoreutz C, Jakobsen SL, Meibom A, Kühl M. Imaging of O<sub>2</sub> dynamics in *Cassiopea* medusae using O<sub>2</sub>-sensitive planar optodes.

Caldwell J, Loussert-Fonta C, Toullec G, Lyndby NH, Haenni B, Taladriz-Blanco P, Espiña B, Rothen-Rutishauser B, Petri-Fink A. Correlative Light, Electron Microscopy and Raman Spectroscopy to Detect and Observe Microplastic Interactions with Whole Jellyfish (submitted)

Toullec G, Lyndby NH, Rådecker N, Banc-Prandi G, Pogoreutz C, Escrig S, Meibom A. Symbiotic metabolism of cassiosomes, the free-living "weapons" of the upside-down jellyfish *Cassiopea*

### **Conferences and presentations**

Poster presentation at the annual Danish Microbiological Society congress 2016.

Poster title: *Green-fluorescent protein like pigments scatter light and enhance coral heating.*

DOI: 10.13140/RG.2.2.12791.42406

Oral presentation at the European Coral Reef Symposium, Oxford 2017, session 15 "Nutrient physiology and ecology of coral reefs".

Presentation title: *Effects of feeding on the radiative energy budget of the coral *Pocillopora damicornis* during thermal stress.*

DOI: 10.13140/RG.2.2.29572.63363